Theoretical Biology

Atsushi Kamimura
Toru Ohira

Group Chase and Escape

Fusion of Pursuits-Escapes and Collective Motions

Springer

Theoretical Biology

Series Editor

Yoh Iwasa, Department of Bioscience, School of Science and Technology, Kwansei Gakuin University, Hyogo, Japan

The "Theoretical Biology" series publishes volumes on all aspects of life sciences research for which a mathematical or computational approach can offer the appropriate methods to deepen our knowledge and insight.

Topics covered include: cell and molecular biology, genetics, developmental biology, evolutionary biology, behavior sciences, species diversity, population ecology, chronobiology, bioinformatics, immunology, neuroscience, agricultural science, and medicine.

The main focus of the series is on the biological phenomena whereas mathematics or informatics contribute the adequate tools. Target audience is researchers and graduate students in biology and other related areas who are interested in using mathematical techniques or computer simulations to understand biological processes and mathematicians who want to learn what are the questions biologists like to know using diverse mathematical tools.

More information about this series at http://www.springer.com/series/15703

Atsushi Kamimura · Toru Ohira

Group Chase and Escape

Fusion of Pursuits-Escapes and Collective Motions

Springer

Atsushi Kamimura
Department of Basic Science
Graduate School of Arts and Sciences
The University of Tokyo
Tokyo, Japan

Toru Ohira
Nagoya University
Nagoya, Aichi, Japan

ISSN 2522-0438 ISSN 2522-0446 (electronic)
Theoretical Biology
ISBN 978-981-15-1730-3 ISBN 978-981-15-1731-0 (eBook)
https://doi.org/10.1007/978-981-15-1731-0

Mathematics Subject Classification (2010): 60G50, 34K50, 60H10

© Springer Nature Singapore Pte Ltd. 2019
This work is subject to copyright. All rights are reserved by the Publisher, whether the whole or part of the material is concerned, specifically the rights of translation, reprinting, reuse of illustrations, recitation, broadcasting, reproduction on microfilms or in any other physical way, and transmission or information storage and retrieval, electronic adaptation, computer software, or by similar or dissimilar methodology now known or hereafter developed.
The use of general descriptive names, registered names, trademarks, service marks, etc. in this publication does not imply, even in the absence of a specific statement, that such names are exempt from the relevant protective laws and regulations and therefore free for general use.
The publisher, the authors and the editors are safe to assume that the advice and information in this book are believed to be true and accurate at the date of publication. Neither the publisher nor the authors or the editors give a warranty, expressed or implied, with respect to the material contained herein or for any errors or omissions that may have been made. The publisher remains neutral with regard to jurisdictional claims in published maps and institutional affiliations.

This Springer imprint is published by the registered company Springer Nature Singapore Pte Ltd.
The registered company address is: 152 Beach Road, #21-01/04 Gateway East, Singapore 189721, Singapore

This book is dedicated to our families.

Preface

Sometimes research begins by chance. The main theme of this book, Group Chase and Escape, is one such example. Neither of the authors knew about the long tradition of chases and escapes. One of the authors (A. K.) was working on theoretical models to explain how primitive cells could have consistently grown and divided. The other author (T. O.) was interested in systems with noise and delay and was studying models of a random walk with delay. The story of our collaboration dates back to the summer of 2008 when a book of chases and escapes by Paul J. Nahin was introduced to the second author by Professor John G. Milton of Claremont University, California, USA. Coincidentally, the authors were together at the University of Tokyo and came up with the idea of expanding the long-standing problem of chases and escapes into a multi-particle system.

Our attempt was to bring together two topics of differing nature. Chases and Escapes have a long tradition in mathematics, and efforts have been made to obtain analytical expressions of pursuit curves. On the other hand, collective motion of a large number of particles is an emerging research area to elucidate universality with the interests of statistical physics. Here, the high degree of freedom of the system makes computer simulation a powerful tool. As a first step to connect the two topics, we kept the concept as simple as possible and extended it to a multi-particle system. This led us to propose the original model released in 2010: each player chases and escapes individually with the nearest opponent without in-group communication (except excluded volumes of the players). Although simple, the model shows emergent collective behavior, such as segregation of pursuers and escapees.

It was fortunate that our attempt attracted some interest, and various extensions of the model have been done. Our intention in writing this book is to summarize the majority of the models and recent developments as well as to provide related topics and possible future directions. In this process, with enjoyment, we have also obtained analytical solutions for a novel problem in chases and escapes.

Collaboration with other colleagues has greatly helped us in extending the models discussed in this book, and gaining deep insight into the problems. We are particularly grateful to N. Ito, S. Matsumoto, R. Nishi, T. Nogawa, T. Hosaka, J. G.

Milton, K. Nishinari, T. Saito and T. Nakamura for working with us. We also thank T. Vicsek and Y. Sugiyama for many useful discussions.

Hopefully, the readers may find some of their interests and enjoy this book. It is, however, important to bear in mind that this book is only a proposal. The successful fusion of the two topics remains to be achieved.

Atsushi Kamimura and Toru Ohira

Acknowledgements

A. K. acknowledges support from the Japan Society for the Promotion of Sciences with which the study presented in this book was mainly done. T. O. also affiliates with Future Value Creation Research Center, Graduate School of Informatics at Nagoya University, and Mathematical Science Team, RIKEN Center for Advanced Intelligence Project. He was in part supported by research funds from Ohagi Hospital (Hashimoto, Wakayama, Japan) as well as by Grant-in-Aid for Scientific Research from the Japan Society for the Promotion of Science No. 16H01175, No. 18H04443, No. 16H03360, and No. 19H01201.

Contents

Chapter 1
Introduction

The main theme of this book, entitled Group Chase and Escape, is a fusion of two different directions of mathematical and scientific research fields. One field deals with the traditional mathematical problems of chases and escapes, and the other is a more recent emerging field of "self-driven" particles to explain collective motions.

In this introduction, we give an overview of this book by briefly describing backgrounds and contents of the subsequent chapters. We first describe the two fields: chases and escapes (section 1.1) and collective motions (section 1.2). Then we move on to briefly explain our proposal, namely, Group Chase and Escape (section 1.3). It follows potential applications and challenges of our proposal (section 1.4).

1.1 Chases and Escapes

Situations relating to chases and escapes are ubiquitous in our daily lives. We see them in detective stories on TV; kids are playing games of tag; cats are chasing mice, and so on. They have also attracted the interest of mathematicians for a long time [71].

The oldest formulation of the problem is said to have been done by Leonardo da Vinci, who considered a cat-chasing-a-mouse problem [32]. The escaping mouse moves at a constant speed along a straight line, which is perpendicular to the line connecting the initial positions between them. The chasing cat also moves at a constant speed with its direction always pointing to the mouse.

Though the problem statement is simple, it took over 200 years before the pursuit curve of the cat was obtained by Pierre Bouguer in 1732 [10]. After that, this problem was presented in a book on differential equations by George Boole, who was a prominent mathematician known for Boolean algebra and logic [9].

A slight generalization of the problem had been studied where the straight line on which the mouse moves is inclined at an arbitrary angle, but the closed-form analytical solution in the absolute frame of reference was obtained only recently in 1991 [17], about half a millennium after Leonardo da Vinci's time!

© Springer Nature Singapore Pte Ltd. 2019

A. Kamimura and T. Ohira, *Group Chase and Escape,*
Theoretical Biology, https://doi.org/10.1007/978-981-15-1731-0_1

Another classic problem from this topic is the case where a target moves in circular motions. The first appearance of a circular pursuit problem was reported in the mathematical puzzle section of an English journal called *Ladies' Diary* [71]. In the 1748 issue, the problem was stated as a spider chasing a fly moving on a semicircular pane of glass.

Since then, the circular pursuit problems surfaced occasionally until the end of 19th century, however, progress was not significant probably because the problems involved coupled nonlinear differential equations and it was generally impossible to obtain analytical solutions in closed form. The problem was often associated with A. S. Hathaway, who stated it clearly in 1920 [2].

Apparently, there were no big leaps until we could use computers to draw the pursuit curves as we will show in Chapter 2.

Investigations of pursuit and evasion problems continue. From around 1990, a new mathematical formulation was developed by Eliezer and Barton [26, 27, 5] which allowed one to consider the problems not only in two-dimensional but also in three-dimensional space. This new approach will be described with examples in Chapter 2.

The problems of "chases and escapes" have also developed in different directions. In the mid-twentieth century, connections were found with the field of game theory. The most notable one was developed into theories of "Differential Games", on which R. Issacs published a classic book in 1965 [41]. In these games, the two players, pursuer and pursued, have strategies so that they can, respectively, minimize and maximize specific objective criteria, which are often the time between the beginning and the termination of the game, or the event of "capture". The pursuer wants to catch the pursued as soon as possible, while the pursued wants to evade for as long as possible. The central question is to find the optimal strategy for each of the players to achieve the conflicting objectives.

A representative example in the differential game is called the "homicidal chauffeur" problem. In this game, the chauffeur (pursuer) tries to run over and capture the slower but more maneuverable pedestrian (pursued). The pursuer has a faster speed, but the pursued has a smaller minimum turn-radius. Surprisingly, various types of strategies and situations for the two players have been found associated with the different speeds and the turn-radius ratios.

Other extensions relating to game theories include Search Game Theories [86]. The main theme is that a chaser tries to locate hiders, who can or cannot move among hiding spots. One notable example is the "Princess and Monster" problem [104]. These hiding spots can also take different forms, such as being connected by networks of various kinds.

Another direction is a fusion of the chase and escape problems with classical mechanics. Analogies and techniques developed in chases and escapes are employed to obtain analytical solutions of curvilinear motion of a particle on an inclined plane [92].

1.2 Collective Motion

The history of investigating multi-particle systems in physics is almost as old as the beginning of classical mechanics. Johannes Kepler, who analyzed astronomical data left by Tycho Brahe, investigated relations between geometry and motions of six planets. As is well known, the Newton's laws were developed based on the work of Kepler.

The work by Daniel Bernoulli in the 18th century is considered as the pioneering work of the kinetic theory of gases. The theory is based on the hypothesis that gases are composed of a huge number of moving particles. In the 19th century, physicists including Rudolf J. E. Clausius, James C. Maxwell and Ludwig E. Boltzmann had further developed the theory leading to statistical physics. Also, the work by Robert Brown led to the theory of Brownian motion by Einstein. Subsequent experiments by Jean B. Perrin confirmed the atomic nature of matter as well as the determination of Avogadro's number.

Collective behaviors and their functions have been of great interest in the field of biology. An example includes investigations of brains composed of neural cells, or neurons [51]. Experimental and anatomical studies begun in the 19th century. J. E. Purkinje, Cammillo Golgi and Ramon Cajal are the names of the pioneering scholars. By the beginning of the 20th century, the notion of the brain and central nervous system as a network of neurons with information processing capability was established.

Theories of the brain as a neural network were sprung in the 20th century. Seminal work was done by the neurophysiologist Warren McCulloch and the mathematician Walter Pitts to connect a network of neurons with computations in 1943 [65]. Following the work, various conceptual and mathematical models and algorithms have been proposed. They include functions of memories, learning, pattern recognition, vision and other sensory systems. Applications to engineering problems and systems, such as constrained optimization problems and robotics, have also been vigorously pursued. In recent years, deep multilayer neural networks and associated algorithms called Deep Learnings have provoked much interest fusing ever more strongly with the field of artificial intelligence [57].

Another line of research has emerged in recent years on collective motions [39, 102] of insects, animals, birds, humans, and automobiles. The phenomena of flocking, grouping and congestions are commonly observed around us. Here, the line of research treats each entity as a "self-propelled" or "self-driven" particle, and a group of them as an aggregate of particles. In contrast to physical matter of atoms and molecules, the movements of the particles are modeled by "coarse-grained" rules and dynamics, and as a result, one tries to elucidate the generality of rich collective behavior.

Investigations of collective motions have been pursued both experimentally and theoretically. For example, careful observation of flying patterns of groups of pigeons has suggested a possible social hierarchy [70]. It is also found that aerodynamic effects are responsible for V-shaped flying patterns of certain birds [82]. Schools of fish such as sardines have been observed and analyzed [33, 34, 81]. The

reaction time for collective response to disturbances such as attacks by larger fish is surprisingly short compared to the swimming speed of individuals. Studies of traffic data have shown for natural congestions without bottlenecks on highways that the head of congestion commonly moves backward approximately with the speed of 20km/h [94].

Various mathematical models have been proposed for theoretical investigations, to explain path formation of ants, pedestrian collective motions, flocks of birds and so on. Among them, we will present two representative theoretical frameworks in Chapter 3: Vicsek model [99] for flocking behavior and the Optimal Velocity model [4] for automotive congestions.

1.3 Group Chase and Escape

We have merged these two lines of research to propose a model of "Group Chase and Escape" [44]. On one hand, it is a simple extension of the traditional chase and escape problems to multiple players: one group chases another group. On the other hand, one can also view this proposal as an extension of the self-propelled particles into a mixture of two groups with different motives. In reality, such situations can be observed when one group of animals chases another, such as wolves chasing deer.

Mathematical analysis of group chase and escape is very challenging. Therefore, we have relied mostly on computational simulations to study the problem and show that a simple model can give rise to rich and complex behavior. In the original proposal of the framework, we first focused on certain quantities such as time for the total catch, average lifetimes of targets, and "cost" of capture by varying the number of chasers and targets. We found two qualitatively different regions for the quantities as a function of the number of chasers.

The most notable behavior of the simple model is the spatial organization of chasers and targets. To connect the two qualitatively-different regions with the spatial organization, we classify chasing processes into several patterns and introduce order parameters to characterize them. It is found that the number of targets decreases intermittently along with the capture of targets. At each event of the capture, the spatial organization of chasers changes drastically. Before the event, the chasers surround the target to be captured, and after that, they move to other remaining targets toward the next capture. Correspondingly, the order parameters change drastically at the events as well.

After introducing the basic model, we will discuss some of the recent developments of group chase and escape by extending the model. The developments will be reviewed by roughly categorizing them into three directions: abilities, reactions and motions.

The first category, "abilities", deals with modifications of abilities of the chasers and the targets for detecting the opponents' positions. Examples include the effects of changing and distributing the detection ranges of the chasers. It also suggests a benefit of division of labor in chasing and escaping.

The second category, “reactions”, deals with modifications of the relationship of pursuit and evasion, and the outcome of the “capture”. One investigated example extends the chasers and the targets to a three-member case [88]. In the example, three different species, A, B, and C, are considered. The species form a triangular relation of chasing and escaping: the first species A chases the second species B, and the species B chases the third species C, which in turn chases the first species A. Here, the captured member is converted to the member of the chasing group, for example, the captured B is converted to another member of A. Another related extension is considered as a vampire problem [75]. In this work, the basic rules for the chasers and the targets are the same as in the basic model. However, with some probabilities, the captured target can be converted into a new chaser rather than simply being removed from the field. It is observed that with this inclusion of conversion, there is a maximum for the time to catch all the targets when we change the initial number of targets.

The third category, “motions”, deals with modifications of the movements of the chaser and the target. Examples include the changes of lattice structures, off-lattice models, and errors in the movement. We also extend the model to facilitate interactions within each group. One investigated example is a model where chasers interact among themselves to repel within a certain distance. This has an effect that the chasers get less in each other’s way, and they tend to spread over the field. It is observed that when the number of chasers is small, this interaction works more effectively to reduce the time for the entire catch.

1.4 Potential Applications and Challenges

The topic of group chases and escapes described above is still at the beginning phase and there are a number of open problems and potentials for further developments and applications.

We will first discuss open problems such as the effects of boundary conditions, characterization of chasing patterns, and development of macroscopic descriptions, that require some theoretical challenges for further developments.

Then, we will present and discuss possible applications of group chases and escapes. The first topic is hunting in nature, in which we will take wolves as one typical example. One promising direction is to model cooperative hunting and compare with ethological studies. The second topic is to apply the framework to problems in engineering such as optimization problems. One attempt with preliminary results is described to employ the idea of chases and escapes for a combinatorial optimization problem. Finally, we make a remark by providing a general perspective of living together.

In the following chapters, we present the main body of the topics as we outlined in this introduction. The structure of the following chapters is as follows.

In Chapter 2, we introduce two classical examples of chases and escapes: a cat-chasing-a-mouse problem (Bouguer’s problem), and chases and escapes with circu-

lar paths. Recent developments are also described to extend the problems to three-dimensional space.

In Chapter 3, we provide a brief introduction of statistical mechanical approaches to collective motions. Then, we review two representative models, namely, the Vicsek model and the Optimal Velocity model.

In Chapter 4, we introduce a basic model to demonstrate group chase and escape. We review the behavior of the model obtained by computer simulations and present analysis to understand the dynamics. In addition, recent developments are described to modify and extend the basic model.

In Chapter 5, as described above, we discuss some open questions and challenges. Also, we point out possible applications of group chase and escape to cooperative hunting by wolves and optimization problems as promising directions for further developments.

Chapter 2
Chases and Escapes

2.1 Introduction

The main interest of chases and escapes, or pursuit and evasion, is to obtain the pursuit curve of the chaser(s) and it has a long history [32]. It is said that the original formulation of the problem dates back to Leonardo da Vinci, who considered a cat-chasing-a-mouse problem. Since then, various problems of chases and escapes have attracted mathematicians, and some analytical results were obtained for specific setups. Because the analytical treatments are generally challenging, the setups have been traditionally restricted to one-to-one cases where a chaser pursues a single target.

In this chapter, we introduce the representative problems of chases and escapes. We start by describing a pursuit curve obtained by the French mathematician Pierre Bouguer in 1732 for the cat-chasing-a-mouse problem where the mouse (target) moves on a straight line. Then, a slight extension of the cat-chasing-a-mouse problem is proposed in which the target's path is on an inclined line. Even though this extension appears to be a small change, the closed-form solution in the absolute frame of reference was obtained only recently in 1991.

We subsequently turn our attention to another classic problem of circular pursuit in which the target moves on a circular path. This problem originates from the mid-18th century, and a clear mathematical formulation was done in 1920. It is noted that this problem involves coupled nonlinear differential equations and that a closed-form solution cannot be obtained. Relating to this problem, a new mathematical formulation was developed by Eliezer and Barton, which allows one to consider the problem beyond two-dimensional space. We present this formulation with examples of chases and escapes in three-dimensional space.

Interest in chases and escapes has grown to expand related topics. In particular, connections with game theories have been developed as an interdisciplinary field of mathematics, operations research, and economics. Such research topics are typically called "Discrete Search Games" [86] and "Differential Games" [41]. We do not

© Springer Nature Singapore Pte Ltd. 2019

A. Kamimura and T. Ohira, *Group Chase and Escape,*
Theoretical Biology, https://doi.org/10.1007/978-981-15-1731-0_2

introduce them in detail here, but a brief introduction of discrete search games is given in Appendix A.

2.2 Chases and Escapes with Straight Lines

Let us start here with one of the simplest representative problems, where the target moves on a straight line.

2.2.1 Bouguer's Problem

The first problem is to obtain the pursuit curve of a chaser to a target moving on a straight line at a constant speed (see Fig. 2.1). The chaser, also with a constant speed, is required to have its velocity vector pointing to the position of the target. This problem is called Bouguer's problem after the French mathematician Pierre Bouguer, who proposed and solved it in 1732 [10].

The main problems are (A) to obtain the analytical expression of the path of the chaser in this setup and (B) to obtain the point at which the chaser captures the target. Both of the problems were solved as follows.

(A) The path of the chaser is given by the following equation with the configurations in Fig. 2.1. Even though we just present the expression of the equation below, it will be derived as a special case of the generalized problem in section 2.2.2.

(i) When the speed of the chaser, denoted by v_C, is different from that of the target, denoted by v_T, the pursuit curve is written as

$$y(x) = \frac{n}{1-n^2}x_0 + \frac{1}{2}(x_0 - x)\left\{\frac{\left(1-\frac{x}{x_0}\right)^n}{1+n} - \frac{\left(1-\frac{x}{x_0}\right)^{-n}}{1-n}\right\}, \tag{2.1}$$

where $n = v_T/v_C$ denotes the ratio of the speeds of the target to the chaser, and x_0 is the initial position of the target in the x-direction.

(ii) When the speeds of the chaser and the target are equal, the pursuit curve is written as

$$y(x) = \frac{1}{2}x_0\left\{\frac{1}{2}\left(1-\frac{x}{x_0}\right)^2 - \ln\left(1-\frac{x}{x_0}\right)\right\} - \frac{1}{4}x_0. \tag{2.2}$$

(B) The position of the point at which the chaser captures the target is given by

$$(x, y) = \left(x_0, \frac{nx_0}{1-n^2}\right),$$

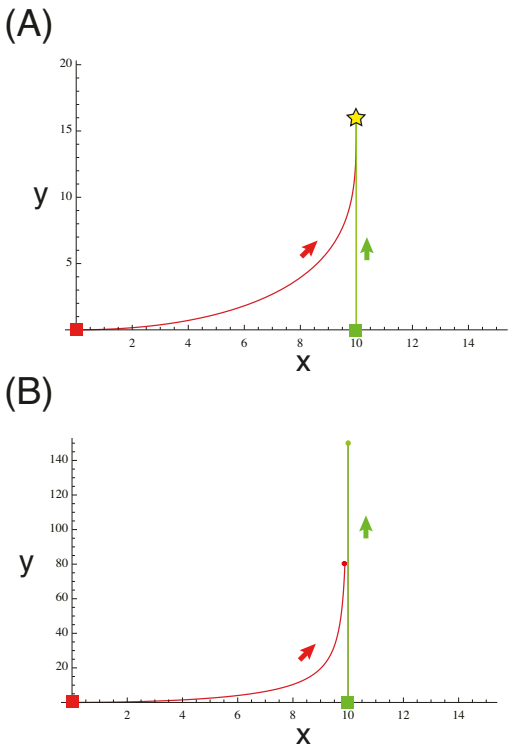

Fig. 2.1 Bouguer's problem: The green line represents the path of the target and the red curve represents the path of the chaser. (A) When the speed of the chaser is larger than that of the target, the target is captured at the position marked by the star. (B) When the speed of the chaser is smaller than that of the target, the chaser cannot capture the target. The initial position of the target, indicated by the green square, is at $(x,y) = (x_0,0)$ with $x_0 = 10$ and that of the chaser, indicated by the red square, is at $(x,y) = (0,0)$. The green and red arrows, respectively, indicate the directions of the motion of the target and the chaser along the paths.

which can be finite only if $n < 1$, i.e., the speed of the chaser is faster than the target. Otherwise, the capture does not take place as shown in Fig. 2.1(B). Note that this is also the case when the speeds are the same, corresponding to the path of Eq. (2.2).

Albeit the simplicity of the problem, one can appreciate from the above results that the analytical expressions are rather intricate.

One can consider variations of the problem. For example, the chaser can move in the direction to the target's anticipated position in the future for an interception, instead of pointing to the target's current position.

2.2.2 Chases and Escapes with Inclined Lines

We now generalize Bouguer's problem [17, 26, 27]. Here, the line on which the target moves is an inclined straight line. The schematic view is shown in Fig. 2.2. The target, denoted by E, now moves on an inclined straight line, starting from the point $A = (0, y_0)$. At the same time, the chaser C starts from the origin, $O = (0,0)$. Let us assume that the target and the chaser move with the constant speeds, v_T and v_C, respectively, and that the chaser C always points its velocity vector toward the target E. The position of E is denoted by $(X(t), Y(t))$, and the problem is to find the analytical expression for the path of C whose position is given by $(x(t), y(t))$.

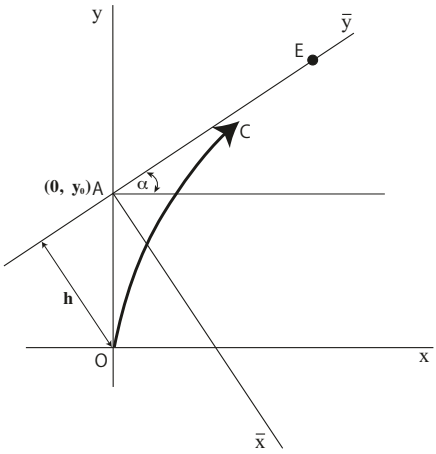

Fig. 2.2 Schematic view of the problem for which the target moves on an inclined line. See the main text for details.

By the condition that the chaser C at $(x(t), y(t))$ always points its velocity vector $(\dot{x}(t), \dot{y}(t))$ to the target E at $(X(t), Y(t))$, there is a relation between their positions,

$$(X(t), Y(t)) = (x(t) + \lambda(t)\dot{x}(t), y(t) + \lambda(t)\dot{y}(t)), \tag{2.3}$$

where $\lambda(t)$ is a function of time and the dot denotes derivative with respect to time t. By denoting the ratio of the speeds v_T and v_C as $n = v_T/v_C$, we also have

$$\dot{X}^2(t) + \dot{Y}^2(t) = n^2(\dot{x}^2(t) + \dot{y}^2(t)). \tag{2.4}$$

The above set of equations (2.3) and (2.4) are the basic equations of the problem: three equations to solve for $x(t), y(t)$, and $\lambda(t)$, given $X(t), Y(t)$, and n. We note that the expression of the equations is generally applicable to chase and escape problems in two-dimensional space.

We now formulate the condition in which the target E moves on a straight line. Here, let us assume, without the loss of generality, that the speed of E is equal to one ($v_T = 1$ and $n = 1/v_C$). By taking t as time with this unit, we have $\dot{X}^2(t) + \dot{Y}^2(t) = 1$. Also the position of the target E is written as $(X(t), Y(t)) = (t\cos\alpha, y_0 + t\sin\alpha)$, where α denotes the angle of the straight line (see Fig. 2.2). Thus, the following set of equations is obtained from Eqs. (2.3) and (2.4) with respect to the position $(x(t), y(t))$ and the velocity $(\dot{x}(t), \dot{y}(t))$ of C,

$$\dot{x}^2 + \dot{y}^2 = \frac{1}{n^2}, \tag{2.5}$$

$$x + \lambda\dot{x} = t\cos\alpha, \tag{2.6}$$

$$y + \lambda\dot{y} = y_0 + t\sin\alpha. \tag{2.7}$$

We have to solve the above set of equations to obtain the analytical expression for the paths of C. In order to make the calculation simpler, we introduce new coordinates $(\bar{x}, \bar{y})$, where the $\bar{y}$ axis is in the direction of the motion of E, while $\bar{x}$ is perpendicular to it with the origin at A (see Fig. 2.2). In the new coordinates, the set of equations (2.5)–(2.7) is given in a simpler form,

$$\dot{\bar{x}}^2 + \dot{\bar{y}}^2 = \frac{1}{n^2}, \tag{2.8}$$

$$\bar{x} + \lambda\dot{\bar{x}} = 0, \tag{2.9}$$

$$\bar{y} + \lambda\dot{\bar{y}} = t. \tag{2.10}$$

We now solve them by eliminating λ from Eqs. (2.9) and (2.10):

$$\bar{y} - \bar{x}\frac{d\bar{y}}{d\bar{x}} = t. \tag{2.11}$$

If we further differentiate both sides by $\bar{x}$, the following equation is obtained:

$$-\bar{x}\frac{d^2\bar{y}}{d\bar{x}^2} = \frac{dt}{d\bar{x}}. \tag{2.12}$$

On the other hand, if we divide Eq. (2.8) by $(\dot{\bar{x}})^2$, we get

$$1 + \left(\frac{d\bar{y}}{d\bar{x}}\right)^2 = \frac{1}{n^2}\left(\frac{dt}{d\bar{x}}\right)^2. \tag{2.13}$$

By eliminating $\frac{dt}{d\bar{x}}$ from Eqs. (2.12) and (2.13), we arrive at

$$1 + \left(\frac{d\bar{y}}{d\bar{x}}\right)^2 = \left(\frac{\bar{x}}{n}\right)^2\left(\frac{d^2\bar{y}}{d\bar{x}^2}\right)^2. \tag{2.14}$$

Since the chaser's curve is concave downward in the coordinate frame of $(\bar{x}, \bar{y})$, this leads to

$$\frac{d^2\bar{y}}{d\bar{x}^2} > 0, \quad (\forall \bar{x}). \tag{2.15}$$

Thus, by taking the square root of Eq. (2.14), the following is obtained with $p \equiv \frac{d\bar{y}}{d\bar{x}}$:

$$\sqrt{1+p^2} = \left(\frac{\bar{x}}{n}\right)\left(\frac{dp}{d\bar{x}}\right). \tag{2.16}$$

We can integrate this equation by separating the variables $\bar{x}$ and p as

$$\frac{dp}{\sqrt{1+p^2}} = \frac{n}{\bar{x}} d\bar{x}, \tag{2.17}$$

which leads to

$$\ln\left[p+\sqrt{1+p^2}\right] = n\left(\ln\bar{x} - \ln\bar{x}_c\right), \tag{2.18}$$

or

$$p+\sqrt{1+p^2} = \left(\frac{\bar{x}}{\bar{x}_c}\right)^n, \tag{2.19}$$

where $\bar{x}_c$ is a constant of integration. If we take the inverse of both sides, we obtain

$$\frac{1}{p+\sqrt{1+p^2}} = -p+\sqrt{1+p^2} = \left(\frac{\bar{x}}{\bar{x}_c}\right)^{-n}. \tag{2.20}$$

Equations (2.19) and (2.20) give

$$p = \frac{d\bar{y}}{d\bar{x}} = \frac{1}{2}\left[\left(\frac{\bar{x}}{\bar{x}_c}\right)^n - \left(\frac{\bar{x}}{\bar{x}_c}\right)^{-n}\right]. \tag{2.21}$$

We integrate this equation with the following initial conditions at $t = 0$ to obtain the pursuit curve,

$$\bar{x}(t=0) = y_0\cos\alpha, \quad \bar{y}(t=0) = -y_0\sin\alpha, \quad p(t=0) = -\tan\alpha. \tag{2.22}$$

Case 1: The speeds of the chaser and the target are different ($n \neq 1$)

The integration of Eq. (2.21) leads to

$$\bar{y} = \frac{n}{1-n^2} y_0\left(1+n\sin\alpha\right) + \frac{1}{2} y_0\cos\alpha \times \left[\frac{1}{1+n}\left(\frac{1-\sin\alpha}{\cos\alpha}\right)\left(\frac{\bar{x}}{y_0\cos\alpha}\right)^{1+n} - \frac{1}{1-n}\left(\frac{1-\sin\alpha}{\cos\alpha}\right)^{-1}\left(\frac{\bar{x}}{y_0\cos\alpha}\right)^{1-n}\right]. \tag{2.23}$$

This equation represents the analytical expression of the path of the chaser, C, in the coordinates of $(\bar{x},\bar{y})$. If one wants the corresponding equation in the original

coordinates of (x,y), one can make the coordinate transform using

$$\bar{x} = xy_0 \sin\alpha - (y - y_0)\cos\alpha, \quad \bar{y} = x\cos\alpha - (y - y_0)\sin\alpha. \tag{2.24}$$

Examples of the path obtained by numerical simulations are shown in Fig. 2.3.

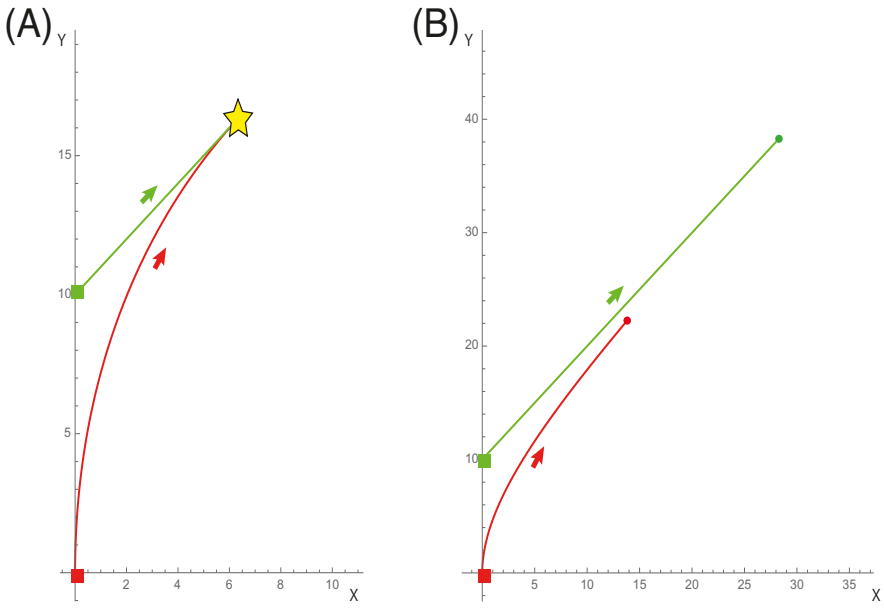

Fig. 2.3 Examples of the pursuit curves with inclined lines. The parameters are (A) $n = 0.5, \alpha = \pi/4, y_0 = 10$ and (B) $n = 1.5, \alpha = \pi/4, y_0 = 10$. The green and red squares indicate the starting points of the target and the chaser, respectively, and the green and red arrows indicate the directions of the motion of the target and the chaser along the paths, respectively.

We also note that by setting

$$\bar{x} = x_0 - x, \quad y_0 = x_0, \quad \alpha = 0, \tag{2.25}$$

the problem reduces to the original Bouguer's problem in section 2.2.1, and Eq. (2.1) is obtained from Eq. (2.23).

Case 2: The speeds of the chaser and the target are equal ($n = 1$)

In the case that the speeds of chaser and target are the same, Eq. (2.21) is written as

$$p = \frac{d\bar{y}}{d\bar{x}} = \frac{1}{2}\left[\left(\frac{\bar{x}}{\bar{x}_c}\right) - \left(\frac{\bar{x}}{\bar{x}_c}\right)^{-1}\right]. \tag{2.26}$$

We integrate this equation with the initial condition

$$\bar{x}_c = \frac{y_0 \cos^2\alpha}{1-\sin\alpha}, \tag{2.27}$$

leading to the following results:

$$\bar{y} = -\frac{1}{2}\left(\frac{y_0\cos^2\alpha}{1-\sin\alpha}\right)\times \left[\ln\frac{\bar{x}}{y_0\cos\alpha} - \frac{1}{2}\left\{\frac{(1-\sin\alpha)\bar{x}}{y_0\cos^2\alpha}\right\}^2 + 2\left(\frac{1-\sin\alpha}{\cos\alpha}\right)\tan\alpha + \frac{1}{2}\left(\frac{1-\sin\alpha}{\cos\alpha}\right)^2\right]. \tag{2.28}$$

If we set

$$\bar{x} = x_0 - x, \quad y_0 = x_0, \quad \alpha = 0, \tag{2.29}$$

the expression Eq. (2.2) in the previous section 2.2.1 is obtained from Eq. (2.28).

Catching up or not

Using the formulation, we can predict if the chaser can catch up with the target or not, as a function of the speed ratio $n = v_T/v_C = 1/v_C$ between the two. First, we note that the distance D between the chaser and the target is proportional to λ from Eqs. (2.3) and (2.4),

$$D = \sqrt{(X-x)^2 + (Y-y)^2} = \lambda v_C = \lambda/n. \tag{2.30}$$

From Eqs. (2.9) and (2.10), we can see that $\lambda(t) \geq 0$. Also by Eqs. (2.8)–(2.10) and (2.21), we obtain

$$\begin{aligned}\lambda(t) &= n\bar{x}\left[1+\left(\frac{d\bar{y}}{d\bar{x}}\right)^2\right]^{\frac{1}{2}} = n\bar{x}\left[1+\frac{1}{4}\left\{\left(\frac{\bar{x}}{\bar{x}_c}\right)^n - 2 + \left(\frac{\bar{x}}{\bar{x}_c}\right)^{-n}\right\}\right]^{\frac{1}{2}} \\ &= \frac{1}{2}n\bar{x}_c\left[\left(\frac{\bar{x}}{\bar{x}_c}\right)^{1+n} + \left(\frac{\bar{x}}{\bar{x}_c}\right)^{1-n}\right].\end{aligned} \tag{2.31}$$

For the case $n < 1$, we can see $\lambda \to 0$ as $\bar{x} \to 0$. This means that the positions of the chaser and the target will coincide at $\bar{x} = 0$ [Eq. (2.3)]. Thus, the chaser can catch up. This is intuitively reasonable because, for $n < 1$, the chaser is faster than the target. The point of the catch-up $(\bar{x}^*, \bar{y}^*)$ is given with $\bar{x} = 0$ in Eq. (2.23),

$$(\bar{x}^*, \bar{y}^*) = \left(0, \frac{ny_0(1+n\sin\alpha)}{1-n^2}\right). \tag{2.32}$$

On the other hand, for the case with $n > 1$, the values of λ [from Eq. (2.31)] and $\bar{y}$ [from Eq. (2.23)] approach positive infinity as $\bar{x} \to 0$. This means that the chaser cannot catch up with the target and the distance between the two increases.

For the case of equal speed $n = 1$, we expect that the chaser cannot catch up with the target if they are initially far separated. This can be seen from Eq. (2.31) as

$$\lambda = \frac{\bar{x}^2}{2\bar{x}_c} + \frac{\bar{x}_c}{2}, \tag{2.33}$$

and it leads to

$$\lambda \to \frac{\bar{x}_c}{2} = \frac{y_0 \cos^2 \alpha}{1 - \sin \alpha}, \quad (\bar{x} \to 0). \tag{2.34}$$

This means that there exists a constant distance $\bar{x}_c/2$ between the chaser and the target even as the time increases, therefore, the chaser cannot catch up with the target.

2.3 Chases and Escapes with Circular Paths

We now turn our attention to the case of circular motions by the target. While the problem is traditionally investigated in two-dimensional space, we will give a brief review on an extension to three-dimensional space, which was done only recently [5].

2.3.1 The Classic Problem in Two-Dimensional space

Let us first look at the problem in which the target moves in a circle (see Fig. 2.4). The rules for the chaser and the target are basically the same as that of the case in the previous section. The chaser always points its velocity vector to the current position of the target. This problem was first proposed in an English journal called *Ladies' Diary* in 1748 [71].

In contrast to Bouguer's problem, the chaser's path for this problem cannot be solved in an analytically closed form. However, certain characteristics are observed in numerical simulations as illustrated in Fig. 2.4. When the speed of the chaser is slower than the target, the chaser cannot catch up with the target. After a long time, however, it also follows a circular path with a smaller radius [Fig. 2.4(a)(b)]. As we show below, the ratio of radii of the two circles is proved to be the same as the ratio of the speeds of the chaser and the target. When the speed of the chaser is faster than the target, the chaser can catch up with the target [Fig. 2.4(c)(d)].

To analyze the movements, we define the problem as shown in Fig. 2.5. The target moves on a circular path of a radius a, and is pursued by a chaser who can move n times faster than the target. Suppose that the initial position of the target at

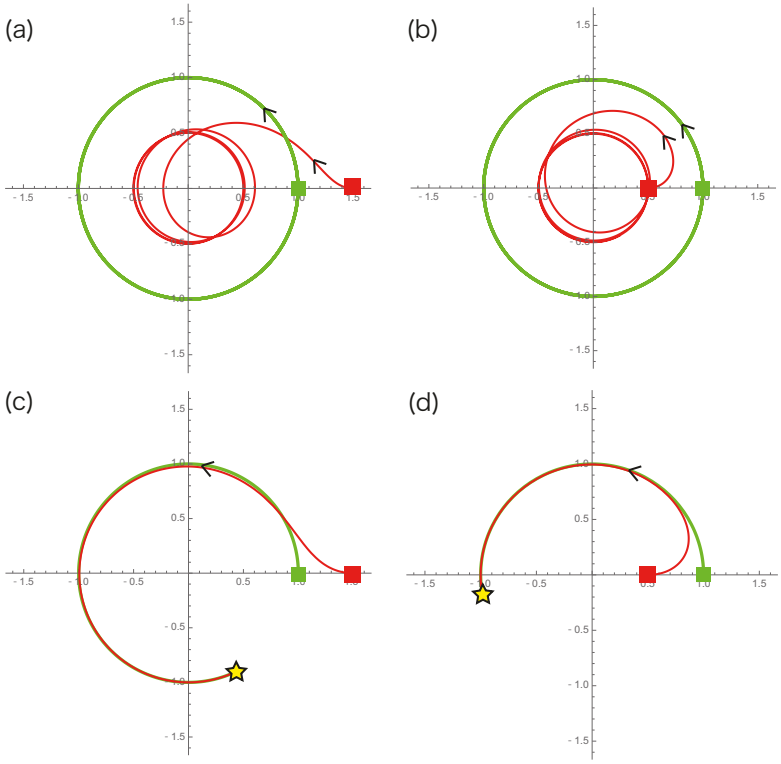

Fig. 2.4 Circular chase and escape: The green circle is the path of the target moving at a constant speed starting from $(x,y) = (1,0)$ indicated by the green square. The red curve represents the pursuit path of the chaser starting from $(x,y) = (1.5,0)$ for (a) and (c), and $(x,y) = (0.5,0)$ for (b) and (d). Both of the starting points are indicated by the red squares. The ratio of the speeds between the chaser and the target are $n = v_T/v_C = 2/1$ for (a) and (b), and $n = 0.95/1$ for (c) and (d). The chaser can catch up with the target for (c) and (d), and never catch up for (a) and (b).

time $t = 0$ is on the x–axis, at $(a,0)$. Because the target moves on the circular path, the position of the target is represented by an angle θ as $(a\cos\theta, a\sin\theta)$. When the target moves from the initial position ($\theta = 0$) to the present position at θ, a distance traveled by the target is $a\theta$. Hence, during the time interval, the chaser moves by a distance of $s = na\theta$ to reach the present position at (x,y). It is assumed that the chaser always points its direction of motion to the target. This makes the tangent at (x,y) to the chaser's pursuit curve pass through the target's instantaneous position.

We denote the angle made by the tangent line and the x–axis by φ, and denote the distance between the chaser and the target by ρ (see Fig. 2.5A). Then, the unit vector in the direction of the tangent line is written as $\mathbf{u} = (\cos\varphi, \sin\varphi)$, and the vector normal to the direction is written as $\mathbf{v} = (\sin\varphi, -\cos\varphi)$. The length of side 1 (see Fig. 2.5B) is obtained by considering the inner product of $\mathbf{p} = (x,y)$ and $\mathbf{v}$ as $\mathbf{p}\cdot\mathbf{v} = x\sin\varphi - y\cos\varphi$. On the other hand, the length is also obtained by considering

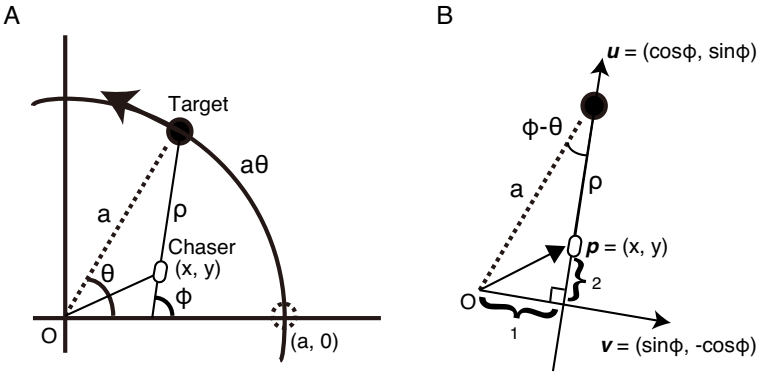

Fig. 2.5 (A) Definition of variables to characterize positions and movements of the chaser and the target. (B) The relative positions of the target and the chaser are extracted from (A).

the triangle of which side 1 is the base and the apex is the position of the target, as $a\sin(\varphi-\theta)$. Thus, the equation of the tangent line to the chaser's pursuit curve is written as

$$x\sin\varphi - y\cos\varphi = a\sin(\varphi-\theta). \tag{2.35}$$

Similarly, the length of side 2 (see Fig. 2.5B) is also obtained in two ways, and the equation of the line normal to the tangent line that passes through (x,y) is

$$x\cos\varphi + y\sin\varphi = a\cos(\varphi-\theta) - \rho. \tag{2.36}$$

By differentiating Eq. (2.35) with respect to θ, one gets

$$\frac{dx}{d\theta}\sin\varphi + x\cos\varphi\frac{d\varphi}{d\theta} - \frac{dy}{d\theta}\cos\varphi + y\sin\varphi\frac{d\varphi}{d\theta} = a\cos(\varphi-\theta)\left(\frac{d\varphi}{d\theta}-1\right).$$

This equation is rewritten as

$$\frac{dx}{d\theta}\sin\varphi - \frac{dy}{d\theta}\cos\varphi + \frac{d\varphi}{d\theta}(x\cos\varphi + y\sin\varphi) = a\cos(\varphi-\theta)\left(\frac{d\varphi}{d\theta}-1\right).$$

From Eq. (2.36), the last term on the left-hand side (in the bracket) is $a\cos(\varphi-\theta) - \rho$. Then, we have

$$\frac{dx}{d\theta}\sin\varphi - \frac{dy}{d\theta}\cos\varphi + a\cos(\varphi-\theta)\frac{d\varphi}{d\theta} - \rho\frac{d\varphi}{d\theta} = a\cos(\varphi-\theta)\frac{d\varphi}{d\theta} - a\cos(\varphi-\theta),$$

or

$$\frac{dx}{d\theta}\sin\varphi - \frac{dy}{d\theta}\cos\varphi - \rho\frac{d\varphi}{d\theta} = -a\cos(\varphi-\theta). \tag{2.37}$$

From the definition of φ, one sees

$$\frac{dy}{dx} = \tan\varphi.$$

Also, since the chaser moves by a distance of $s = na\theta$ to reach the present position at (x, y), and

$$\frac{dx}{ds} = \cos\varphi,$$

then

$$ds = \frac{dx}{\cos\varphi} = nad\theta,$$

and so

$$\frac{dx}{d\theta} = na\cos\varphi. \tag{2.38}$$

The chain rule of calculus gives

$$\frac{dy}{d\theta} = \frac{dy}{dx}\cdot\frac{dx}{d\theta} = \tan\varphi na\cos\varphi,$$

or

$$\frac{dy}{d\theta} = na\sin\varphi. \tag{2.39}$$

Thus, Eq. (2.37) is rewritten by inserting Eqs. (2.38) and (2.39) as

$$na\cos\varphi\sin\varphi - na\sin\varphi\cos\varphi - \rho\frac{d\varphi}{d\theta} = -a\cos(\varphi-\theta),$$

or

$$\rho\frac{d\varphi}{d\theta} = a\cos(\varphi-\theta). \tag{2.40}$$

This equation is one of the differential equations to explain the movements of the chaser.

Another equation is also obtained as follows. By differentiating Eq. (2.36) with respect to θ, one gets

$$\frac{dx}{d\theta}\cos\varphi - x\sin\varphi\frac{d\varphi}{d\theta} + \frac{dy}{d\theta}\sin\varphi + y\cos\varphi\frac{d\varphi}{d\theta} = -a\sin(\varphi-\theta)\left(\frac{d\varphi}{d\theta}-1\right) - \frac{d\rho}{d\theta}.$$

This equation is rewritten as

$$\frac{dx}{d\theta}\cos\varphi + \frac{dy}{d\theta}\sin\varphi - \frac{d\varphi}{d\theta}(x\sin\varphi - y\cos\varphi) = -a\sin(\varphi-\theta)\left(\frac{d\varphi}{d\theta}-1\right) - \frac{d\rho}{d\theta}.$$

From Eq. (2.35), the last term on the left-hand side (in the bracket) is $a\sin(\varphi-\theta)$, and we have

$$\frac{dx}{d\theta}\cos\varphi + \frac{dy}{d\theta}\sin\varphi - a\sin(\varphi-\theta)\frac{d\varphi}{d\theta} = -a\sin(\varphi-\theta)\frac{d\varphi}{d\theta} + a\sin(\varphi-\theta) - \frac{d\rho}{d\theta},$$

or

$$\frac{dx}{d\theta}\cos\varphi + \frac{dy}{d\theta}\sin\varphi = a\sin(\varphi-\theta) - \frac{d\rho}{d\theta}. \tag{2.41}$$

Thus, Eq. (2.41) is rewritten by inserting Eqs. (2.38) and (2.39) as

$$na = a\sin(\varphi-\theta) - \frac{d\rho}{d\theta},$$

or

$$\frac{d\rho}{d\theta} = a\left[\sin(\varphi-\theta) - n\right]. \tag{2.42}$$

To sum up, the following set of differential equations is obtained by differentiating Eqs. (2.35) and (2.36) with respect to θ:

$$\rho\frac{d\varphi}{d\theta} = a\cos(\varphi-\theta), \tag{2.43}$$

$$\frac{d\rho}{d\theta} = a\left[\sin(\varphi-\theta) - n\right]. \tag{2.44}$$

It is not possible to solve these equations analytically. However, we are still able to give some insights into the nature of the chaser's trajectory. By introducing a variable $\omega = \varphi - \theta$, we have $d\omega/dt = d\varphi/dt - 1$. Here, we assume $\theta = t$ because the target moves on the circular path at a constant speed. Then, Eq. (2.43) becomes

$$\rho\frac{d\omega}{dt} + \rho = a\cos\omega. \tag{2.45}$$

Also, Eq. (2.44) is written as

$$\frac{d\rho}{dt} = a\sin\omega - an. \tag{2.46}$$

Differentiating Eq. (2.46) with respect to t, we have

$$\frac{d^2\rho}{dt^2} = a\cos\omega\frac{d\omega}{dt},$$

or

$$\frac{d\omega}{dt} = \frac{d^2\rho/dt^2}{a\cos\omega}.$$

By substituting it into Eq. (2.45), we obtain

$$\rho\frac{d^2\rho}{dt^2} + a\rho\cos\omega = a^2\cos^2\omega. \tag{2.47}$$

This equation suggests that in a steady-state solution which satisfies

$$\frac{d\rho}{dt} = \frac{d^2\rho}{dt^2} = 0,$$

the chaser also moves on a circular path (see Fig. 2.6), so that the chord between the chaser and the target rotates but its length ρ is a constant, where

$$\rho = a\cos\omega.$$

At the steady state, one also gets $n = \sin\omega$ from Eq. (2.46). Then,

$$\rho = a\sqrt{1-n^2}. \tag{2.48}$$

Writing the radius of the circular path of the chaser by R, the Pythagorean theorem says

$$R^2 + \rho^2 = a^2.$$

Then,

$$R = \sqrt{a^2 - \rho^2} = \sqrt{a^2 - a^2(1-n^2)} = \sqrt{a^2 n^2} = na.$$

Hence, when $n \leq 1$, the chaser cannot catch up with the target, and that the chaser's pursuit curve eventually becomes a circle with the radius $R = na$.

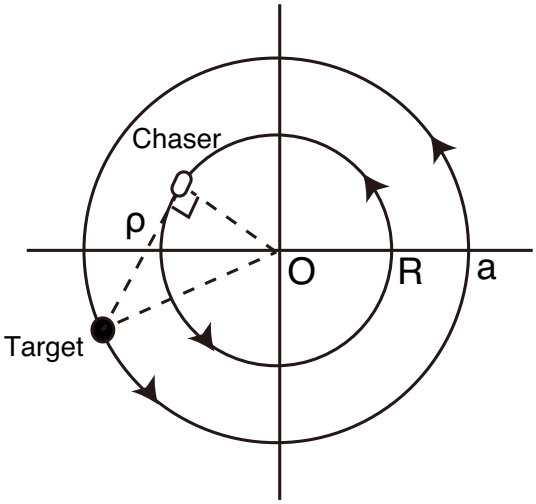

Fig. 2.6 In the steady state $d\rho/dt = 0$ and $d^2\rho/dt^2 = 0$, the chord joining the chaser and the target rotates, but its length (ρ) remains unchanged.

2.3.2 Extension to Three-Dimensional Space

In considering general problems of chases and escapes in three-dimensional space, the following approach can be taken by extending the method described for two-dimensional space in the previous section. Here, we denote the position of the target by (X,Y,Z) and that of the chaser by (x,y,z). The ratio of the speeds between the two is given by $n = v_T/v_C$. We derive the set of equations by the condition that the chaser always points its velocity vector to the position of the target.

In the same manner as for Eqs. (2.3) and (2.4), one writes

$$(X,Y,Z) = (x+\lambda\dot{x}, y+\lambda\dot{y}, z+\lambda\dot{z}), \tag{2.49}$$

$$\dot{X}^2+\dot{Y}^2+\dot{Y}^2 = n^2(\dot{x}^2+\dot{y}^2+\dot{z}^2). \tag{2.50}$$

The problem is to obtain the solution for the four functions, $x(t), y(t), z(t), \lambda(t)$, from the four first-order non-linear differential equations, given $X(t), Y(t), Z(t)$, and n. We have assumed that the chasers and the targets are both moving, respectively, with constant speeds, but this condition can be relaxed as long as the ratio n remains constant.

Because the set of the differential equations is nonlinear, it is generally difficult to obtain solutions. Here, we will present only a few special solutions for the setups explained below without showing derivations in detail. The interested readers may refer to the paper by Barton and Eliezer [5] for their derivations and other solutions.

2.3.2.1 Circular Cylindrical Helices

The first example is where the target moves in a circular cylindrical helix of constant pitch, a straightforward extension of the two-dimensional circular chases and escapes in section 2.3.1. The derivation of the path is somehow in the reverse direction because we first specify the path of the chaser. Let us consider the case where the chaser is moving in a circular cylindrical helix of equal pitch, which is represented by the following equation with a constant pitch p:

$$x = \cos t, \quad y = \sin t, \quad z = \left(\frac{p}{2\pi}\right)t. \tag{2.51}$$

Then, from Eq. (2.49), the target is at the location given below:

$$X = \cos t - \lambda \sin t, \quad Y = \sin t + \lambda \cos t, \quad Z = \left(\frac{p}{2\pi}\right)(t+\lambda). \tag{2.52}$$

If we assume that λ is a constant at this point and introduce a new parameter α by

$$\cos\alpha = \frac{1}{\sqrt{1+\lambda^2}}, \tag{2.53}$$

one can show that the position of the target (2.52) is rewritten as

$$X = \sqrt{1+\lambda^2}\cos(t+\alpha), \quad Y = \sqrt{1+\lambda^2}\sin(t+\alpha), \quad Z = \left(\frac{p}{2\pi}\right)(t+\lambda). \quad (2.54)$$

This expression represents that the path of the target is a circular cylindrical helix with the radius of $\sqrt{1+\lambda^2}$ and the pitch p. For these paths, it can be further shown that $n = v_T/v_C > 1$ and that the distance between the chaser and the target is a constant $\lambda\sqrt{1+p^2/4\pi^2}$. This indicates that the distance between the two does not change when the chaser moves slower than the target. Projecting the motions onto the two-dimensional $x-y$ plane corresponds to the long-time limit case of the circular chase and escape in section 2.3.1. One example of paths of the chaser and the target is shown in Fig. 2.7.

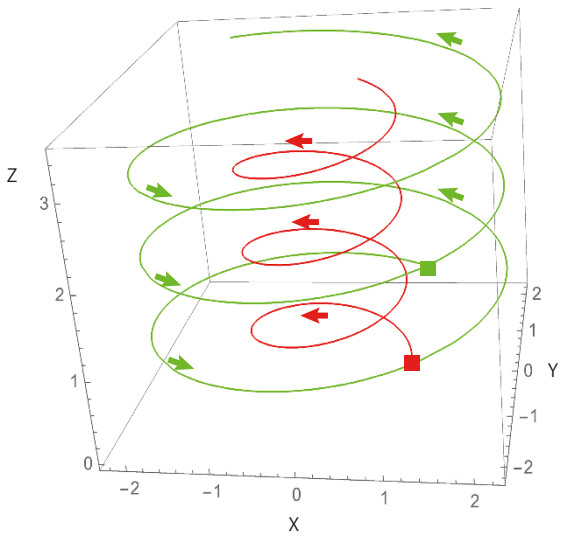

Fig. 2.7 Circular chase and escape in three-dimensional space: The red helix represents the path of the chaser starting from the point $(1,0,0)$, while the green one represents the path of the target starting from $(1,2,1/\pi)$. The parameters are $p = 1.0$ and $\lambda = 2.0$. The green and red arrows, respectively, indicate the directions of the motion of the target and the chaser along the paths.

2.3.2.2 Equiangular Spiral Helix

The second example is a spiral. The positions of the chaser and the target are, respectively, given by the following equations:

$$x = e^{-t}\cos t, \quad y = e^{-t}\sin t, \quad z = Bt, \quad (2.55)$$

and

$$X = e^{-t}\cos(t+\pi/2), \quad Y = e^{-t}\sin(t+\pi/2), \quad Z = B(t+1), \tag{2.56}$$

where B is a parameter. One example is shown in Fig. 2.8. At $t = 0$, the chaser starts at $(1,0,0)$, while the target starts at $(0,1,B)$ (both starting points are located outside the space in Fig. 2.8).

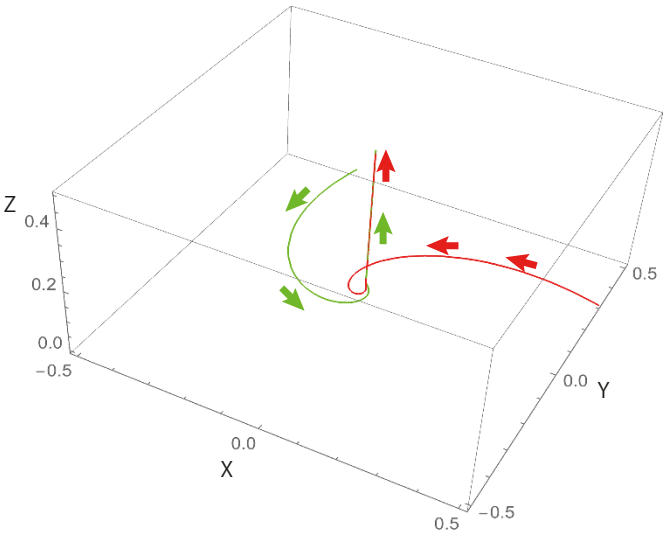

Fig. 2.8 Circular chase and escape with equiangular spiral helix in three-dimensional space: The red helix represents the path of the chaser starting from $(1,0,0)$, while the green one represents the path of the target starting from $(0,1,B)$. The parameter B is set as $B = 0.2$.

Here, we assume that the chaser and the target move at an equal constant speed ($n = 1$). As time progresses, the paths of both the chaser and the target appear as if they climb up and wind around the z axis. The distance D between the chaser and the target is greater than B, and approaches B in the limit of infinitely long time, i.e., the chaser cannot catch up with the target.

If we set $B = 0$, the motions of the chaser and the target are restricted to the two-dimensional plane as shown in Fig. 2.9. In this case, both of them fall into the origin in the long-time limit.

We can also consider another kind of spiral. For example, the following equations represent the spirals for both moving toward the origin:

$$x = e^{-t}\cos t, \quad y = e^{-t}\sin t, \quad z = Be^{-2t}, \tag{2.57}$$

$$X = e^{-t}\cos(t+\pi/2), \quad Y = e^{-t}\sin(t+\pi/2), \quad Z = -Be^{-2t}. \tag{2.58}$$

In this example, the chaser starts at $(1,0,B)$ to move downwards to the origin, and the target starts at $(0,1,-B)$ to move upwards to the origin. Typical paths are

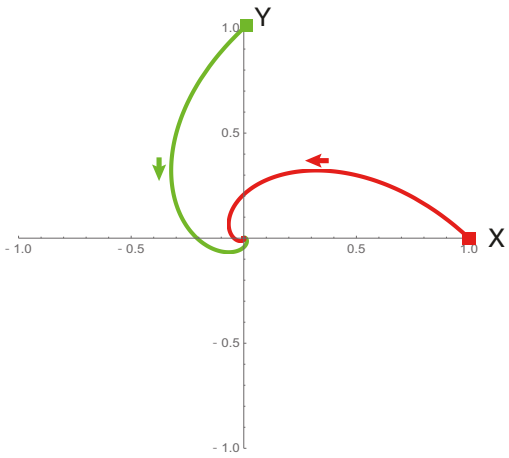

Fig. 2.9 Circular chase and escape with equiangular spiral helix to be projected onto the two-dimensional plane by fixing $B = 0$: The red helix represents the path of the chaser, while the green one represents the path of the target. The green and red arrows, respectively, indicate the directions of the motion of the target and the chaser along the paths.

shown in Fig. 2.10. We note that, by fixing $B = 0$, this example also reduces to the two-dimensional motions as described in Fig. 2.9.

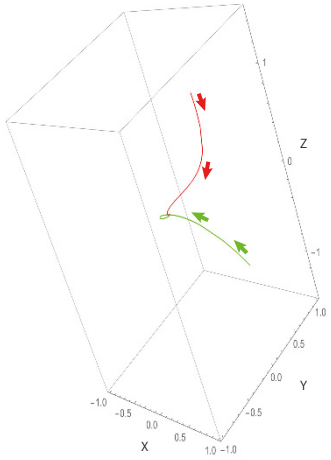

Fig. 2.10 Circular chase and escape with equiangular spiral-helix in three-dimensional space: The red helix represents the path for the chaser starting from $(1, 0, B)$, while the green one represents the path for the target starting from $(0, 1, -B)$. The parameter B is fixed as $B = 1.3$. The green and red arrows, respectively, indicate the directions of the motion of the target and the chaser along the paths.

Chapter 3
Collective Motion

3.1 Introduction

In everyday life, we observe various kinds of collective behavior [80], for example, in flocks of birds [12, 36], schools of fish [68], herds of animals [31], colonies of insects [19], and also in crowds of humans [38] and car traffic [39]. It also appears at microscopic scales such as colonies of bacteria [100], molecular motors [89], and also in artificial particles and robots [98]. They often exhibit eye-catching elegant ordered movements at various scales. Of particular interest is that such behavior emerges spontaneously, i.e., apparently in the absence of leaders or rulers, or any pre-established hierarchical structures.

Over the past few decades, an increasing number of attempts have been made to observe and describe flocking. Based on numerous observations, a tendency to adopt the direction of motion of the neighbors is the main reason for ordered motion, and apparently, very similar behavior can occur in different systems. This convinces the community of physicists to try to understand them as universal behavior in a system composed of a large number of "self-propelled" agents, and naturally leads to the idea of applying methods of statistical physics to the description of the collective behavior of organisms.

One of the main goals of the recent research trends, still to be achieved though, is to establish a systematic classification of the types, or the universality, of collective motion applicable to all, from collections of molecules to groups of humans. Meanwhile, flocking has been attracting biologists to answer why they come together, and what the advantages are to their functions. The main, commonly assumed advantages of flocking are: 1) defense against predators, 2) more efficient exploration for resources or hunting, and 3) improved decision making in larger groups.

Since the late 1980s, computer scientists have also recognized the power of unity from algorithmic viewpoints. The collective behavior of decentralized, self-organized systems is called swarm intelligence [8, 22]. The main advantage of collective behavior is efficiency for optimization; examples include stochastic diffusion searching [6], ant colonies [22] and particle swarm optimization [52].

© Springer Nature Singapore Pte Ltd. 2019

A. Kamimura and T. Ohira, *Group Chase and Escape,*
Theoretical Biology, https://doi.org/10.1007/978-981-15-1731-0_3

In this chapter, we briefly introduce concepts of statistical mechanics to explain phase transition in equilibrium systems. We then introduce two theoretical models to explain flocking and traffic jams as a phase transition in non-equilibrium systems.

3.2 Brief Introduction of Statistical Mechanical Approach

3.2.1 Phase Transition

The term phase transition is most commonly used to describe transitions between solid, liquid and gaseous states of matter. Water, the most familiar matter in our lives, has three states, solid (ice), liquid (water) and gas (vapor). We know that they are all composed of the same molecules, H_2O, but it is amazing to have the states of the different macroscopic characters only by changing temperatures. In addition, the transitions between the states have extremely clear and precise regularity. Under the pressure of one atmosphere, by gradually increasing temperature, ice transition to water precisely at 0 °C, and, as one increases it further, another transition occurs at 100 °C from water to vapor.

Even though physical properties of water, such as density and viscosity, change between the temperatures 0 and 100 °C, the states between them are rather quantitative and can be changed without the macroscopically obvious qualitative differences of water. Therefore, it is reasonable to characterize, as a "phase", the collection of states between which the properties of the system are changed without the qualitative differences.

One may naively expect that the qualitative difference between phases is due to a qualitative change in each molecule of H_2O. For example, one may imagine that the structure or interaction rules of the molecules sharply change at the temperature and, consequently, result in the macroscopic character of water. However, based on statistical mechanics, temperature is just a parameter for microscopic molecules to determine the "average" of thermal noises, and the energetic character is, actually, fluctuating between molecules. Therefore, it is impossible for the molecules to change the structure or interaction rules discontinuously at a specific temperature.

The qualitative differences at phase transitions are not due to qualitative change of the microscopic rules. Even if the microscopic rules do not change, the qualitative differences occur when the degree of freedoms (molecules) is sufficiently large in the system. In other words, the phase transition is a kind of cooperative phenomenon so that the origins cannot be reduced to characteristics of each component.

3.2.2 Order Parameters and Symmetry

In a general sense, a phase transition is a process during which a system undergoes a transition from one phase to another as a function of one or more external parameters (e.g. temperature, pressure etc.). More specifically, phase transitions are defined by the change of one or more specific variables called order parameters. The order parameters measure the degree of order across the boundaries between phases. The name "order" comes from the observations that a phase transition often (but not necessarily) involves a symmetry-breaking process. For example, the cooling of a fluid into a crystalline solid breaks continuous translation symmetry: each spatial point in the fluid has the same properties, but each spatial point in a crystal does not unless the points are chosen from the lattice points of the crystal lattices. Typically, the high-temperature phase contains more symmetries than the low-temperature phase due to spontaneous symmetry breaking. Mathematically speaking, the value of the order parameter is usually zero in a high-temperature disordered phase and non-zero in a low-temperature ordered phase.

In the case of collective motion, the commonly adopted order parameter is the average normalized velocity ϕ,

$$\phi = \frac{1}{Nv_0} \left| \sum_{i=1}^{N} \mathbf{v}_i \right|, \tag{3.1}$$

where N is the total number, and v_0 is the average absolute velocity of particles in the system. When the motion of particles is disordered, the velocities of the individual particles are in random directions; then, the average in Eq. (3.1) gives a small magnitude of the vector. On the other hand, if the motion of particles is ordered and the velocities of the particles are in parallel to a specific direction, the average gives a vector of absolute velocity close to Nv_0; therefore, the order parameter ϕ is close to one. If the microscopic rules of particles' motion have rotational invariance (i.e., the dynamics of the system are isotropic), the transition from the random motions to the parallel motion in a specific direction corresponds to a breaking of the rotational symmetry.

If the order parameter changes discontinuously from one phase to another, we refer to this kind of phase transition as a first-order transition. On the other hand, if the order parameter changes continuously but its derivative is discontinuous, the phase transition is referred to a second-order (continuous) transition.

3.2.3 Critical Exponent

Following conventional definitions in statistical mechanics, the behavior of a system near second-order transition is often referred to as critical phenomena. Near the critical point at which phase transition occurs, the behavior of physical quantities to describe the system such as pressure, density, and heat capacity are characterized by

critical exponents. The behavior of the physical quantity Φ asymptotically follows a power law as $\Phi \approx |T - T_c|^{\nu}$ $(T \to T_c)$, where T_c is the value at the critical point of the controlled parameter T, and ν is the critical exponent.

The most commonly known example is the transition at the Curie temperature between ferro- and paramagnetic materials. Above this temperature, some materials lose their permanent magnetic (ferromagnetic) properties, to be replaced by induced magnetism (paramagnetism). At this point, the behavior follows for heat capacity $C_H(T) \approx |\varepsilon|^{\alpha}$, magnetization $M \approx |\varepsilon|^{\beta}$, and susceptibility $\xi \approx |\varepsilon|^{\gamma}$ where $\varepsilon = \frac{T - T_c}{T_c}$. Interestingly, the values of the critical exponents depend only on a few factors such as spatial dimensions, symmetry of the system and interaction ranges, and the other details in the system do not matter. Therefore, different systems sharing the essential factors exhibit identical behavior of the critical exponent, and such a collection of systems is referred to as belonging to the same universality class.

Another surprising observation is that these critical exponents are related to each other and expressions called scaling laws can be formulated, such as $\alpha + 2\beta + \gamma = 2$.

3.2.4 Spin Models

One of the most basic models to study the phase transition is the Ising model for ferromagnetism. The model consists of discrete variables that represent magnetic dipole moments of atomic spins, and they are in one of two states ($+1$ or -1) [Fig. 3.1(A)]. The spins are arranged in a lattice and each interacts with its neighbors and with an external magnetic field. The two-dimensional square-lattice Ising model is one of the simplest statistical-mechanics models to show a phase transition.

In the absence of an external field, the state ($+1$ or -1) of each spin flips due to fluctuations at finite temperatures. At high temperature, the fluctuations are large so that the state of each spin is almost random, and changes frequently. On the other hand, at low temperature, the interaction between spins is relevant for determining the state of the spins. To quantitatively investigate this, energy is defined as the Hamilton function of the states of the spins on the grids as

$$H(\sigma) = -\sum_{\langle ij \rangle} J_{ij} \sigma_i \sigma_j,$$

where the sum is over pairs of adjacent spins. The notation $\langle ij \rangle$ denotes that the sites i and j are nearest neighbors, and σ_i and σ_j denote the states of the spins ($+1$ or -1), respectively. J_{ij} denotes the interaction energy between the spins at i and j, and, for ferromagnetic interactions, $J_{ij} = J > 0$ for all pairs. When the spins are in the same state $\sigma_i = \sigma_j = +1$ or -1, the interaction energy is $-J$, and, when they are in the opposite states, the energy is J.

In equilibrium states at temperature T, the probability to occupy a specific configuration σ is given by the Boltzmann distribution $\exp\{-\beta H(\sigma)\}/Z$, where $\beta = (k_B T)^{-1}$ and $Z = \sum_{\sigma} \exp\{-\beta H(\sigma)\}$. The probability to have a configuration

state with lower energy increases as T decreases. Because the interaction energy is lower when the spins are in the same state with the neighboring sites, the probability that the spins are in the same state ($+1$ or -1) increases as T decreases. Actually, the model undergoes a phase transition between an ordered and a disordered phase in two dimensions or more. In the ordered phase, the spins are aligned to be in the same state, $+1$ or -1. On the other hand, the spins are randomly in the states of $+1$ or -1 in the disordered phase.

The magnetization is generally considered as the order parameter, which is the average value of the spin $M = \frac{1}{N}\sum_{i=1}^{N}\sigma_i$. The magnetization has a non-zero value in the ordered phase, while it is zero in the disordered phase. The phase transition also accompanies a symmetry-breaking process: the discrete symmetry breaks between the spin configurations in which they are aligned to $+1$ or -1 states. The critical exponents of the ferromagnetic transition in the Ising model establish an important universality class in which a variety of different phase transitions share the same behavior near the critical point. For example, the critical exponents in the spatial dimension $d_S = 2$ are known as $\alpha = 0$, $\beta = 1/8$ and $\gamma = 7/4$; these satisfy the scaling law $\alpha + 2\beta + \gamma = 2$.

The XY model is also one of the basic models in statistical mechanics. In the model, the spin variable is a two-component unit-vector $\mathbf{s}_i = (s_i^x, s_i^y)$ [Fig. 3.1(B)]. Using the angle variable θ_i of the spin, the unit vector is also written as $\mathbf{s} = (\cos\theta_i, \sin\theta_i)$. The spins are arranged in a lattice and each interacts with its neighbors. In the Ising model, the spins are in either of up ($+1$) or down (-1) states. In the XY model, the spin can rotate in the plane of the lattice.

The energy of the XY model is defined as the Hamilton function of the states of the spins on the grids as

$$H(\sigma) = -J\sum_{\langle ij\rangle}\mathbf{s}_i\cdot\mathbf{s}_j = -J\sum_{\langle ij\rangle}\cos(\theta_i - \theta_j),$$

where the sum is over pairs of the nearest neighbors. The interaction energy is lower as the two spins are aligned, i.e., as θ_i is closer to θ_j. Even though the XY model shares the same trends with the Ising model in which the spins are aligned as temperature decreases, the two-dimensional XY model does not exhibit the phase transition in which the spontaneous magnetization has a non-zero value. More generally, it is proved as the Mermin–Wagner theorem that continuous symmetries cannot be spontaneously broken at finite temperature in systems with sufficiently short-range interactions in dimensions $d_S \leq 2$. The two-dimensional XY model does not exhibit the normal second-order phase transition; however, the model is known to exhibit a different kind of phase transition called the Kosterlitz-Thouless transition.

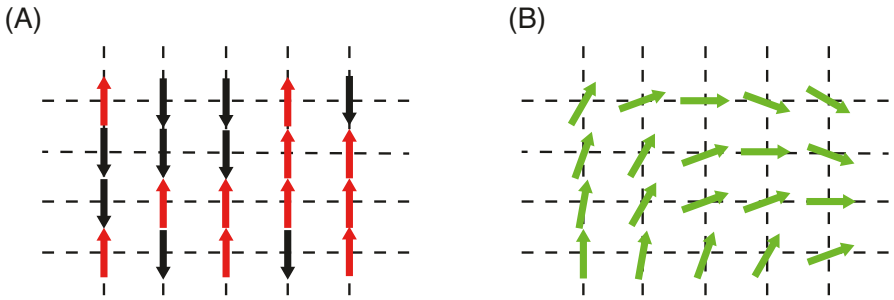

Fig. 3.1 Cartoon of the spin models. (A) Ising model: the spins on each grid of the square lattice are in one of two states ($+1$ or -1), denoted by up and down arrows, respectively. (B) XY model: the state of the spins is written as $\mathbf{s}_i = (\cos\theta_i, \sin\theta_i)$.

3.3 Collective Motion as Phase Transitions in Non-equilibrium Systems

Phase transitions can occur in both equilibrium and non-equilibrium systems. In contrast to phase transitions of the materials composed of atoms and molecules, collective motion is a truly non-equilibrium phenomenon. On one hand, there are possible analogies with the equilibrium phenomena, and the language and the characterizations of the various aspects in equilibrium phase transitions are still suitable for understanding and interpreting observed non-equilibrium phenomena in collective motions.

On the other hand, there are some specific features of collective motion such as giant number fluctuations and jamming, which obviously do not occur in systems at equilibrium.

3.4 Vicsek Model

Among the number of models that have been proposed and developed to explain collective motion from a microscopic description, the most commonly known and well-studied one is referred to as the Vicsek model [99]. The Vicsek model has attracted broad interest from wider audiences and is considered as one of the standard models in the field of collective motions. Several variants are proposed based on the original model.

One of the first widely known flocking models was made by Reynolds, and the primary motivation was to produce a visual appearance of coherently flying objects similar to birds in computer animation: he called the objects “boids” [84]. The boids move along trajectories determined by three basic steering rules: (a) separation, (b) alignment, and (c) cohesion. Each object interacts only with its neighboring objects

within a certain distance (local flock-mates). In separation, each tries to separate itself in order to avoid crowding local flock-mates and collisions. The alignment rule keeps each object steering its direction towards the average heading direction of its surrounding flock-mates. The third rule, cohesion, moves each toward the average position of local flock-mates, to keep them together.

In order to give a quantitative interpretation of the behavior of flocking, the Vicsek model was introduced based on a statistical-physics-type approach and mathematical refinement of the computer model for flocking simulations. The model describes the overdamped dynamics of a collection of N self-propelled particles characterized by their off-lattice position $\mathbf{x}_i(t)(i = 1,...,N)$ at time t. In the model, all particles move with a fixed speed of v_0, and are allowed to change the direction of their velocity vectors. Reflecting the alignment rule, each particle tries to align its direction with the average direction of its neighbors within a given interaction distance of R.

The velocity $\mathbf{v}_i$ of the i-th particle is given by

$$\mathbf{v}_i(t+1) = v_0 \frac{\langle \mathbf{v}(t) \rangle_R^i}{|\langle \mathbf{v}(t) \rangle_R^i|} + fluctuation, \tag{3.2}$$

where $\langle \mathbf{v}(\mathbf{t}) \rangle_R^i$ is the average velocity of particles within a circle of radius R centered at the i-th particle.

The speed of particles is constant and the velocity is updated by changing the direction based on the average velocity and fluctuations. The fluctuation is introduced in the angle $\langle \theta^i \rangle$ of the average velocity over the surroundings to update the orientation angle θ_i. The dynamics of the angle are given by

$$\theta_i(t+1) = \langle \theta^i \rangle(t) + \xi(t), \tag{3.3}$$

where $\xi(t)$ is the random number taken from a uniform distribution in the interval of $[-\eta\pi, \eta\pi]$. Hence, the parameter η represents the strength of fluctuations. Finally, the position of the particle is updated as

$$\mathbf{x}_i(t+1) = \mathbf{x}_i(t) + \mathbf{v}_i(t+1). \tag{3.4}$$

The only parameters of the model are the density ρ (the number of particles in a volume R^{d_S}, where d_S is the dimension), the velocity v_0 and the level of fluctuations η.

Even though it is simple, the Vicsek model exhibits a rich variety of collective motion patterns, by varying the parameters and initial conditions. Of particular interest is that the model displays phase transition from a disordered to an ordered (particles moving in parallel) state as we change fluctuation strength parameter η. The dynamics of the model are isotropic in space so that no preferred direction is given a priori. However, when the alignment term is stronger than the noise effect, the particles collectively develop global orientation: particles move in a specific direction. For order parameter ϕ, the normalized average velocity is typically suitable $\phi = \frac{1}{Nv_0} |\sum_{i=1}^{N} \mathbf{v}_i|$, and schematic behavior of the order parameter versus the noise

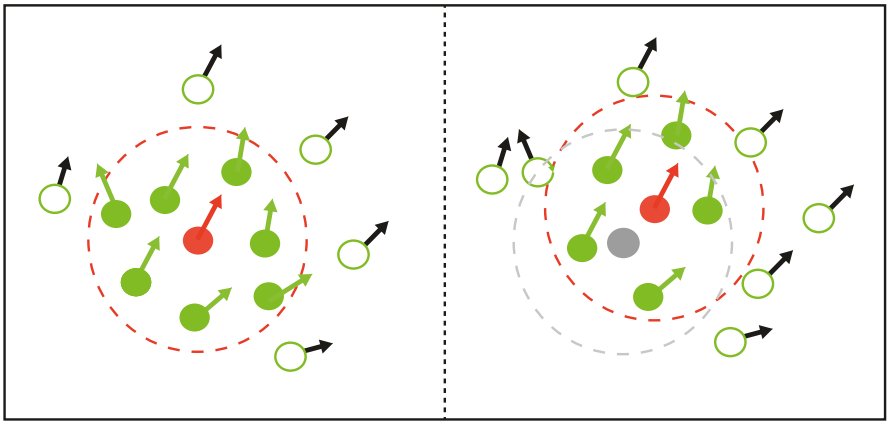

Fig. 3.2 Cartoon of the Vicsek model. The velocity of i-th particle (indicated by the red circle) is given by the average velocity of particles (green filled circles) within a circle of radius R (red dashed circle) and fluctuations. In the next time step, the particles contributing to the average velocity can change.

strength η is shown in Fig. 3.3. At low noise levels, the particles collectively move in a specific direction and ϕ is close to unity in the ordered phase. On the other hand, at high noise levels, the particles move in random directions and ϕ is close to zero in the disordered phase.

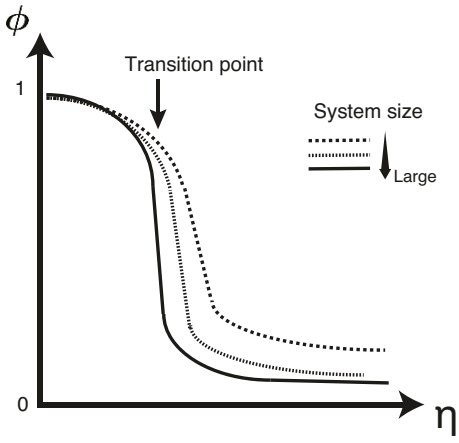

Fig. 3.3 Schematic behavior of the order parameter ϕ as a function of the strength of fluctuations η. As the noise strength η decreases, the order parameter transitions to increasing. As the system size increases with fixed density, the transition points become sharp.

In the original paper, a second-order transition from disordered to ordered phase was shown to exist. In particular, in the thermodynamic limit, the model was argued to exhibit a phase transition analogous to the continuous ones in equilibrium systems as $\phi \approx [\eta_c(\rho) - \eta]^\beta$ and $\phi \approx [\rho - \rho_c(\eta)]^\delta$, which defines the behavior of the order parameter ϕ at the critical point, as in the case of a standard second-order transition, β and δ are the critical exponents, η is the noise strength, ρ is the particle density. $\eta_c(\rho)$ and $\rho_c(\eta)$ are the critical noise and density, respectively in the limit of infinite system size. The continuous nature of the transition has been a matter of some debate. In fact, the type of the phase transition depends on the way in which the noise is introduced into the system. The original model is so-called angular-noise type in which the noise perturbs the final angle as in Eq. (3.3), exhibiting the continuous one. On the other hand, when the noise perturbs velocity of the individual particles before averaging, the model produces discontinuous first-order phase transitions.

One interesting property in the Vicsek model is its ability to exhibit the long-range order in two-dimensional space. According to the Mermin–Wagner theorem, continuous symmetries cannot be spontaneously broken at finite temperature with sufficiently short-range interactions in dimensions $d_S \leq 2$. In fact, the two-dimensional XY model does not exhibit long-range order at finite temperatures. The contradiction could naturally occur because the Vicsek model does not satisfy the conditions required by the theorem to apply. The following properties of the model are probably, but not surely, origins of the long-range order: 1) the system is in non-equilibrium (e.g. particle interactions do not conserve momentum), 2) particles move and originate effective long-range interactions (flocks merge and dismember, carrying information across the system), 3) the system is not translationally invariant (particle positions are distributed inhomogeneously in space).

Another intriguing property of the model is giant number fluctuations. The number of particles in a fixed area of the system fluctuates over time because the particles are moving around in the system. The extent of the fluctuations is typically characterized by the average number of particles $\langle n \rangle$ and the standard deviation $\Delta n = \sqrt{\langle (n - \langle n \rangle)^2 \rangle}$. As the average number of particles increases in the area, the standard deviation also increases. In equilibrium systems, the relationship is generally written as $\Delta n \propto \langle n \rangle^\alpha$ with $\alpha = 0.5$. In the ordered phase of the Vicsek model, the standard deviation increases faster ($\alpha \approx 0.8$) than the equilibrium relationship, that is, inhomogeneity of spatial distribution is more giant, and dense and sparse areas of the particles are more defined.

3.5 Optimal Velocity Model

3.5.1 One Dimension

We introduce here another theoretical model, namely the Optimal Velocity model, to describe traffic jams on motorways [4]. Studies from engineering, mathematics, op-

eration research, and physics have suggested a great variety of models from different modeling approaches (see [39] and references therein for reviews). Among various models for traffic jams, the model introduced here assumes agent-based modelings in continuous space, in which each agent (vehicle) follows simple rules of motion to form collective behaviors. In this sense, the spirit of the model is similar to that of the Vicsek model [99].

The main principle of the model is to assume that each vehicle has an optimal velocity as a function of the distance between the vehicle and that is running immediately ahead of it. It models a natural response of a driver of the vehicle: he/she accelerates the vehicle to shorten the distance if it is too large, and decelerates it if it is too small.

3.5.1.1 Model

Here, we consider N vehicles, and they are running in a traffic lane of length L with a periodic boundary condition (see Fig. 3.4). The dynamics of the i-th vehicle ($i = 1, 2, ...N$) are governed by the following differential equations:

$$\frac{dx_i}{dt} = v_i, \tag{3.5}$$

$$\frac{dv_i}{dt} = a\{V(x_{i+1} - x_i) - v_i\}, \tag{3.6}$$

where x_i and v_i denote the position and the velocity of the i-th vehicle. The model introduces an optimal velocity $V(\Delta X)$ as a function of the distance $\Delta X = x_{i+1} - x_i$. Here, the $(i+1)$-th vehicle is running immediately ahead of the i-th vehicle.

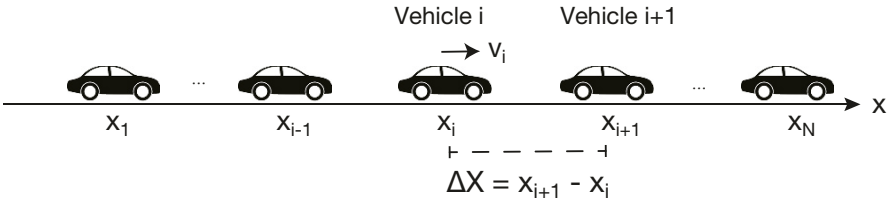

Fig. 3.4 Schematic figure of the one-dimensional optimum velocity model. N vehicles are running in a traffic lane of length L with a periodic boundary condition. The i-th vehicle at the position x_i with the velocity v_i is running immediately behind the $(i+1)$-th vehicle.

From the right-hand side of Eq. (3.6), the velocity v_i increases, i.e., the vehicle accelerates, if v_i is below the optimal velocity $V(\Delta X)$, and decreases if v_i is above the optimal. The parameter a ($a > 0$) is a constant denoting the timescale of the response of the driver: larger a indicates more rapid responses (acceleration or deceleration). We assume that the shape of the function $V(\Delta X)$ is as shown in Fig. 3.5:

it increases monotonically with ΔX for small ΔX, and is saturated at an upper limit for large ΔX. In the simulations below, we adopt $V(\Delta X) = \tanh(\Delta X - 2) + \tanh(2)$.

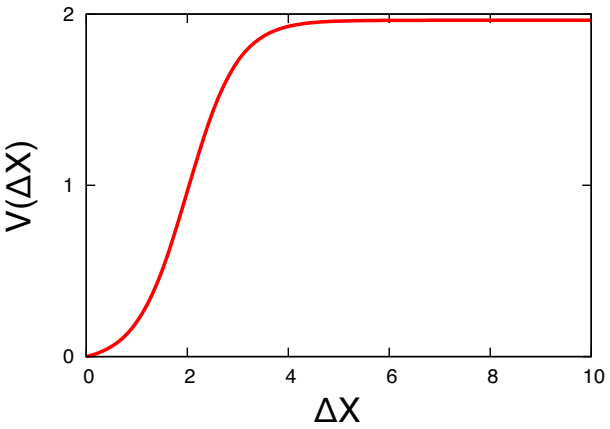

Fig. 3.5 Shape of the optimal function $V(\Delta X) = \tanh(\Delta X - 2) + \tanh(2)$.

3.5.1.2 Stability in Linearized Theory

The model has two free parameters, the density of the vehicles, $\rho = N/L$, and the timescale of the responses a.

Equation (3.6) has a uniform solution written as

$$x_n^{(0)}(t) = \bar{b}n + V(\bar{b})t \tag{3.7}$$

where $\bar{b} = L/N$. We call this solution the "uniform flow" without congestion, in which vehicles are uniformly distributed with identical spacing $\bar{b}$, and run with the same velocity $V(\bar{b})$.

Let us investigate the stability of the solution by linearizing equations (3.5) and (3.6). Let y_i be a small deviation from the solution $x_n^{(0)}$,

$$x_n = x_n^{(0)} + y_n, \qquad |y_n| \ll 1. \tag{3.8}$$

By neglecting higher orders of y_n, the linearized equation is obtained as

$$\frac{d^2 y_n}{dt^2} = a\left\{V'(\bar{b})\,(y_{n+1} - y_n) - \frac{dy_n}{dt}\right\}. \tag{3.9}$$

The solution of this equation is obtained by expanding the Fourier series with $e^{i\alpha_k n}$ as

$$y_n = \sum_k A_k \exp\left(i\alpha_k n + zt\right), \tag{3.10}$$

$$\alpha_k = \frac{2\pi}{N}k \qquad (k = 0, 1, 2, ..., N-1), \tag{3.11}$$

where z satisfies

$$z^2 + az + aV'(\bar{b}) = aV'(\bar{b})e^{i\alpha_k}. \tag{3.12}$$

Each α_k corresponds to each eigenmode, and for a given $V'(\bar{b})$, we have a complete set of the eigenmodes $\{\alpha_k\}$.

The "uniform flow" is unstable if the amplitude of an eigenmode grows with time, that is, the real part of z is positive. On the other hand, if the real part is negative, the oscillation of the mode shrinks. Here we rewrite Eq. (3.12) as

$$\left(\frac{z}{a}\right)^2 + \frac{z}{a} + \frac{V'(\bar{b})}{a} = \frac{V'(\bar{b})}{a}e^{i\alpha_k}, \tag{3.13}$$

and assume that $z = a(u + iv)$. The solution for $u = 0$, i.e., $z = iav$ satisfies the condition

$$-v^2 + \frac{V'(\bar{b})}{a} + iv = \frac{V'(\bar{b})}{a}e^{i\alpha_k}. \tag{3.14}$$

The $(V'(b), \alpha)$ plane is separated into stable ($u < 0$) and unstable ($u > 0$) regions by the critical curve $u(V'(\bar{b}), \alpha) = 0$. From Eq. (3.14), the critical curve satisfies

$$V'(\bar{b}) = \frac{a}{2\cos^2\frac{\alpha}{2}}. \tag{3.15}$$

In order for the uniform flow to be stable, every u corresponding to the complete set of α_k should be negative. Both sides of Eq. (3.14) are shown in the polar coordinate plane Fig. 3.6 of $(V'(b), \alpha)$ for (i) $V'(\bar{b})/a = 1$ and (ii) $1/2$. Each solution for α_k is on the circle of radius $V'(\bar{b})/a$ in the plane, and the right region from the green curve corresponds to the $u > 0$ region. If the circle intersects with the green curve, then there exists at least one positive u solution, therefore, the flow is unstable. Thus, the flow is stable if $V'(\bar{b}) < \frac{a}{2}$ because $u < 0$ for all modes α_k, and unstable if $V'(\bar{b}) > \frac{a}{2}$ because at least one u mode can be positive.

From the linear stability analysis, one can show that the phase diagram is obtained as in Fig. 3.7. The uniform flow of the vehicles is unstable when $a < 2V'(\bar{b})$, where $\bar{b} = L/N$. Note that the stability is determined by the values of the sensitivity a of drivers and the derivative of the optimum velocity function $V(\bar{b})$.

In the stable region, each vehicle runs at equal interval $\bar{b} = L/N$ and its velocity is equal to the optimum velocity for the interval without congestion. However, with the parameters for the unstable region, small perturbations present in the system can grow and finally lead to congestion. The most notable prediction by this simple model is that the phenomena of "natural" traffic jam arise without any bottleneck such as inherent spatial inhomogeneities on the traffic lane.

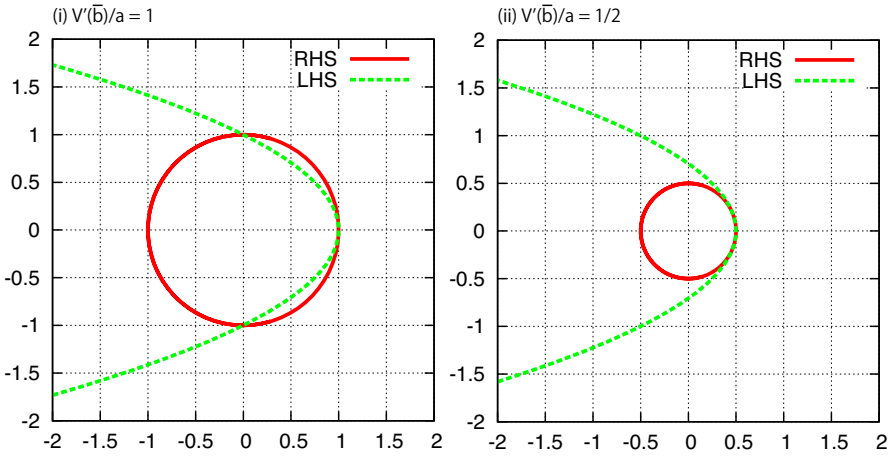

Fig. 3.6 The region of stability criteria in the $(V'(\bar{b}), \alpha)$ polar coordinate plane for (i) $V'(\bar{b}/a) = 1$ and (ii) $V'(\bar{b}/a) = 1/2$. The right- and left-hand sides of Eq. (3.14) are shown by red and green curves, respectively.

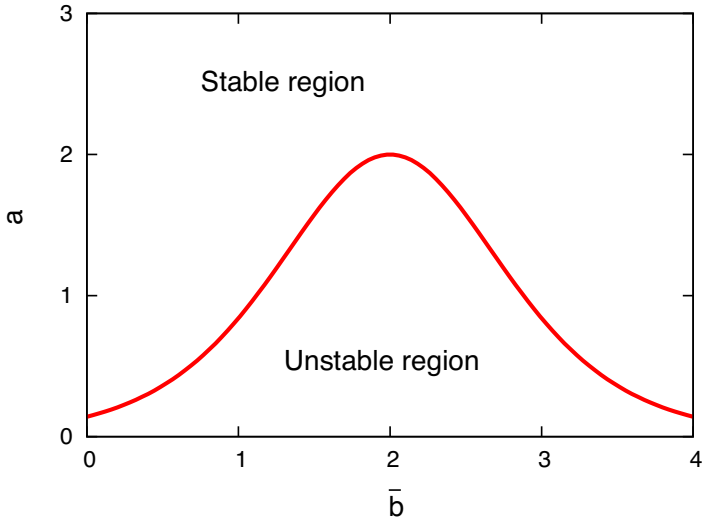

Fig. 3.7 Phase diagram for the stability of the flow. The uniform flow of the vehicles is unstable when $a < 2V'(\bar{b})$, and stable when $a > 2V'(\bar{b})$, where a is the sensitivity of the drivers, $\bar{b} = L/N$, and $V'(\bar{b})$ is the derivative of the optimum velocity function.

3.5.1.3 Numerical Simulations

In Fig. 3.8, we show the simulation results with parameters for unstable regions. Initially, each vehicle runs approximately uniformly. However, small perturbations introduced in the initial positions gradually destabilize the uniform flow and finally cause congestion. From the viewpoint of statistical physics, a phase transition occurs from free-moving phase to congestion phase as the density of vehicles ($N/L = 1/\bar{b}$) increases and passes through the certain value.

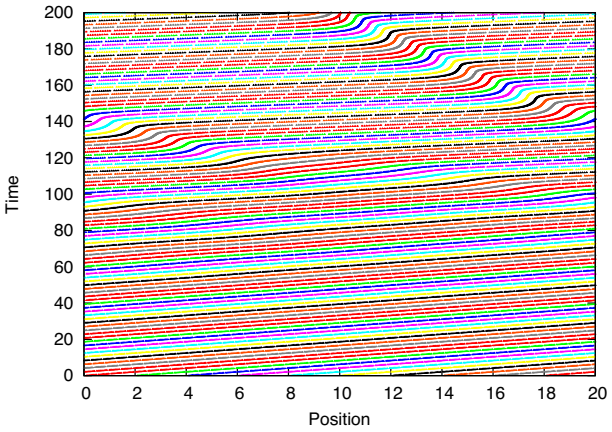

Fig. 3.8 Time evolution of the position in x of each vehicle. Different vehicles are denoted by different colors. Parameters are $N = 10$, $L = 20$, $a = 1$. Initially, each vehicle is located approximately at an equal interval $L/N = 2$ with small perturbations. The perturbation is introduced to each vehicle by randomly shifting between $[-0.01, 0.01]$ from the position at the equal interval.

This phase transition has also been confirmed by experiments in a circular lane [94], and further details including an indication of metastability and validity of the optimum velocity model have been investigated by a larger indoor circuit experiment in the Nagoya Dome [96].

3.5.2 Two Dimensions

The one-dimensional Optimal Velocity model was extended to the two-dimensional OV model [72, 73] to explain the collective motion of pedestrians and animals. For the collective motion of pedestrians, the study fits nicely into recent trends of describing the motion of pedestrians as if they are subject to "social forces", originally proposed by Helbing and Molnár [37]. In the approach, we consider each pedestrian as an agent, and each follows microscopic dynamics of motions which are determined by interactions between the agents. Similar to Newton's equation of

motion, the change of the motion of an agent is caused by forces acting on the agent. The forces are, however, not directly exerted by the pedestrians' environment, but they are a measure for the internal motivations of the individuals to perform certain actions (movements). Generally, the equation of motion for agent j ($j = 1, ..., N$) is written as

$$\frac{d\mathbf{v}_j(t)}{dt} = \frac{v_j^0 \mathbf{e}_j^0(t) - \mathbf{v}_j(t)}{\tau_j} + \sum_{i \neq j} \mathbf{f}_{ji}(t), \tag{3.16}$$

where the first and second terms on the right-hand side denote self-driven and external forces, respectively. In the self-driven terms, $\mathbf{e}_j^0$ denotes a unit vector in the desired direction the agent wants to move, v_j^0 is the optimum speed, and τ_j denotes a timescale in which the agent adjusts its velocity to the optimum velocity. The external forces in the second term denote interactions between agents j and i. Typically, the interactions are introduced as repulsive forces to model general tendencies to avoid collisions with the agent i and the boundaries of the system such as walls.

In the original work by Helbing and Molnár [37], the simple social force model demonstrates the self-organization of several observed collective effects of pedestrian behavior. They include the development of lanes in initially disordered pedestrian crowds with opposite walking directions, and oscillatory changes of the walking direction at narrow passages. In addition, a jammed state is observed in which the oppositely moving particles block each other.

The self-organization due to the collective effects of pedestrian behavior is also observed in the Optimal Velocity model by naturally extending the one-dimensional model to two-dimensions as we will explain below. The equation of motion for a particle with the index j is given by

$$\frac{d\mathbf{x}_j(t)}{dt} = \mathbf{v}_j(t), \tag{3.17}$$

$$\frac{d\mathbf{v}_j(t)}{dt} = a \left[\left\{ \mathbf{V}_0 + \sum_k \mathbf{F}(\mathbf{x}_k(t) - \mathbf{x}_j(t)) \right\} - \mathbf{v}_j(t) \right], \tag{3.18}$$

where $\mathbf{x}_j = (x_j, y_j)$ and $\mathbf{x}_k = (x_k, y_k)$ are the position of j-th and k-th particles, respectively. $\mathbf{V}_0$ is a constant vector to express "desired velocity": a particle moves with the desired velocity when there is only a single particle in the system. Equation (3.18) corresponds to Eq. (3.16) by replacing the sensitivity a with $1/\tau_j$, $\mathbf{V}_0$ with $v_j^0 \mathbf{e}_j^0(t)$, and the summation term of $\mathbf{F}$ with the interaction term of $\mathbf{f}_{ji}(t)$. The vector $\mathbf{F}$ indicates interactions between particles, and

$$\mathbf{F}(\mathbf{x}_k - \mathbf{x}_j) = f(r_{kj})(1 + \cos\phi)\mathbf{n}_{kj}, \tag{3.19}$$

$$f(r_{kj}) = \alpha \left[\tanh \beta (r_{kj} - b) + c \right], \tag{3.20}$$

where $r_{kj} = |\mathbf{x}_k - \mathbf{x}_j|$, $\cos\phi = \frac{\mathbf{V}_0 \cdot (\mathbf{x}_k - \mathbf{x}_j)}{|\mathbf{V}_0| r_{kj}}$ and $\mathbf{n}_{kj} = (\mathbf{x}_k - \mathbf{x}_j)/r_{kj}$. The strength of the interaction is determined by the distance r_{kj} between j-th and k-th particles and the

angle ϕ between $\mathbf{x}_k - \mathbf{x}_j$ and $\mathbf{V}_0$. Because of the term $(1+\cos\phi)$, a particle is more sensitive to particles in front than those behind.

Types of the interaction are controlled by the parameter c. For $c = -1$, the interaction is repulsive, $f < 0$. For $-1 < c < 1$, the interaction can be repulsive for short distance and attractive for long distance. Here, the model with only repulsive interactions can be applied to pedestrians and the model with repulsive and attractive interactions are applied to explaining the collective motion of animals.

For the repulsive interaction ($c = -1$), homogenous flow is a solution to the equations in which particles are moving in the desired direction by forming a triangular structure, and linear stability analysis can be done to obtain the phase diagram to see how unstable modes arise depending on the parameters [72].

Also, in the counter flow, the model exhibits a lane formation similar to that of pedestrian flow. When half the number of particles have the desired velocity in the opposite direction, clear lanes can be formed; a typical snapshot is shown in Fig. 3.9. The lane formation is stable probably for parameters with which the unidirectional flow is stable. When the distance between particles is smaller than the critical value above which the flow is stable, particles cannot move smoothly, and a blocking state emerges where their motion is prevented by other particles moving in the opposite direction (Fig. 3.10).

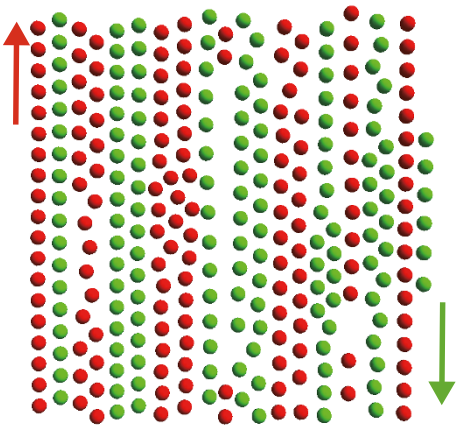

Fig. 3.9 Formation of lanes in the counter flow. Red and green particles prefer to move upward and downward, respectively. Parameters are $N = 300$, $L = 30$, $a = 2$, $b = 1.0$, $c = -1$, $\alpha = 0.25$, $\beta = 2.5$.

The effect of the attractive interaction on the stability has been also studied [73].

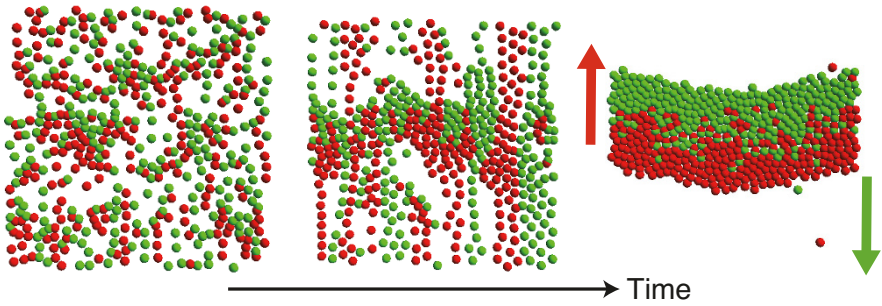

Fig. 3.10 Development of blocking state in the counter flow. Parameters are $N = 500$, $L = 30$, $a = 2$, $b = 1.0$, $c = -1$, $\alpha = 0.25$, $\beta = 2.5$.

Chapter 4
Group Chase and Escape

4.1 Introduction

We have combined the research fields of "Chases and Escapes" and "Collective Motion" described in the previous chapters to propose a concept of "Group Chase and Escape" [44] by investigating simple models.

One can view the concept as a natural extension of chases and escapes, which are typically investigated in one-to-one cases, to multiple players. On the other hand, the models we explain below also fit into a kind of collective motion with two groups of self-propelling particles whose aims (preferred movements) dynamically change with their opponents' positions [101]. It can be also viewed as an ideal simplification of phenomena such as hunting of a group of deer by a pack of wolves.

As the basic model, we first introduce in section 4.2 a simple rule for chasers and targets: each chaser prefers to get closer to the nearest target, while each target wants to get away from the nearest chaser. Even with this simple rule, mathematical analysis of group chase and escape is quite intricate and challenging. Instead, we adopt computational simulations to investigate the models.

In order to understand the nature of the model, we first calculate macroscopic quantities, i.e., the time to catch all the targets from initial conditions, and average lifetimes of targets. In particular, we see how the quantities depend on the number of chasers and/or initial targets in section 4.2.1. We found two qualitatively different regions for the time to catch all the targets as a function of the number of chasers. Although the time monotonically decreases as the number of chasers increases, it shows faster decreases in a region with a smaller number of chasers, while the decrease is slower in a region with a large number of chasers.

To explain the two distinctive regions from microscopic viewpoints of chasing processes, we have introduced order parameters to classify the capturing process in section 4.2.2. In the region with the smaller number of chasers, spatial segregations of chasers and targets are commonly observed, and the number of targets decreases in an intermittent way. The introduced parameters are capable of explaining the intermittent decreases of targets.

© Springer Nature Singapore Pte Ltd. 2019

A. Kamimura and T. Ohira, *Group Chase and Escape,*
Theoretical Biology, https://doi.org/10.1007/978-981-15-1731-0_4

After describing the basic model, we turn our attention to extending the model for possible applications to real problems. A variety of extensions of the basic model are described and discussed in section 4.3: extending the two groups of chasers and targets to three groups, a model which introduces conversion of captured targets to chasers, to include effects of interactions among chasers, differences in speed, the lattice structures, and delay in chasing processes.

4.2 Basic Model

Let us describe the basic model, which we proposed in [44]. We consider a two-dimensional square lattice of size $L_x \times L_y$. Periodic boundary conditions are imposed.[1] Here, we consider excluded volume of particles so that at most one particle, a chaser or a target (escapee), can occupy each site.

The chasers and targets play tag by hopping between the sites. The following rules are applied for hopping: a target moves to evade its nearest chaser, while a chaser hops to close in on its nearest target. Here, we denote positions of a target and a chaser, respectively, by (x_T, y_T) and (x_C, y_C). The distance between them is calculated as

$$d = \sqrt{(x_T - x_C)^2 + (y_T - y_C)^2}. \tag{4.1}$$

Each target calculates the distance for all chasers in order to identify the chaser with a minimum d, i.e., the nearest to the target. If there are more than two chasers who are equally near (equal d), the target chooses one of them randomly. Then, the target hops to its nearest site in the direction to increase the distance from the chaser. The hopping rule is shown in Fig. 4.1. Generally, the target has two or three possible sites to which to hop. In the case of two possible sites (Fig. 4.1(A)), one of them is chosen with an equal probability $1/2$. When the target has three possible sites to increase the distance (Fig. 4.1(B)), one of these is chosen with an equal probability $1/3$.

Similarly, the rule for each chaser is defined such that it hops to close in on its nearest target. A chaser determines the nearest target by calculating distances in the same way as for a target. The chaser, then, hops to its nearest site that decreases the distance. Generally, each chaser has a single site to hop to (Fig. 4.1(B)), or two possible sites to choose from with equal probability $1/2$ (Fig. 4.1(A)).

By the excluded volume of particles introduced here, if the chosen sites are occupied, chasers and targets cannot move, except in "catch events" explained below, and they stay in their original sites. (Here, we first choose one of the nearest sites by the probabilities above, so that the chasers or the targets do not move even if the other nearest sites are empty.)

When a target is in a site nearest to a chaser, the chaser catches the target by hopping to the site, and then the target is removed from the system. We call this a

[1] Validity of the conditions to real problems is discussed in Chapter 5.

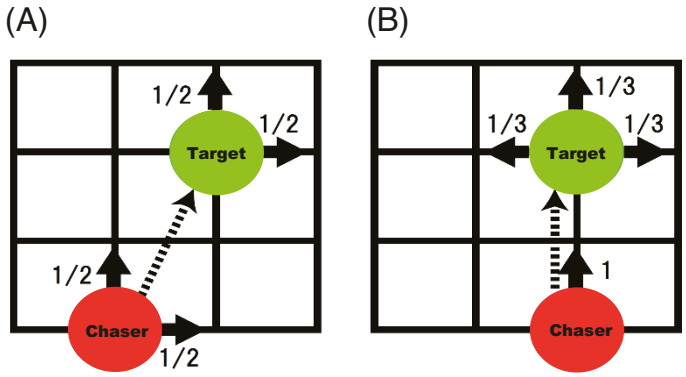

Fig. 4.1 Hopping rules for chasers and targets. While chasers hop to close in on their nearest targets, targets hop to evade their nearest chasers. Dotted arrows from chaser to target indicate that the chaser hops to close in on the target, and the target hops to get away from the chaser. Solid arrows show possible hopping directions with indicated probabilities. (A) Generally, they have two choices. (B) When the chaser and the target are in the same x or y-axis, the chaser has one choice, while the target has three choices.

"catch event". After the catch, the chaser pursues the remaining targets in the same manner.

We now describe how we proceed with computer simulations. Initially, N_C^0 chasers and N_T^0 targets are randomly distributed in the lattice. In accordance with the above hopping rules, every chaser and target are to hop by one site (this implies that we are considering the case that the speeds of chaser and targets are the same). To do this, we first determine the next hopping site for chasers and targets. Then, we move all chasers (the update is done in a random sequential order). If a chaser hops to a site a target occupies, the chaser catches the target, and the caught targets are removed from the field. After this, we move all the remaining targets.

Consequently, the number of targets, N_T, monotonically decreases along with the catches, while the number of chasers, N_C, remains a constant N_C^0. It is noteworthy here that we assume the timescales in the chase and escape processes are much shorter than typical lifetimes of particles, thus intrinsic birth and death of chasers and targets are not considered in the basic model. A possible extension is discussed in section 4.3. Simulations are carried out until all targets have been caught by chasers, i.e., $N_T = 0$. The results are averaged over 10^4 samples.

4.2.1 Simulation Results

4.2.1.1 Lifetimes of Targets

First, let us define the time length for the entire catch T as the simulation steps it takes for the chasers to catch all the targets. Their distribution is shown in Fig 4.2. Since the time T can be also interpreted as a "lifetime" of the final target, Fig. 4.2 represents the probability distribution of the lifetime. When the number of chasers N_C is larger than that of targets N_T, the distribution basically shows a parabolic shape on the log–log scales, suggesting a log-normal distribution. This distribution can be obtained even when both chasers and targets are moving as conventional symmetric random walks (see also section 5.3.1.2). However, as N_C decreases and approaches values approximately equal to N_T, it deviates from the log-normal distribution, reflecting the effect of chase and escape.

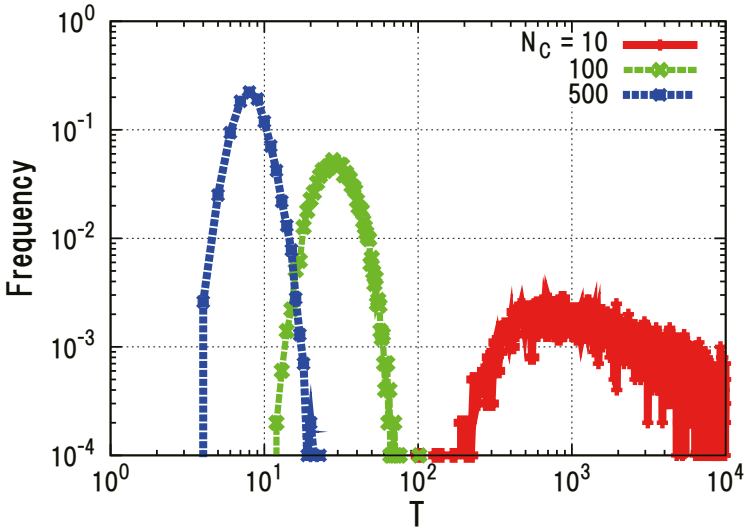

Fig. 4.2 Distribution of time for the entire catch T for the numbers of chasers $N_C = 10, 100, 500$. The linear size of the system is $L_x = L_y = 100$ and the initial number of targets is $N_T^0 = 10$. Modified from [44]. © Deutsche Physikalische Gesellschaft. Reproduced by permission of IOP Publishing. CC BY-NC-SA

Naturally, the time T decreases as the number of chasers increases because it is intuitively reasonable that the targets are caught up sooner when there are more chasers. We note that because we are considering the case where the chasers and the targets have the same speeds, an individual chaser generally cannot catch up with targets. Thus, the catch event typically occurs when chasers surround each individual target, as depicted in Fig. 4.3. Although an individual chaser independently tries

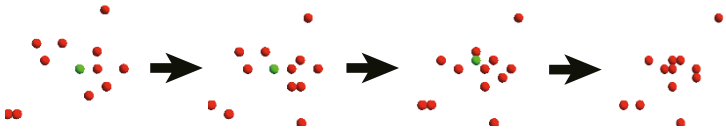

Fig. 4.3 Snapshots of a catch event with time evolution from left to right. Red and green circles denote chasers and target, respectively. Modified from [44]. © Deutsche Physikalische Gesellschaft. Reproduced by permission of IOP Publishing. CC BY-NC-SA

to catch a target, it appears as if the group of chasers cooperates to catch a target. In section 4.2.2, we try to quantify this group behavior.

If we further look at the lifetime distribution of all targets, then we obtain the results shown in Fig. 4.4. The distribution first shows large drops at the left (at the point the lifetime is equal to one), then increases and peaks at a typical time, which gets shorter (shifts to the left) for a larger number of chasers. After the peak, it decreases again.

The large drops at the point the lifetime is equal to one indicate that a number of catch events occur at the initial first step. This is because, in the initial condition, targets can be positioned in the nearest neighboring sites to chasers, i.e., $d = 1$. Then, the targets are caught by the chasers in the next step. However, if the initial distances between targets and chasers are larger than $d = 1$, the targets can momentarily evade the chaser. Then, the number of catch events decreases, causing the drop in the figure.

Besides the first drop, the distribution has a peak. The value of these peak positions can be inferred as a typical lifetime of the targets. It can be interpreted to represent a timescale for chasers to form a spatial structure from the random initial condition to surround and catch targets.

Let us now turn our attention to investigate how the lifetimes of the longest-living (final) and typical targets change with the numbers of chasers N_C and initial targets N_T^0. The lifetime of the final targets is equal to the time for the entire catch T, as described above. The typical lifetime is defined here as $\tau = \sum t(N_T^{t-1} - N_T^t)/N_T^0$, where N_T^t denotes the number of targets at t so that $(N_T^{t-1} - N_T^t)$ represents the number of targets with a lifetime t. In Fig. 4.5, we show how T and τ change with the number of chasers N_C for a fixed $N_T^0 = 10$. Both T and τ show similar dependences.

For moderately small N_C, the lifetimes decrease as $N_C^{-\alpha}$ with $\alpha \approx 3$. The power-law dependence is valid for a region where the ratio of N_C to N_T^0 is less than approximately 5. However, as N_C increases further, the lifetimes show a crossover to slower decreases, which are approximately fitted by another power law $N_C^{-0.75}$. At the right end, both of them approach one where the sites are filled with chasers so that both typical and longest-living targets can survive only in one time step. The two distinctive regions are found and characterized by the different dependences on the number of chasers. Even though the powers of the dependences sensitively depend on the details of the model, the two distinctive regions are generally observed

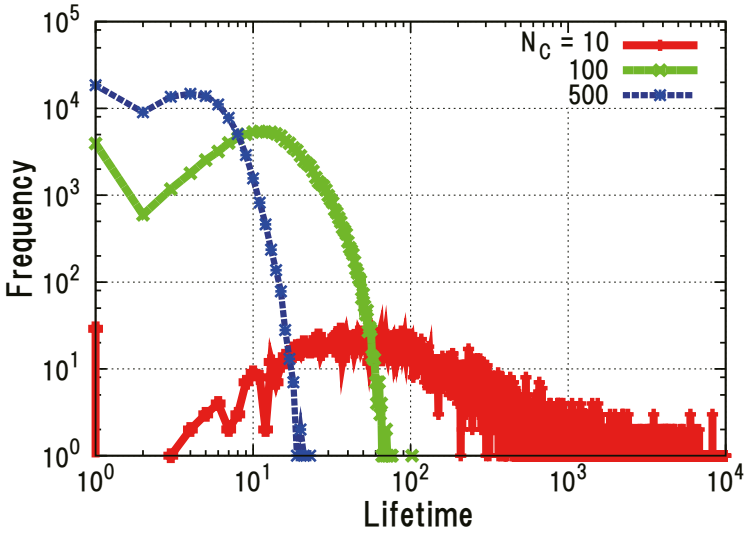

Fig. 4.4 Lifetime distribution of targets for $N_C = 10$, 100, and 500. Parameters are identical with those of Fig. 4.2. Modified from [44]. © Deutsche Physikalische Gesellschaft. Reproduced by permission of IOP Publishing. CC BY-NC-SA

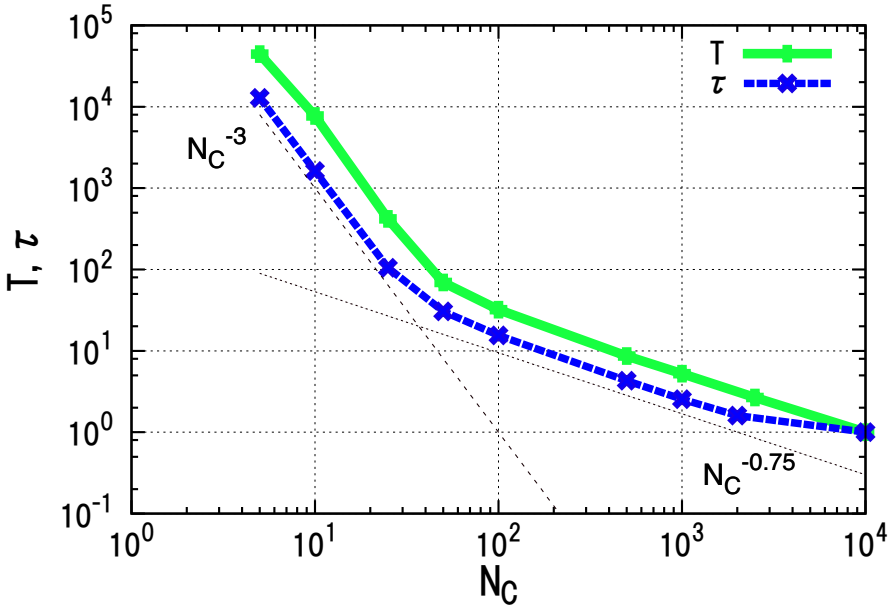

Fig. 4.5 Lifetime of final (T) and typical (τ) targets as a function of N_C for fixed $N_T = 10$. The power-law dependences N_C^{-3} and $N_C^{-0.75}$ are also shown as dotted lines. Modified from [44]. © Deutsche Physikalische Gesellschaft. Reproduced by permission of IOP Publishing. CC BY-NC-SA

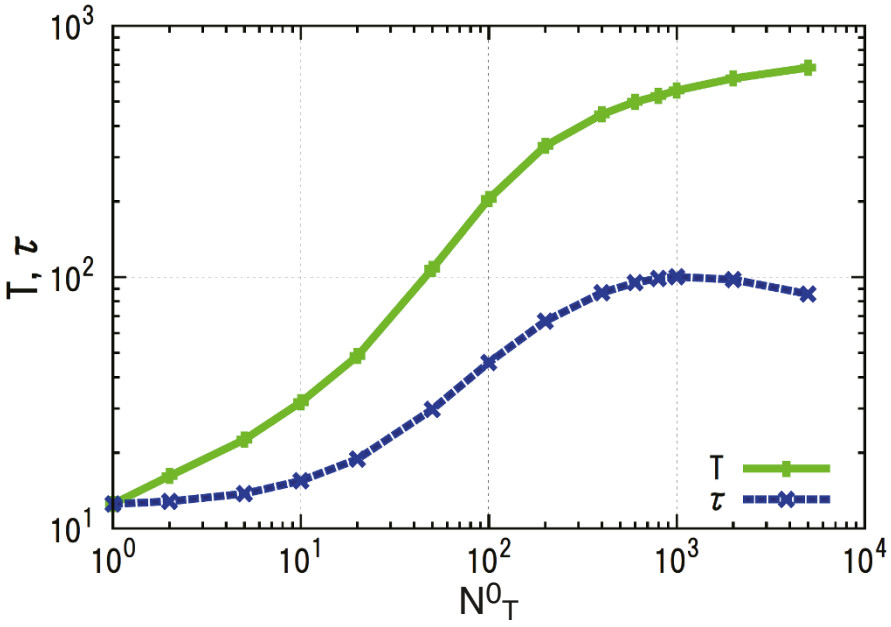

Fig. 4.6 Lifetime of final (T) and typical (τ) targets as a function of N_T for fixed $N_C = 100$. Modified from [44]. © Deutsche Physikalische Gesellschaft. Reproduced by permission of IOP Publishing. CC BY-NC-SA

in subsequent studies (see section 4.3). As we will show in section 4.2.2, the two regions are also characterized by typical catching processes.

We next investigate how the lifetimes change with the initial number of targets N_T^0 for a fixed $N_C = 100$, as shown in Fig. 4.6. As N_T increases, the lifetime of final targets monotonically increases. On the other hand, the lifetime of typical targets peaks around $N_T = 10^3$ and slightly decreases again. We show typical snapshots in Fig. 4.7. From the initial condition, targets evade chasers at first by producing clusters of targets. As shown in the left snapshot, we can see the clusters of targets appear where targets get close to each other. Then a group of chasers gets closer to the clusters to catch up targets. It is intuitively efficient for the group of chasers to catch targets by surrounding the cluster of targets because the number of targets can be caught, more or less, by a single enclosure event. The peak of the lifetime may represent such effects.

Also, it is of interest to know the most "efficient" number of chasers N_C for a given number N_T^0 of targets. We have evaluated this by focusing on a quantity $c = N_C T / N_T^0$: the number of work-hours T for which N_C chasers are deployed (total cost) divided by the initial number of targets N_T^0. Thus, this quantity represents the unit cost for the group of chasers to finish the task per target.

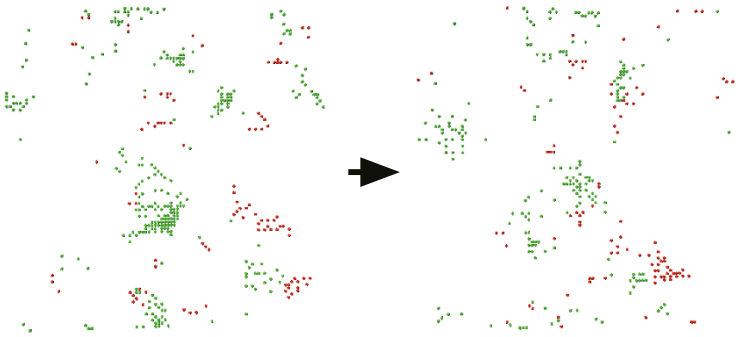

Fig. 4.7 Snapshots of the system for $N_C = 100$ and $N_T^0 = 1000$. Red and green points represent chasers and targets, respectively. Clusters of targets are typically observed during the chasing and escaping processes. Modified from [44]. © Deutsche Physikalische Gesellschaft. Reproduced by permission of IOP Publishing. CC BY-NC-SA

We have plotted this unit cost function for different chasing and escaping rules in Fig. 4.8. Here, the cost is plotted by changing the number of chasers N_C for a fixed N_T^0. We found that there is a minimum in this cost for the chase and target case (indicated by C&T). This means there is an optimal number of chasers N_C^* to finish

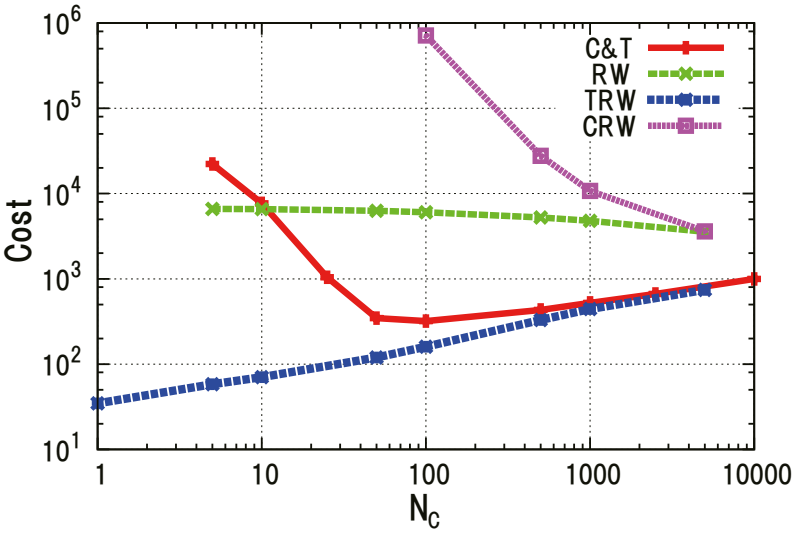

Fig. 4.8 Cost $c = N_C T / N_T^0$ vs. the number of chasers N_C for $N_T^0 = 10$ in following four cases: the original chasers and targets (C&T), both chasers and targets are random walkers (RW), targets are random walkers (TRW), and chasers are random walkers (CRW). Modified from [44]. © Deutsche Physikalische Gesellschaft. Reproduced by permission of IOP Publishing. CC BY-NC-SA

the given chasing task most efficiently. When the speed of targets is as fast as that of chasers, an individual chaser cannot catch up with targets, so it cannot finish the task alone by itself. Instead, a group of chasers catches a target by surrounding it so that the target cannot escape from them. In this case, a number of chasers substantially more than targets is necessary to finish the task efficiently. On the other hand, as the number of chasers exceeds the optimal number to surround the targets, excessive chasers result in increased cost. The right side of the figure, $N_C = 9990$, confirms that the system is fully occupied, so that the targets are caught in one simulation step, leading to the cost $c = 1 \times 9990/10 = 999 \sim 10^3$.

Such a minimal cost is realized as a result of both chase and escape processes. In Fig. 4.8, we also show the costs in different cases: both or either chaser and target follow a random walk process in which the chasers/targets randomly hop to one of the four nearest neighboring sites. We observe that when the targets are random walkers (TRW), the cost monotonically increases along with the number of chasers. On the other hand, when the chasers (CRW) or both (RW) are random walkers, they monotonically decrease.

4.2.2 Quantitative Analysis of Chasing Processes

In this subsection, we investigate the chasing processes of our model in more detail. One of the most fascinating features of the model is the spatial segregation of chasers and targets (Fig. 4.7). In order to quantitatively analyze and characterize this, we classify chasing processes into several patterns.

As a simple classification, we focus on one-particle-to-many-opponents situations in chasing processes. Fig. 4.9 shows the classified patterns of chasers in which many chasers pursue one target (A to C), and those of targets in which many targets escape from one chaser (D to F). The situation of each pattern is explained as follows:

(A) A number of chasers follow a target in a linear formation.
(B) Chasers surround a target. A catch of the target typically follows this pattern.
(C) One chaser drives a target into a group of chasers. This is a transient behavior often observed leading to pattern B.
(D) Targets escape in a linear formation from a single chaser.
(E) Targets scatter away from a chaser isotropically or by dividing into small groups. This pattern frequently appears right after a chaser invades into a cluster of targets.
(F) One chaser runs after a target, while nearby targets escape in different directions of the chaser.

In order to highlight the advantages of group formations, we introduce order parameters q_k and p_k to distinguish the above patterns. By this characterization, we clarify relations between the microscopic pursuit patterns and the macroscopic quantities introduced in the previous subsection.

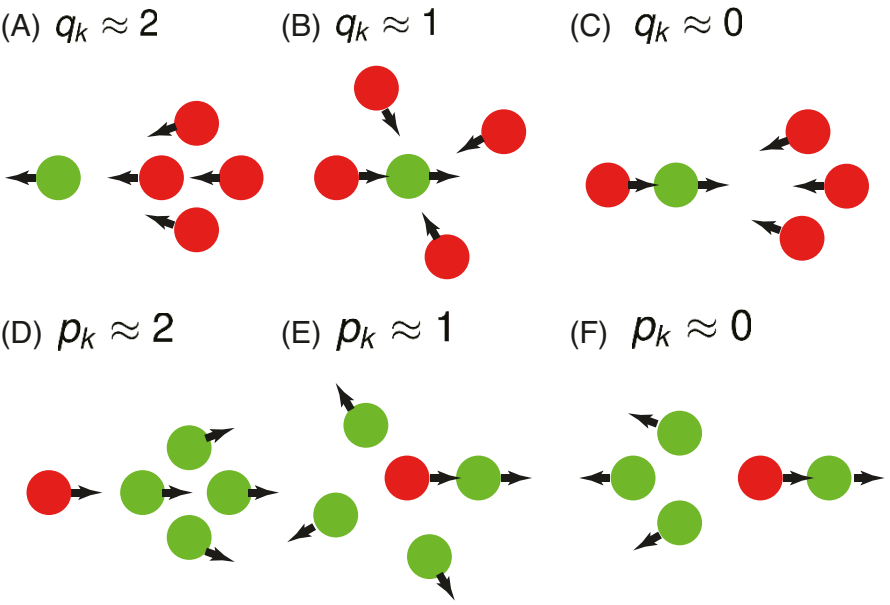

Fig. 4.9 Chasing and escaping patterns characterized by parameters q and p. Situations A, B, and C represent patterns of chasers around a target with corresponding values of q. In contrast, situations D, E, and F represent patterns of targets around a chaser with corresponding values of p. Modified from [49] with permissions (© 2015 Springer Japan).

First, let us introduce a parameter q_k to distinguish patterns A to C, to reflect the viewpoint of targets. At each time step, we focus on every remaining target indexed by k, and the $n_k^C + 1$ chasers ($n_k^C \geq 1$) which chase the target k. Here, we index the nearest chaser as $i = 0$ and the other chasers as $i = 1, ..., n_k^C$. For each target k, we define the order parameter q_k as

$$q_k = \frac{1}{n_k^C} \sum_{i=1}^{n_k^C} (\hat{r}_{ik} \cdot \hat{r}_{0k} + 1), \tag{4.2}$$

where $\hat{r}_{0k}$ denotes a unit vector pointing the direction from the nearest chaser $i = 0$ to the target k, while $\hat{r}_{ik}$ are unit vectors from the i-th chaser to the target k. Fig. 4.10(i) illustrates the calculation of q_k when the target k is chased by two chasers. By this parameter, the three patterns A, B, and C can be characterized as $q_k \sim 2, 1$, and 0, respectively. We also introduce the average of q_k for all the remaining $\tilde{N}_T$ targets which are chased by more than two chasers,

$$\bar{q} = \frac{1}{\tilde{N}_T} \sum_{k=1}^{\tilde{N}_T} q_k. \tag{4.3}$$

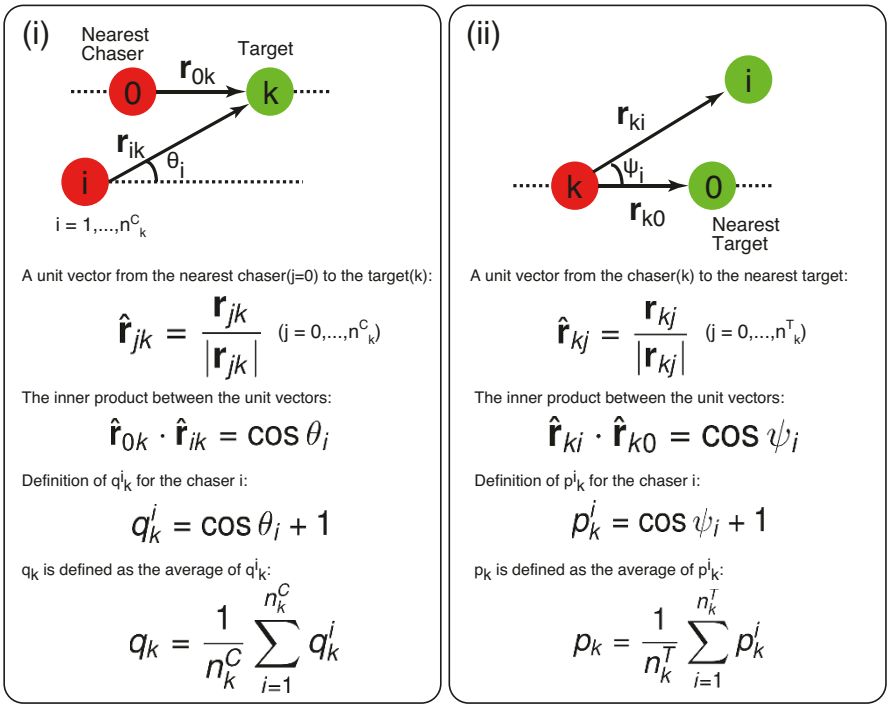

Fig. 4.10 Illustrations for calculating order parameters (i) q_k and (ii) p_k for the case of three players. Modified from [49] with permissions (© 2015 Springer Japan).

In the catching events, pattern B is frequently observed because the chasers need to surround the target. The advantage of this parameter q is that we can identify and distinguish pattern B from patterns A and C, irrespective of the group size and spatial inhomogeneities of chasers, because of the angular sensitivity of the inner product.

Fig. 4.11 shows the time evolution of $\bar{q}$ for different numbers of chasers. When the number of chasers is much larger than the initial number of targets ($N_C = 200$; blue curve), almost all targets are initially surrounded by chasers. Thus the initial $\bar{q}$ is close to one. In addition, $\bar{q}$ is almost constant through the time course because most of the targets are immediately caught with pattern B. On the other hand, when the number of chasers is as small as the initial number of targets ($N_C = 10$; red curve), $\bar{q}$ initially fluctuates, and eventually approaches two. This result indicates that the remaining targets generally evolve to be chased by a group of chasers as in pattern A. This can be explained as follows. The catching event typically results in aggregation of chasers as in pattern B. After the event, the chasers tend to chase the same single nearest target, leading to pattern A, as the remaining targets become small. For an intermediate number of chasers ($N_C = 30$; green curve), a dominant pattern in the final stage depends on initial configurations, therefore, the values of $\bar{q}$

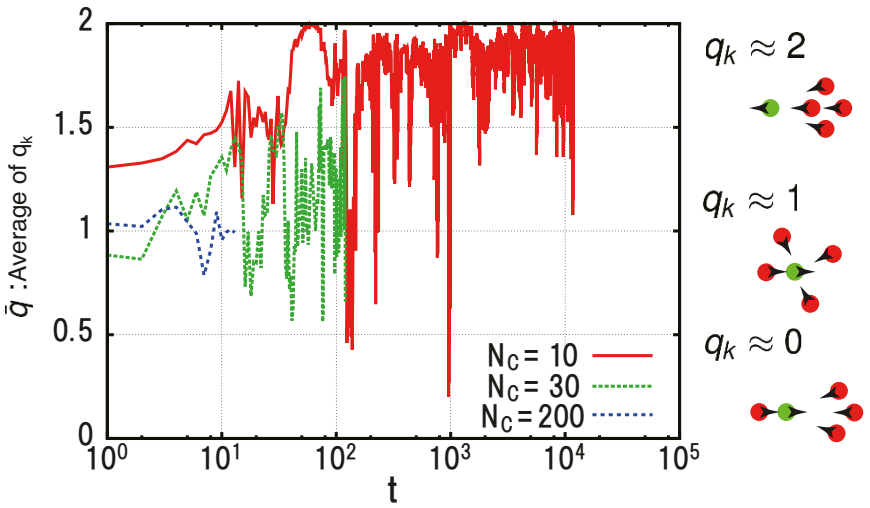

Fig. 4.11 Time evolution of order parameter $\bar{q}$ (the average of q_k) for the numbers of chasers, $N_C = 10, 30, 200$. Initially 10 targets are randomly placed on the square lattice with $L_x = L_y = 100$. On the right, the chasing patterns for $q_k \approx 2, 1, 0$ are shown for a reference. Modified from [49] with permissions (© 2015 Springer Japan).

are between one and two. A ratio of samples in which pattern A appears increases as the number of chasers decreases.

Now let us turn our attention to capturing patterns by examining the time evolution of $\bar{q}$ and the number of targets, $N_T(t)$. In Fig. 4.12, we show $\bar{q}$ and $N_T(t)$ for the parameters $N_T^0 = 10$ and $N_C = 5$. The values of $\bar{q}$ fluctuate just below the value two (red curve), but it clearly shows spike-like decreases at the decrement timings of targets (green curve). This indicates that the chasing patterns of chasers, typically in pattern A, transiently change to patterns B and C, to surround and capture targets. At capturing events, chasers aggregate, and after the capture, they form a larger group, typically, to chase a single nearest target. This makes the rapid recovery of the value of $\bar{q}$ to two.

This parameter $\bar{q}$ also explains the two distinct regions of the time for the entire catch T and typical lifetime τ of targets in Fig. 4.5 (also in [44]). As shown in Fig. 4.13, the times T and τ have two different regions in the dependences on N_C, approximately fitted by the two power laws N_C^{-3} and $N_C^{-0.75}$, and the boundary between the two regions is approximately at $N_C = 50$ for $N_T^0 = 10$. With parameter q, it is clarified that the difference between the two regions comes from a different frequency in the appearance of patterns A, B and C. As explained in Fig. 4.11, $\bar{q}$ stays near one (pattern B) when N_C is much larger than N_T^0, and $\bar{q}$ at approximately two (pattern A) appears frequently when N_C becomes smaller. Here, we quantify them by calculating the ratio ϕ of simulation samples which achieve $\bar{q} > 1.8$ through the time course from the initial configuration until catching all targets. In Fig. 4.13, the boundary between the two regions approximately coincides with the point of $\phi \sim 0$.

In short, for the region of small N_C, pattern A is dominant, while for the region of large N_C, almost all targets are rapidly captured with pattern B or C.

The parameter q clarifies how a single target is pursued by a group of chasers. However, the parameter is not sufficient for explaining all the behavior the model exhibits. In particular, when the number of targets is larger than that of chasers, $N_T^0 > N_C$, drastic decreases in N_T are observed as shown later, and the parameter is insufficient to quantify the observation. The drastic decrease in N_T suggests that a cluster of aggregated targets is formed, and a number of chasers round up the targets. To confirm this, we introduce another parameter p to reflect the viewpoint of chasers.

The introduction of p is analogous to that of q. At each time step, we focus on every chaser indexed by k, and $n_k^T + 1$ targets escaping from the chaser k. The order parameter, p_k, for the chaser k is defined as

$$p_k = \frac{1}{n_k^T} \sum_{i=1}^{n_k^T} (\hat{r}_{ki} \cdot \hat{r}_{k0} + 1), \tag{4.4}$$

and

$$\bar{p} = \frac{1}{N_C} \sum_{k=1}^{N_C} p_k, \tag{4.5}$$

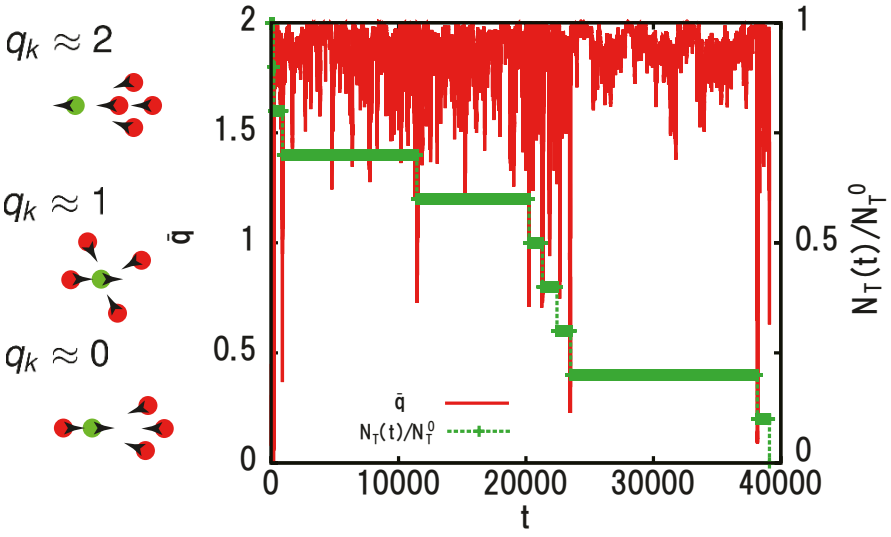

Fig. 4.12 Time evolution of the pattern parameter $\bar{q}$ (red) and the ratio of the remaining targets, $N_T(t)/N_T^0$ (green), for the parameters $N_T^0 = 10$ and $N_C = 5$. On the left, the chasing patterns for $q_k \approx 2, 1, 0$ are shown for a reference. Modified from [49] with permissions (© 2015 Springer Japan).

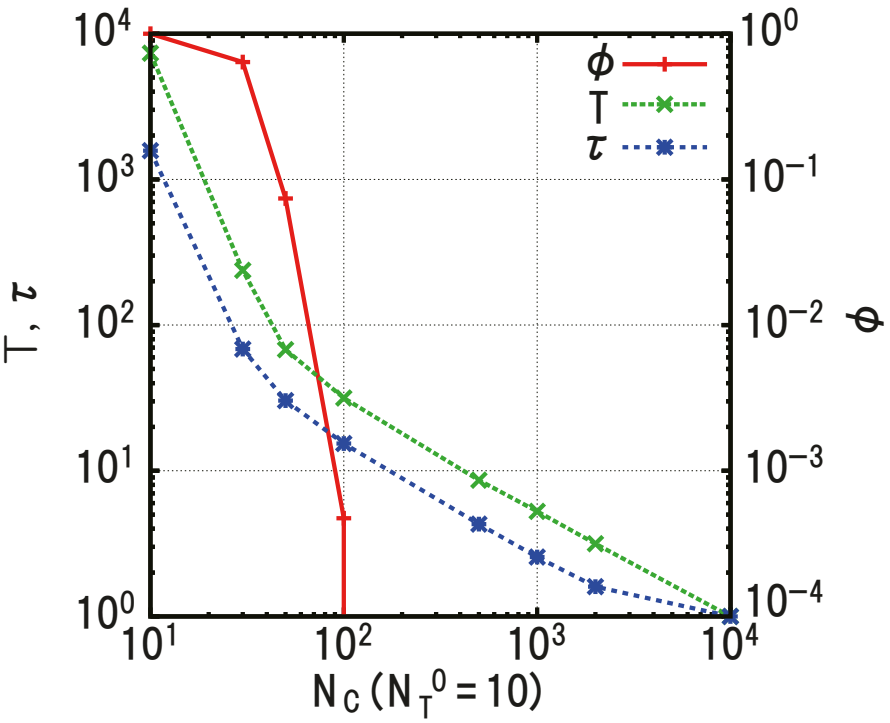

Fig. 4.13 Dependence of the time for the entire catch T, typical lifetime τ and the ratio of simulation runs ϕ on the number of chasers N_C. The quantity ϕ denotes the ratio of simulation samples which achieve $\bar{q} > 1.8$ during the time course from an initial condition until all the targets are captured. Modified from [49] with permissions (© 2015 Springer Japan).

where $\hat{r}_{k0}$ and $\hat{r}_{ki}$ denote unit vectors in the directions toward the chaser k from the nearest ($i = 0$) and i-th targets ($i = 1, ..., n_k^T$) escaping from it, respectively. Fig. 4.10(ii) also illustrates the calculation of p_k when two targets escape from the chaser k. By this parameter, the three patterns D, E, and F can be characterized as $p_k \sim 2, 1$, and 0, respectively. These patterns are illustrated in Fig. 4.9.

The introduction of p, together with q, helps us understand the drastic decrease of the number of targets. As an example, Fig. 4.14 shows the time evolution of $\bar{p}$ (green curve), $\bar{q}$ (red curve) and $N_T(t)$ (blue curve) with $N_T^0 = 50$ and $N_C = 10$. The drastic decrease of $N_T(t)$ occurs around $t = 2700$. Before the event, $\bar{p}$ (green) remains around two for a certain period. This indicates that the targets form an aggregated cluster to escape from a chaser (see pattern D in Fig. 4.9), and it is also confirmed by the upper left snapshot in Fig. 4.14. After the drastic decrease, $\bar{p}$ rapidly decreases approximately to one exhibiting pattern E (Fig. 4.9). The simultaneous behavior of $\bar{p}$ and drastic decrease of $N_T(t)$ explains the collective catch by a round up of chasers.

When the initial number of targets (N_T^0) is fixed to be small (Here, we fix $N_T^0 = 10$), each individual chasing and escaping process is reflected in the time evolution of the averages $\bar{p}$ and $\bar{q}$. As we increase the number of particles and expand the

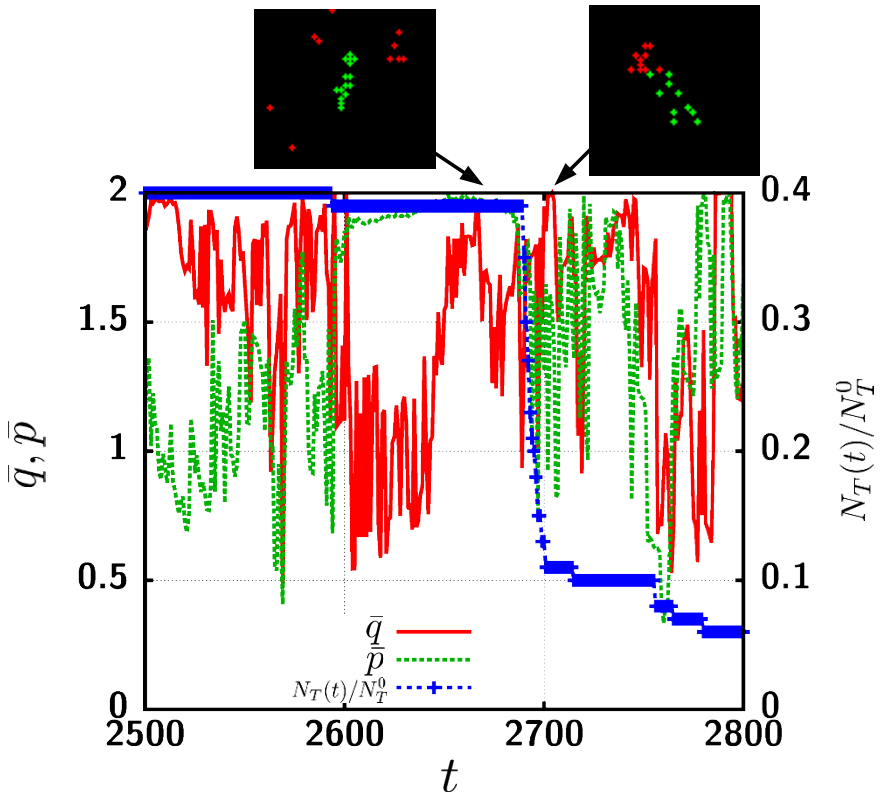

Fig. 4.14 Time evolution of $\bar{q}, \bar{p}$ and $N_T(t)/N_t^0$ around a drastic decay of target with $N_T^0 = 50$ and $N_C = 10$. Modified from [49] with permissions (© 2015 Springer Japan).

system size, such an individual chasing and escaping may not be reflected well by $\bar{p}$, $\bar{q}$ because they are averaged over particles. However, we suggest that the parameters are still useful to characterize typical (dominant) behavior of the system.

Here, we show such an example: the system size is expanded to $L_x = L_y = 2048$ (Fig. 4.15). Even in this larger system, the parameters show similar behavior if the number of targets is sufficiently low. In this case, the averages $\bar{p}$ and $\bar{q}$ can reflect the dynamical changes of q_k and p_k of each individual k because the inner products in the definition of q_k and p_k are less sensitive to the number of chasers and targets, and spatial irregularities of particles. Also in this case, samples in which $\bar{q}$ reaches two disappear for $N_C/L^2 > 0.01$, where L denotes a linear system size.

On the other hand, for a higher density of targets, the parameters exhibit different behavior. Fig. 4.15 shows the time evolution of $\bar{q}$ and $\bar{p}$ with $N_T^0 = 2^{18}, N_C = 2^{14}, 2^{15}, 2^{16}$. In the cases $N_T^0 > N_C$, pattern B is initially dominant for the chased targets as $\bar{q} \sim 1$. In addition, $\bar{p} \sim 1$ indicates that the dominant pattern at the initial stage is pattern E, i.e., most of the targets momentarily escape. In the middle stage $[10 \leq t \leq 100]$, a plateau region appears in $\bar{q}$ and $\bar{p}$ for each N_C. This indicates that

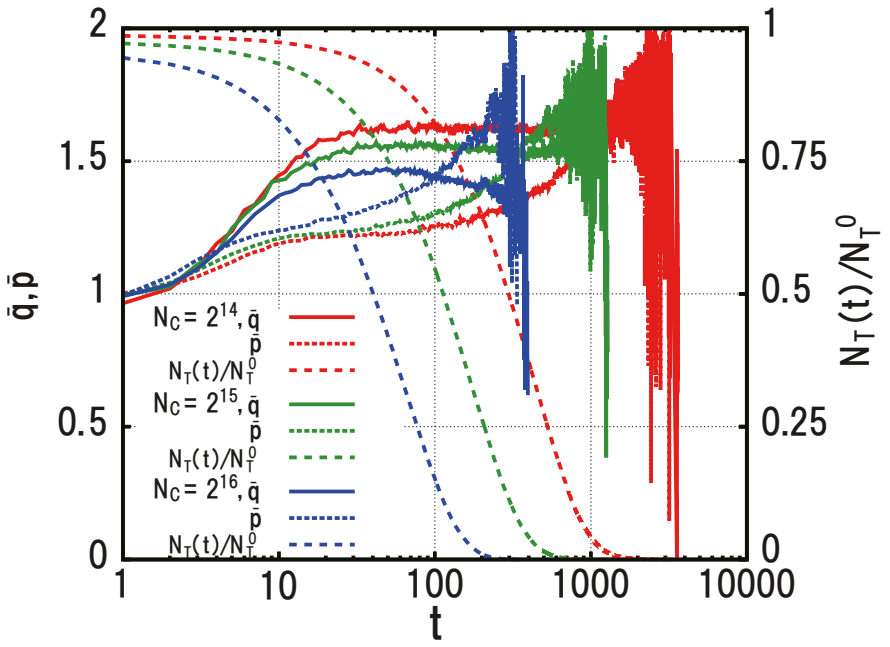

Fig. 4.15 Time evolution of $\bar{q}, \bar{p}$ and $N_T(t)/N_T^0$ with $N_T^0 = 2^{18}, N_C = 2^{14}, 2^{15}, 2^{16}$. The system size is $L_x = L_y = 2048$. Modified from [49] with permissions (© 2015 Springer Japan).

the ratio of appearance in the patterns is constant while the number of targets is decreasing (see dashed curves in Fig. 4.15). The values of $\bar{q}$ in this region increase as N_C decreases. In contrast, $\bar{p}$ is greater than one but far less than two, therefore, targets escape almost with pattern E and occasionally with pattern D. This behavior of $\bar{q}$ and $\bar{p}$ leads to a consequence that, in the plateau region, the majority of targets escape when the chasers chase a relatively small number of targets. This behavior can be interpreted as if the number of targets work as "decoy" targets because chasers are attracted only to the targets.

After the plateau region, the values start to fluctuate as the remaining targets become small. It is noteworthy that the value of $\bar{q}$ gets closer to two even though $N_C/L^2 > 0.01$. This is not observed when the initial density of targets is low. It indicates that pattern A occurs more likely when chasers chase a number of "decoy" targets during the initial and the plateau stages.

4.3 Recent Developments in Group Chase and Escape

In this section, we review and discuss a variety of extensions and modifications of our original model described in section 4.2. The developments can be roughly categorized from the viewpoint of models into three: abilities, reactions and motions.

Developments in abilities refer to modifications of the abilities of the agents for detecting the opponents' positions. Developments in reactions refer to modifications of the model on how the targets change their species and mortality when they are captured; in the original model, the targets are removed from the system. Finally, developments in motions refer to modifications on rules of spatial movements and restrictions of particles.

4.3.1 Abilities

As one of the directions to extend the model, we consider two examples for the agents to restrict their abilities to detect the opponents' positions. The first example is the case when each chaser has limited search distance to find the nearest target. The second example is the case when the abilities of chasers to detect the targets' positions are distributed in the group.

4.3.1.1 When Each Chaser has Limited Search Distance for the Nearest Target

We can extend our model to include the search range of each chaser [44]. In the basic model, chasers can find targets over an unlimited distance. However, in reality, chasers search for targets in their vicinities. This is also the same for targets. Targets may be able to recognize the existence of only nearby chasers.

The search range l can be introduced as follows. When a chaser searches for the nearest target, the search area is limited to the range $\sqrt{(x_T - x_C)^2 + (y_T - y_C)^2} < l$, where (x_C, y_C) and (x_T, y_T), respectively, denote the positions of the chaser and the target in x and y-directions. If the chaser finds a target in the search range, it moves with the chase-and-escape hopping. If not, it follows the random-walk hopping. For the movement of targets, the search range can also be introduced in the same manner. Here we note that the model is equivalent to the random walkers if the value of l is zero. On the other hand, the model approaches the basic model as the range increases to the system size. As shown in [44], the time for the entire catch T decreases as l increases, and it exponentially approaches the time $T_{C\&T}$ for the original chase-and-escape case.

The system can exhibit interesting spatial structure when the search range is different between chasers and targets [44]. For example, we assume an unlimited search range for targets, while the range for chasers is sufficiently short. For an appropriately low number of chasers, targets gather in relatively low-density areas of chasers and momentarily hide from chasers because the short-range chasers cannot recognize their positions (Fig. 4.16). After a long time, chasers can find the group of targets and finally catch them. Examining the catching processes in relation to such spatial pattern formations remains an interesting topic to be investigated.

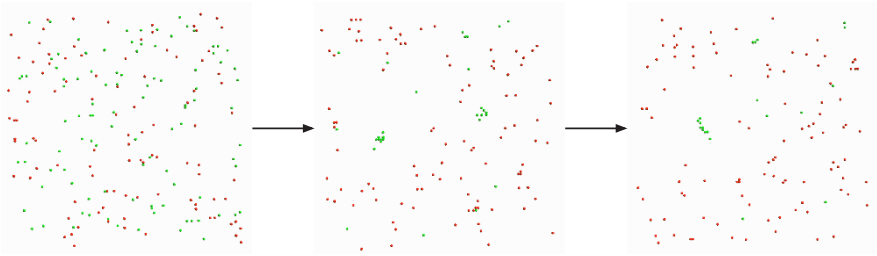

Fig. 4.16 Snapshots of the system with time evolution from left to right. While targets (green dots) have unlimited search range, chasers (red dots) have the search range $l = 5$. The numbers of chasers and targets are fixed to $N_C = N_T^0 = 100$. Modified from [44]. © Deutsche Physikalische Gesellschaft. Reproduced by permission of IOP Publishing. CC BY-NC-SA

4.3.1.2 When the Search Range is Distributed among Chasers

We also consider another extension of our model. This extension is to distribute the search ability among chasers. For example, in the group of chasers, some could have a long search range, while the others follow the random-walk hopping or have a short search range.

One example is where a group of chasers consists of two types: smart chasers and random walkers. Here, we refer to chasers with unlimited search range as smart chasers. On the other hand, the random walkers have a search range of zero. The cost we introduced as $c = N_C T / N_T^0$ enables us in this case to quantify the efficiency of the chasing. Here we assume that all the targets have unlimited search range.

In Fig. 4.17, we show the cost as a function of the number of smart chasers N_C^S. The two curves indicate the two cases: One (red curve) is the case when only the N_C^S smart chasers are present in the system and pursue the targets, and the other (green curve) is the case when $N_C - N_C^S$ random walkers also join the pursuit in addition to N_C^S smart chasers (the total N_C is fixed to 100). For both cases, the cost monotonically decreases as the number of chasers increases. In particular, for the mixed group of smart chasers and random walkers, a small number of smart chasers, say five to ten, drastically drop the cost. One interesting question is, when only a small number of smart chasers are available, which strategy will be better: let only the smart ones chase targets, or should random walkers join them? The cost clarifies that which strategy is better depends on the number of available smart chasers: for a small number of smart chasers, the latter case (green curve) is more efficient, while if many smart chasers available, the former strategy (red curve) gives lower costs.

Another study investigates the effect of smart chasers and random walkers on the average time for the entire catch [62]. By introducing random walks to the chasers, they show that the average time is reduced through the formation of pincer attack configuration. Here, the chasing in a "division of labor" way is essential to the reduction of the time because such an effect is not observed when all the chasers uniformly mix the strategies of chasing and random hopping.

A recent study suggests an enhancement of collective efficiency by the coexistence of highly stochastic ants and normal or weakly stochastic ants in the same colony to achieving the optimal foraging behavior [91]. This highlights the importance of the division of labor in insect societies [7].

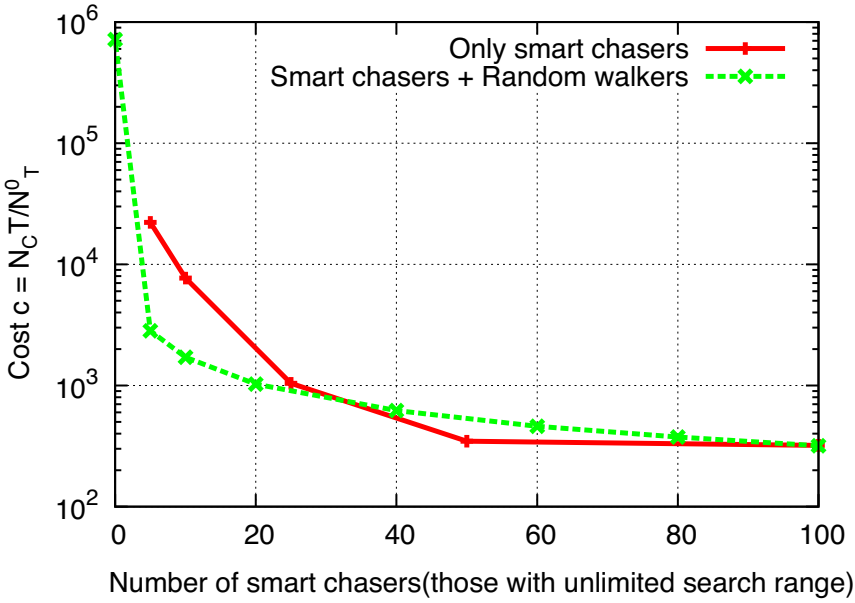

Fig. 4.17 Cost $c = TN_C/N_T^0$ by changing number of smart chasers N_C^S for fixed $N_T^0 = 10$. Modified from [44]. © Deutsche Physikalische Gesellschaft. Reproduced by permission of IOP Publishing. CC BY-NC-SA

4.3.2 Reactions

In the original model, captured targets are removed from the system to model typical predator–prey interactions: predators kill their prey to feed on them. This model assumes the timescales in the chase–escape processes are much shorter than typical lifetimes of organisms and reproduction timescales of chasers. An infectious disease may be one of the possible exceptions where capturing events and increase in the number of chasers are directly related, thus, one cannot neglect birth of chasers. Susceptible targets can be infected to become additional infective chasers when the targets are touched by the chasers.

Nishi et al. investigate such a vampire problem [75], in which a target converts to a chaser when captured, instead of removing it as in the original model. Numerical

simulations show that the conversion causes the lifetimes of targets to show non-monotonic dependence on the initial number of targets, resulting in the existence of a maximum lifetime. We will explain the results in the following subsection.

Sato extends the problem to a three-species case [88]. He considers three kinds of species A, B, and C; particles in species A act as chasers for species B, those in species B are the chaser for species C, and those in species C are the chasers for species A. The particle converts to a chaser when captured, thus, the total number of the three species is constant. Using a mean-field approximation, the time evolutions of the ratios of species are given by

$$\frac{d}{dt}\left(\frac{N_A}{N_0}\right) = 4\frac{N_0}{N_S}\frac{N_A}{N_0}\left(\frac{N_B}{N_0} - \frac{N_C}{N_0}\right), \tag{4.6}$$

$$\frac{d}{dt}\left(\frac{N_B}{N_0}\right) = 4\frac{N_0}{N_S}\frac{N_B}{N_0}\left(\frac{N_C}{N_0} - \frac{N_A}{N_0}\right), \tag{4.7}$$

$$\frac{d}{dt}\left(\frac{N_C}{N_0}\right) = 4\frac{N_0}{N_S}\frac{N_C}{N_0}\left(\frac{N_A}{N_0} - \frac{N_B}{N_0}\right), \tag{4.8}$$

where N_A, N_B, N_C, respectively, denote the number of A, B, and C. N_S denotes the total number of sites in the system, and $N_0 = N_A + N_B + N_C$. The factor 4 indicates the number of nearest neighbor sites for each particle in the square lattice. The solution for the ratio of species A, B, and C shows oscillations of species with constant phase intervals. For example, an increase in number of A, at a first moment, results in a decrease of B, and an increase of C. The increase of C results in a decrease of A and an increase of B. Then the increase of B causes a decrease of C and an increase of A. In this way, the three species cyclically oscillate and coexist. Numerical simulations of a random-walk model also confirm the oscillation and coexistence of the three species.

In the model of chasing and escaping for the three-species case, the numbers of species also show oscillatory behavior in the initial stage of simulations. In contrast, he finds that the chasing and escaping make the system unstable and, consequently, one of the species dominates the system and the other two species become extinct.

4.3.2.1 Vampire Problem

Here, we briefly review the work by Nishi et al., who investigated a vampire problem [75]. In this extension, a target can be converted to a chaser when captured, instead of being removed as in the original model.

In the extended model, the basic rules of motion for the chasers and targets are the same as in the basic model. However, we introduce a possibility of converting the captured target into a new chaser rather than simply removing it from the system. This process is shown in Fig. 4.18. We assume that these removal and conversion actions take place with probability $1 - P_V$ and P_V, respectively.

If the removal action is chosen, the chaser hops to the position of its nearest target and the target is removed as in the basic model. On the other hand, if the conversion

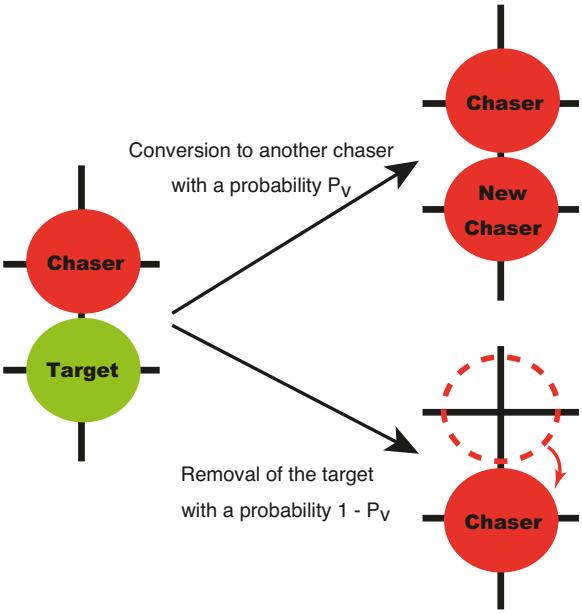

Fig. 4.18 In the vampire problem, the captured target (indicated by green) is converted to a new chaser (red) with a probability P_V, and is removed as in the original model with a probability $1-P_V$.

action is chosen, the chaser does not move, and the nearest target is converted into a new chaser. We note that $P_V = 0$ corresponds to a situation in which all the captured targets are removed, leading to the original model. $P_V = 1$ represents the case in which all the captured targets become chasers.

In order to investigate the effect of this extension, we performed numerical simulations. The size of the system is $L_x = L_y = 100$. We have N_C^0 chasers and N_T^0 targets at the start, and randomly distribute them over the square lattice. We measure the time for the entire catch T and the typical lifetime of targets defined as $\tau = \Sigma t(N_T^{t-1} - N_T^t)/N_T^0$. We average the times T and τ for 1000 samples. Also, for comparison, we simulate the random walk model, where both chasers and targets follow a simple random walk.

We compute T and τ as a function of N_T^0 with a fixed initial number of chasers as $N_C^0 = 100$. We chose the probability of conversion as $P_V = \{0, 0.25, 0.5, 0.75, 1\}$ and results are shown in Figs 4.19 and 4.20. The essential result in Fig. 4.19 is that the quantity T has maxima for the cases $P_V > 0$ in both the chasing-and-escaping and the random-walking models. This was not observed with the basic model without conversion ($P_V = 0$). If we turn our attention to τ, the maxima exist, irrespective of the conversion, for the chasing and escaping. For the random walking case, however, τ stays almost constant at $P_V = 0$ and monotonically decreases with increasing N_E^0 for $P_V > 0$.

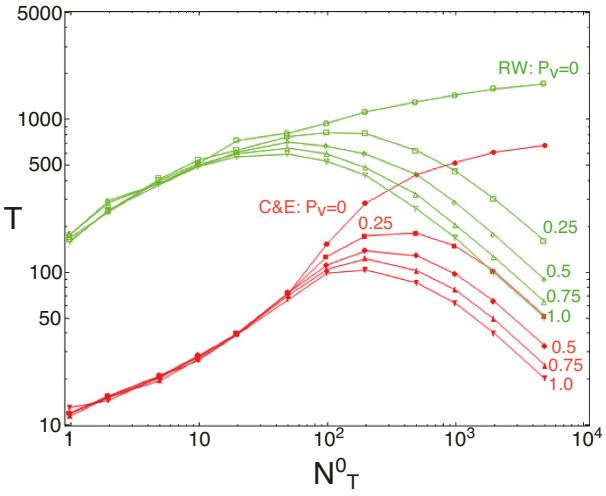

Fig. 4.19 Relation between the time for the entire catch T and the initial number of targets N_T^0 with various P_V for the two cases: chases and escapes (C & E) and random walks (RW). Modified from [75] with permissions (© 2011 Elsevier B. V.).

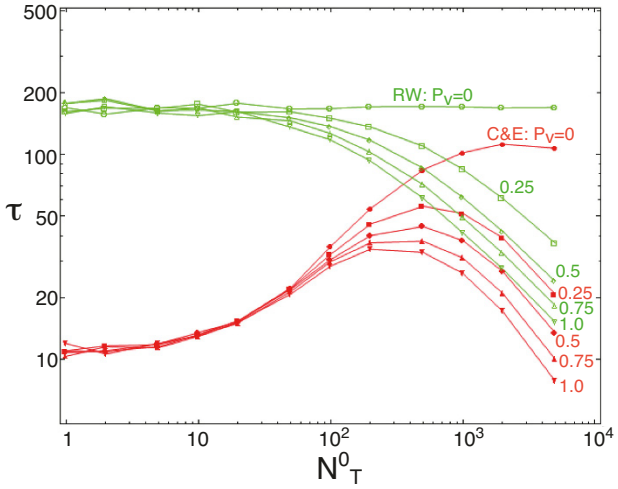

Fig. 4.20 Relation between the typical lifetime τ and the initial number of targets N_T^0 with various P_V for the two cases: chases and escapes (C & E) and random walks (RW). Modified from [75] with permissions (© 2011 Elsevier B. V.).

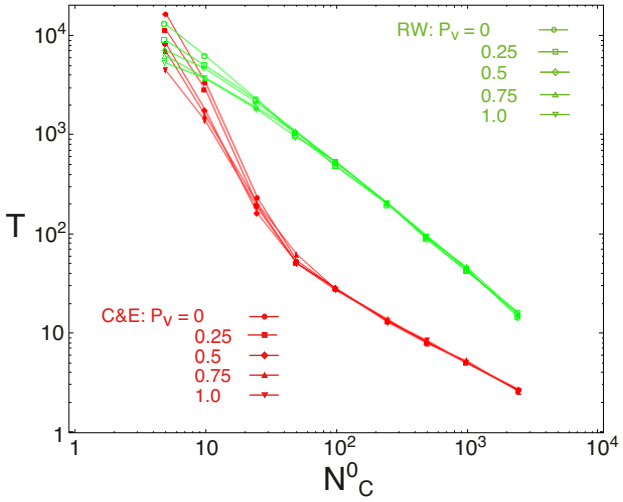

Fig. 4.21 Relation between T and N_C^0 with various P_V for the two cases: chases and escapes (C & E) and random walks (RW). The number of initial targets is fixed as $N_T^0 = 100$. Modified from [75] with permissions (© 2011 Elsevier B. V.).

We can understand these results qualitatively. First, the existence of a maximum T can be explained as follows. In the basic group-chase-and-escape model ($P_V = 0$), T increases as N_T^0 increases. When N_T^0 is small, the conversion process would not be relevant because the increase of chasers by the catch-up of targets is small. However, as N_T^0 increases, the chasers catch targets more frequently and convert them into new chasers leading to, probably, a fast spread of a chain of conversions. This spread would drastically decrease the entire lifetime T. Hence, these two factors lead to the maximum of T as a function of N_T^0. The same argument would be applied to the existence of the maximum of τ for the chasing and escaping case. Also, the monotonic decrease of T for the random walkers can be attributed to the factor of the spread of conversions. Note that the maximum τ in $P_V = 0$ was observed in the original model (Fig. 4.6). For the random walk cases, it is noteworthy that, in Fig. 4.19, the time T with $N_T^0 = 1$ (left end) is larger than the time with $N_T^0 = 5000$ (right end) for large values of P_V, i.e., chasing just one target without conversions takes longer than chasing 5000 targets with frequent conversions.

We also plot the time T as a function of N_C^0 in Fig. 4.21. The initial number of targets is fixed at $N_T^0 = 100$, and the probability P_V of the conversion is set as $\{0, 0.25, 0.5, 0.75, 1\}$. The other parameters are the same as in Figs 4.19 and 4.20.

For the chasing and escaping cases, the time T for different P_V converges for larger N_C^0. In other words, the lines do not depend on P_V above the critical number

of the initial chasers. On the other hand, there is a spread in the slope approximately below the critical number of the initial chasers around $N_C^0 \approx 40$: T decreases as P_V increases. It is noteworthy that the decrease of T by the conversion is more significant for the case of chase and escape than the random walker.

The difference in the relevance of conversions below and above the critical number of initial chasers reflects the essential number of chasers to catch the targets. In concrete, there is a critical number of chasers, beyond which adding more chasers is not as effective. Our results indicate that this critical number also exists even with conversions $P_V > 0$. This understanding is consistent with the result showing that the critical point does not depend on $P_V > 0$, but is dictated by a large number of chasers.

Up to now, the number of targets monotonically decreases by the catch-up events, irrespective of the processes of removal and conversions so that the targets are bound to become extinct. The conversions from targets to chasers make the situation more advantageous for the chasers. One may consider additional processes for targets to resist extinction. Proliferation processes for the targets can be one such example. Interested readers are referred to the original publication [75].

In summary, we introduced a conversion rule from captured targets to chasers. We found, through numerical simulations, that the conversion rule provides the optimum initial number of targets to produce the maximum lifetime T for the group of targets. While this maximum is also observed in the random walk rule, the conversion does not affect the qualitative difference with respect to the changes in the initial number of chasers.

4.3.3 Motions

One of the essential motions in the original model is that chasers and targets move with an equal speed. Different speeds of chasers and targets drastically change the catching process, because the fast chasers do not need to surround their targets to capture them. This suggests the two distinct regions of the time for the entire catch would not be observed in this case and, in fact, the region for the small number of chasers vanishes when the speed of chasers is faster than that of targets. Iwama and Sato found that only a few fast chasers are sufficient for this observation [42]. As intuitively expected, the effect of fast chasers is more relevant for the region with the small number of chasers than that with the large number.

The lattice structure also plays an essential role in spatial restrictions of particles' movement. While the square lattice would give the simplest model, investigations on various lattice structures can be considered if it alters the surrounding dynamics of chasing and escaping: one such example is the honeycomb lattice [105].

Individual-based off-lattice models with pursuit and evasion have been developed by Angelani [1] as well as by the present authors [63]. Angelani develops an off-lattice model based on the modeling of self-propelled organisms by Vicsek et al.[99] explained in section 3.4. The velocity of each particle, labeled by i, is updated by

$$\mathbf{v_i}(t+\Delta t) = v_0 \hat{\mathbf{v}}_\mathbf{i}^{(int)}(t), \tag{4.9}$$

where $\hat{\mathbf{v}}_\mathbf{i}^{(int)}$ is a unit vector, determined by following intra- and intergroup interactions:

$$\hat{\mathbf{v}}_\mathbf{i}^{(int)} = R_\eta[\hat{\mathbf{v}}_\mathbf{i}^{(al.)}] + \beta \mathbf{f}_\mathbf{i}^{(rep.)} + \gamma \mathbf{f}_\mathbf{i}^{(CT)}. \tag{4.10}$$

The first term describes the self-propulsion and alignment effect, where the particle i tends to align with an average velocity summed over the particles within a circle of radius R centered at the particle i. The operator R_η describes the effect of noise, as introduced in the Vicsek model. The second term describes a repulsive force preventing particle overlap. The third term describes the chase or escape force, and he chooses the form

$$\hat{\mathbf{f}}_\mathbf{i}^{(CT)} = p\hat{\mathbf{r}}_{ik_i}, \tag{4.11}$$

where k_i denotes the closest target (chaser) to any chaser (target) within a radius r_s (sighting radius) of particle i, $\mathbf{r}_{ik_i} = \mathbf{r}_i - \mathbf{r}_{k_i}$, $p = -1$ for chasers and $p = +1$ for targets.

Two distinct catch regimes are observed: a fast regime at a high ratio of predators to prey, and a slow regime when the ratio is less than about 5, in agreement with the results in the lattice models. Further, "spike-like" events are also observed, corresponding to cage trapping of a prey coop by many predators converging on it. In addition, he also considers another form of the escape force for targets, by weighted average over particles within the sighting radius as

$$\mathbf{f}_\mathbf{i}^{(T)} = \sum_{j \in S_i^{(sight.)}} h(r_{ij})\hat{\mathbf{r}}_{ij}, \tag{4.12}$$

where $h(r)$ is the weight function as a function of distance r. He examines two weight functions, the power law $h(r) = r^{-w}$, and the exponential $h(r) = e^{-kr}$. Particularly in the case where targets move faster than chasers $v_T/v_C > 1$, the weight average strategy improves the efficacy of escaping: the survival time has a maximum with an optimal weight exponent $w = 2$, and $k = 1$.

Recently, Janosov et al. have proposed a bio-inspired realistic agent-based model in continuous space and discrete time within closed boundaries for the case when the target is significantly faster than the chasers. Their framework includes three important and general features in various predator–prey systems: inertia, time delay and noise. In addition to the existence of an optimal number of chasers in two and three dimensions, their approach reproduces more realistic properties of pursuit observed in nature, such as emergent encircling and the target's zigzag motion [43].

Qualitatively different dynamics by the effect of time delay can also be demonstrated by extending the circular chase and escape problem introduced in section 2.3, with a state-dependent time delay (see Appendix B). In the problem, a target moves on a circular path with a constant velocity, while a chaser moves towards the target and tries to capture it. Here, we introduce a time delay τ for the chaser to recognize the position of the target, and τ is defined as an increasing function of the distance ρ between the chaser and the target as $\tau \propto \rho$. As a result, the chaser's

pursuit curve points to past positions of the target by the time τ. The dynamics of the chaser become exquisitely sensitive to the relative positions of the chasers and targets, and produce a complex chasing trail of the chaser [77].

The effect of time delay is also essential to model virtual stick balancing, an experimental paradigm for investigating complex visuomotor tracking tasks [67]. Here, trajectories of tracking a target resemble pursuit curves of a chaser (see Appendix C).

4.3.3.1 When Fluctuations Affect the Movements of Chasers/Targets

Fluctuations and noises inevitably arise and are widely relevant in a variety of systems. For example, predatory microbes hunt their prey by chemotaxis, in which they sense the concentration of a chemical which is secreted by the prey and diffuses through the space [90]. The signal of the chemical is typically noisy, and detection and decision-making by the predator are also implemented by inherently stochastic chemical reactions. Even though some biochemical signaling pathways can efficiently extract relevant information from the noise signals [54, 55, 47], the effect of fluctuations in their movements remains elusive.

We propose here another extension by modifying the motions of particles to introduce such fluctuations. In the original hopping rule, chasers/targets must choose the next site to decrease/increase distances to the nearest targets/chasers. We introduce fluctuations to these decisions. When a chaser chooses the next hopping site, the hopping probabilities are defined as follows. For each of the four nearest-neighbor sites, we define $\Delta l_i = \pm 1$ where i denotes the indexes of the four sites $(i = 1,2,3,4)$. If hopping to a site i decreases the distance to the nearest target, we assume $\Delta l_i = -1$. If it increases, we assume $\Delta l_i = 1$. Then, we define the hopping probability of the chasers as $p_i^C = \exp(-\Delta l_i/T_f)/\Sigma_i \exp(-\Delta l_i/T_f)$, where we introduce T_f as a "temperature". In the same manner, we define Δl_i for targets. When hopping to a site i increases the distance from the nearest chaser, we assume $\Delta l_i = 1$. If it decreases, we assume $\Delta l_i = -1$. We define the hopping probability for targets as $p_i^T = \exp(\Delta l_i/T_f)/\Sigma_i \exp(\Delta l_i/T_f)$.

When the temperature T_f is sufficiently high, the value of Δl_i is not relevant and the hopping probability is approximately equal to the random-walk model, i.e., the chasers/targets hop to one of the four neighboring sites, each with a probability $1/4$. As the temperature decreases, the hopping probability increases for chasers/targets to decrease/increase the distance, approaching the chase-and-escape model.

Fig. 4.22 shows the time for the entire catch T as a function of the temperature T_f for different numbers of initial targets N_T^0. The number of chasers N_C is fixed to 100. For all lines, on the left and right ends, the values of time for the entire catch are equal to those of the original chase-and-escape and random-walk models, respectively. In between, we found non-trivial behavior. When N_T^0 is small (for lower curves), the time monotonically increases from left to right. However, when N_T^0 becomes large to the order of N_C (for upper curves), they show a minimum around $T_f = 1$. Here, we note that the shapes of the distributions also change with T_f. But

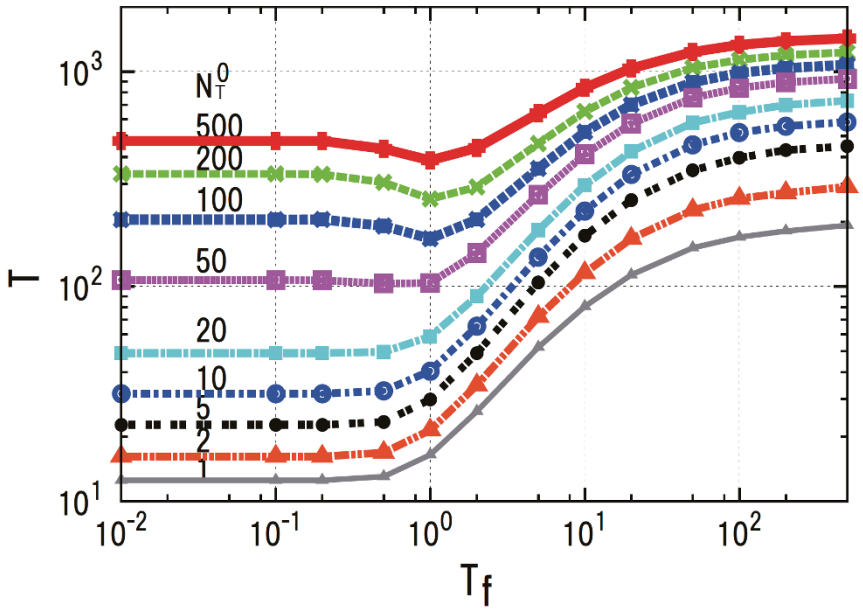

Fig. 4.22 Time for the entire catch, T, as a function of temperature T_f. Curves from top to bottom are for $N_T^0 = 500, 200, 100, 50, 20, 10, 5, 2, 1$. For all lines, we fix $N_C = 100$. Modified from [49] with permissions (© 2015 Springer Japan).

we confirmed that the distribution with $T_f \sim 1$ is clearly located at a smaller value of time compared to those of the chase-and-escape and random-walk models.

Interestingly, a certain amount of fluctuation reduces the time, making it easier for chasers to catch targets [46]. We may relate this observation to a phenomenon called "Stochastic Resonance" [103, 11, 28]. Stochastic resonance has been studied in various fields from the stance that an appropriate level of noise or fluctuation can provide constructive or beneficial effects. In particular, we note the similarity of collective effects of stochastic resonance with a simple model of a computer network traffic, where the appropriate level of fluctuation in the direction of passing packets by routers led to reducing the overall congestion of the network [76].

We also consider a case where chasers and targets have different "temperatures", respectively, T_f^C and T_f^T. In Fig. 4.23, we show the time for the entire catch as functions of T_f^C and T_f^T. When we change the temperature T_f^C for chasers with fixed T_f^T for targets, the time monotonically increase with T_f^C and it rapidly increases around $T_f^C = 1$. On the other hand, when we change T_f^T for targets with fixed T_f^C for chasers, the time monotonically decreases with T_f^T and, in particular, shows a rapid decrease around $T_f^T = 1$. The case where there exists a minimum around $T_f = 1$ in Fig. 4.22 is obtained by tracing the surface of T in Fig. 4.23 with $T_f^T = T_f^C$ (see the caption for details). This result suggests that the synchronous changes of

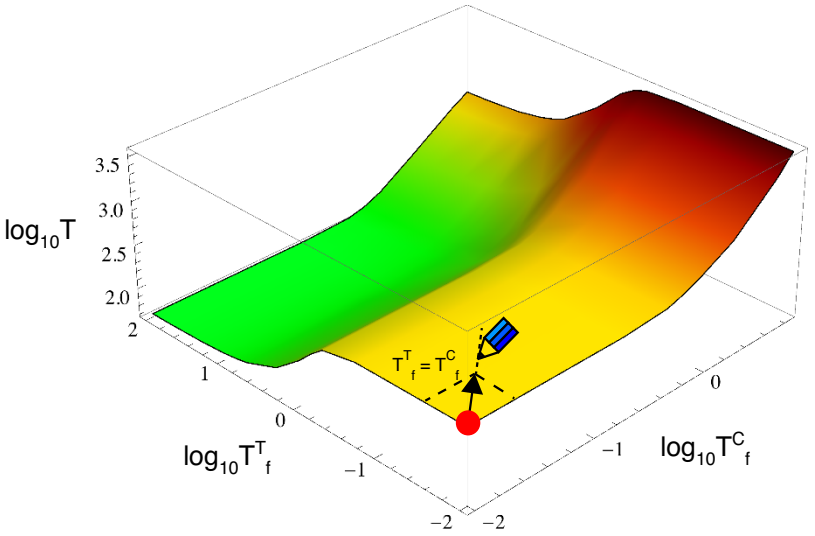

Fig. 4.23 Time for the entire catch, T, as functions of temperatures T_f^C and T_f^T. The case where there exists a minimum around $T_f = 1$ in Fig. 4.22 is obtained by tracing the surface of T by fixing $T_f^T = T_f^C$. Imagine that one draws a line on the surface, starting from the point $T_f^C = T_f^T = 10^{-2}$ (indicated by the red circle) to the direction of the arrow. At first, the values of the time T along the line are approximately constant (in the yellow region), but the line gradually penetrates into the green region, i.e., the time along the line decreases. Tracing the line further, it again enters the yellow region, thus, the time along the line increases. In this way, the time T has a minimum around $T_f^C = T_f^T = 1$ in Fig. 4.22. Here, we fix $N_C = 100$ and $N_T^0 = 200$. Modified from [49] with permissions (© 2015 Springer Japan).

the "temperatures" between chasers and targets are essential to achieve the non-monotonic dependence of the time in Fig. 4.22.

4.3.3.2 Interaction among Chasers

As another extension to motions of the basic model, we include a new element: a local communication among chasers such that the chasers do not get too close to each other. We name this extension the chasers' local interaction (CLI) strategy. It can be considered as an extension to reflect realistic situations. For example, this kind of intentional repulsion among chasers has been observed in real wolf-pack huntings [69]. A study to include such interactions in a simulation model with a single target is shown to reproduce some aspects of a wolf-pack hunting ethogram. We investigate the effect on the collective behaviors of group chase and escape.

The model is extended by adding a rule for the chasers' motion. A chaser focuses on the nearest player (chaser or target) and moves by the following rule.

(A) When the nearest player for the chaser 1 is a target 1, chaser 1 moves to a site to approach target 1.

(B) When the nearest player to chaser 1 is another chaser 2, chaser 1 moves to a site to get away from chaser 2.

Rule (A) is the same as in the basic model, while rule (B) is the new addition to introduce the repulsive interactions between chasers. Fig. 4.24 shows an example of this new rule.

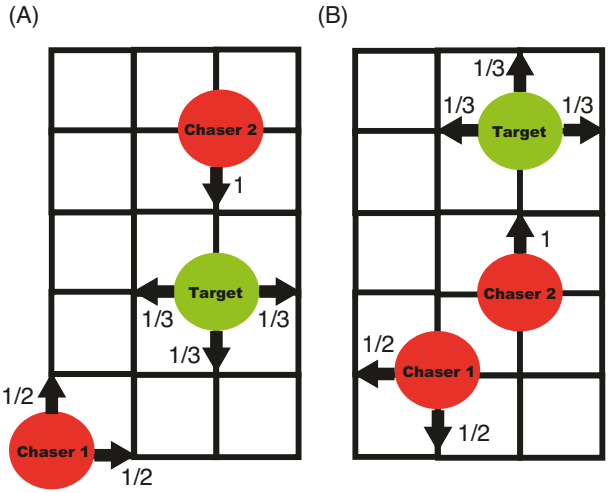

Fig. 4.24 Moving rules of chasers' local interaction (CLI) strategy for chasers (red circle) and targets (green circle). Solid arrows are the possible moving directions with indicated probabilities. (A) This is when the nearest neighbor to chasers is a target. Hence, chaser 1 and chaser 2 move to close in on the target, and chaser 1 has two choices and chaser 2 has one choice to move to the target in this example. (B) This is when the nearest neighbor for a chaser is another chaser. Hence, chaser 1 moves away from chaser 2, and chaser 1 has two choices to get away from chaser 2 in this example. Modified from [87] with permissions (© 2015 Elsevier B. V.).

We now present how this extension affects the collective behavior of the basic model. Numerical simulations are carried out using the basic model and the CLI strategy on a two-dimensional square lattice $L_x = L_y = 100$ with a periodic boundary condition.

First, let us show the spatial spread of chasers by the CLI strategy. Representative snapshots are shown in Fig. 4.25. They clearly indicate that the chasers with CLI strategy spread out over the field more than those in the basic model.

We next examine the difference quantitatively. Simulations are carried out for three different numbers of targets $N_T^0 = 10, 25$ and 50 with different number of chasers. Fig. 4.26 shows the time for the entire catch T and the cost function $c = N_C T / N_T^0$. They are averaged over 1000 individual runs.

We observe that when the numbers of the chasers are small, the CLI strategy works more effectively than the hopping rule in the basic model, i.e., the time for entire catch T are reduced from the basic model for each N_T^0. This suggests that the spatial spread of chasers as observed in Fig. 4.25 effectively help surround the

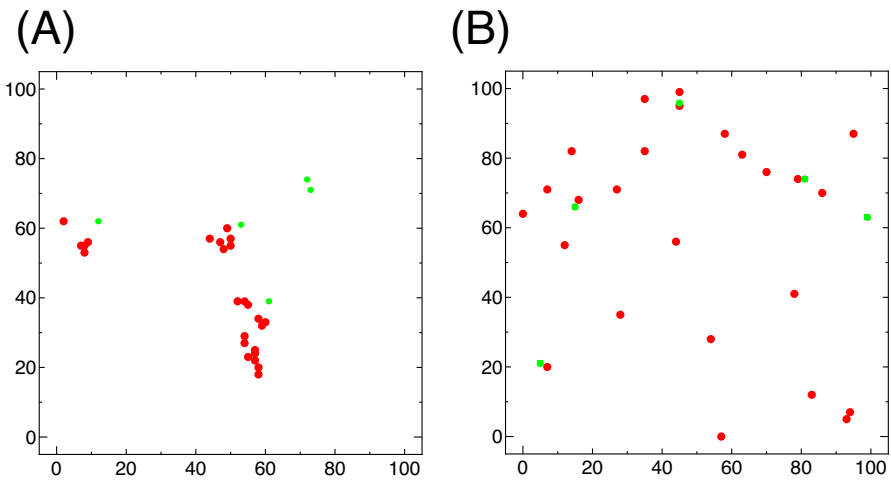

Fig. 4.25 Typical snapshots in (A) the basic model and (B) the model with the CLI strategy. The numbers of chasers N_C and the initial targets N_T^0 are 25. Red and green circles represent chasers and targets, respectively. The snapshots are at when the numbers of surviving targets decrease to $N_T = 5$. We can clearly see that approximately three aggregates of chasers are formed for the basic model, but no such aggregates are formed for the CLI strategy. Modified from [87] with permissions (© 2015 Elsevier B. V.).

targets and, consequently, chasers can complete the capture of all targets within a shorter time. Also, with the CLI strategy, the decrease of the time T by increasing the number of chasers is less evident compared to the basic model. On the other hand, when the numbers of chasers are large, the CLI strategy performs worse than the basic model, i.e., it takes more time to catch all targets than the case in the basic model. In this case, the field is substantially covered by chasers so that the CLI strategy appears to obstruct other chasers' movement rather than spreading. Hence, direct motions to the targets work better for chasing than spatial spreading of chasers.

We also investigate how the numbers of remaining targets decrease with simulation steps in both cases. For the basic model, aggregates of chasers are formed as the number of targets decreases, and they effectively make it more difficult for the chasers to impound targets. Therefore, we expect that, as the number of remaining targets gets smaller, the simulation steps between successive catching events get longer.

Fig. 4.27 compares the number of the remaining targets along with the simulation steps for $N_T^0 = 10, 25$ and 50. At the beginning of each simulation, the number of remaining targets decreases linearly with simulation steps so that the chasers catch the targets at approximately constant step intervals in both the basic model and that with the CLI strategy. However, for the basic model, the steps it takes to catch next targets get remarkably long, as the number of remaining targets decreases (blue curve). Indeed, we observe that catching a few final targets takes up a large portion

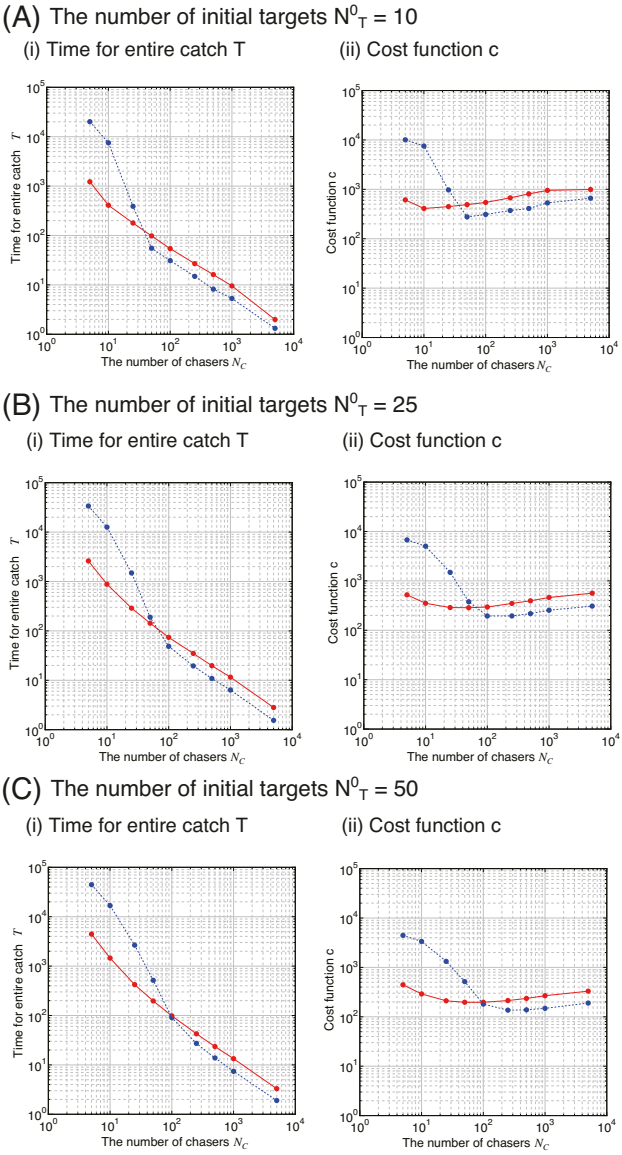

Fig. 4.26 For the three initial numbers of targets (A) $N_T^0 = 10$, (B) 25 and (C) 50, (i) the time for entire catch T and (ii) the cost function c as a function of the number of chasers N_C are shown, where the solid curve (red) is for the model with the CLI strategy and the dotted curve (blue) is for the basic model. The data is obtained for $N_C = 5, 10, 25, 50, 100, 250, 500, 1000$ and 5000. Note the logarithmic scale. Modified from [87] with permissions (© 2015 Elsevier B. V.).

of the total time for entire catch T, when the initial number of targets is less than the number of chasers. On the other hand, for the model with the CLI strategy, the chasers catch the targets approximately at a constant rate throughout the simulations.

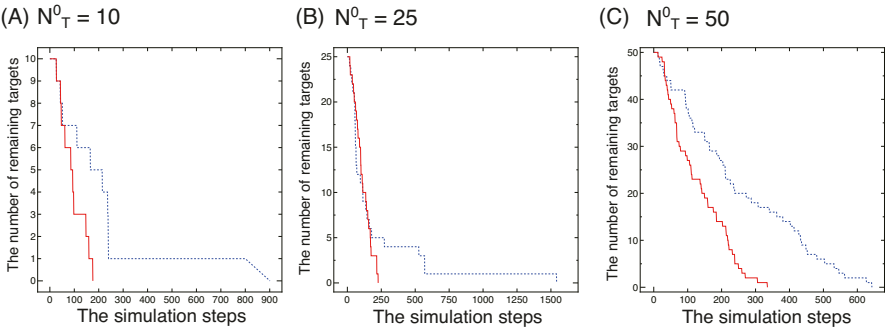

Fig. 4.27 Evolution of the number of remaining targets. The initial numbers of targets N_T^0 are (A) 10, (B) 25, and (C) 50. The solid curve (red) is the model with the CLI strategy and the dotted curve (blue) is for the basic model. For all cases, $N_C = 25$. Modified from [87] with permissions (© 2015 Elsevier B. V.).

When the number of chasers is large, on the other hand, the CLI strategy gives negative effects, i.e., it takes more time to catch all the targets than the basic model. Fig. 4.28 shows how the number of remaining targets decreases along with the simulation steps: the original model surpasses the CLI strategy with increasing number of chasers.

Overall, the interaction among chasers to spread out over the field is more effective when their number is small. In particular, the effectiveness is notable at the final stage of catching a few remaining targets. On the other hand, with a substantial number of chasers, a strategy with direct motions toward targets works better. Investigation of the effect of switching the strategies between spreading and chasing in real examples is one of the perspectives to be investigated for possible applications of the model.

Here, we investigate the direct interaction among chasers to spread out over the field. In Appendix D, we discuss a possibility of such spreading, even in the absence of interactions, in relation to developing strategies in game theory.

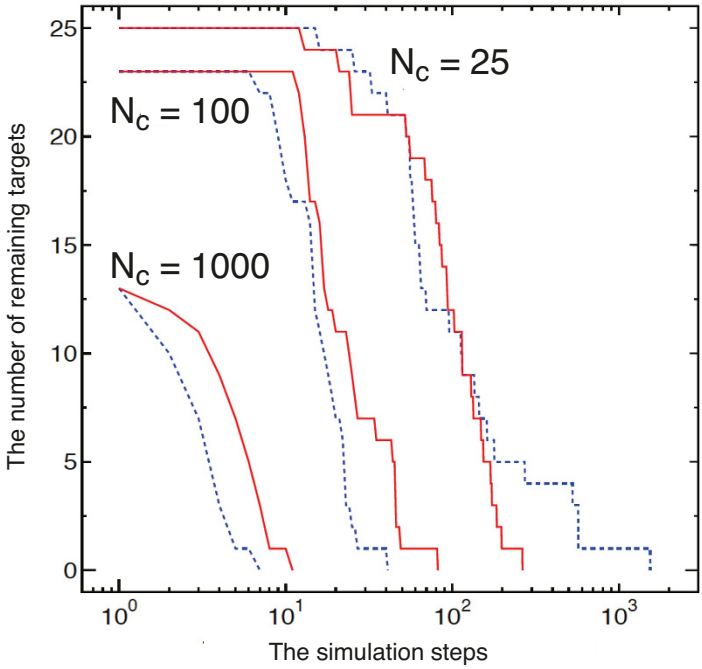

Fig. 4.28 Evolution of the number of remaining targets with different numbers of chasers N_C. The solid curve (red) is for the CLI strategy, and the dotted curve (blue) is for the original model. The initial number of the targets is $N_T^0 = 25$. Modified from [87] with permissions (© 2015 Elsevier B. V.).

Chapter 5
Potential Applications and Challenges

5.1 Introduction

We have reviewed in Chapter 4 the basic model and its extensions of group chase and escape. Naturally, there are still a fair number of open problems and directions relating to the topic ranging from realistic modelings for applications of the results to empirical observations in both technical and conceptual aspects.

In this final chapter, we discuss some of these issues relating to group chases and escapes and provide possible future directions for further developments. We start with theoretical issues relating to the basic model.

First, it is pointed out that the boundary conditions play crucial roles in chasing and escaping processes. The periodic boundary conditions we imposed in the basic model may not be as relevant to real situations where solid boundaries exist, and the effects of walls affect the results. However, the basic model still elucidates the general tendency of having an optimal number of chasers given the number of targets. Methods to evaluate more quantitatively the effects of boundary conditions need to be developed.

Second, characterizations of chasing patterns and their dependence on initial conditions are challenging issues. We observe two patterns of chasing: one is a linear formation chasing from one direction and the other is the surrounding formation around the targets. These patterns appear in a mixed manner, and sometimes co-exist over the field. We have introduced several quantities to characterize these; however, it is not trivial to fully characterize and quantify all the chasing patterns. In particular, some initial conditions are more likely to lead to a certain configuration pattern of chases and escapes. How the stability, as well as co-existence of multiple patterns, are linked to initial configurations is yet to be explored.

Third, possible developments of macroscopic continuum description of group chase and escape are discussed. The basic model we propose for chasing and escaping is based on microscopic units of chasers and targets. In contrast, the macroscopic continuum description in terms of spatial density and the average velocity is often useful for its numerical efficiency, analytical investigations and comparison

© Springer Nature Singapore Pte Ltd. 2019

A. Kamimura and T. Ohira, *Group Chase and Escape,*
Theoretical Biology, https://doi.org/10.1007/978-981-15-1731-0_5

with empirical data. We briefly review the macroscopic description for flocking and traffic models.

We then turn our attention to potential applications of group chases and escapes. The first possible example is hunting in nature. Even though it is not common, we have some species which perform cooperative hunting of prey, such as lions, wolves, and dolphins. Ethological and theoretical studies suggest the possibility that a rather simple set of rules is enough to explain the chases and escapes in reality. Also, the classical theoretical model of predator–prey systems is the Lotka–Volterra equation. It will be a promising problem to compare the behavior of group chase and escape models with the solutions of such differential equations. Nonlinear dependence of the efficiency of hunting on the size of groups, also observed in the basic model, is another interesting topic to explore further from ethological perspectives.

The second example is to apply the chase and escape processes to optimization problems. There have been numerous recent works in the field of Collective Intelligence and Swarm Intelligence, in which an interest of the field is whether intelligence can emerge from a large number of autonomous agents. One of the representative problems for such emergent intelligence is an optimization problem. We describe here one such attempt to apply the idea of group chases and escapes for the problems. In concrete, an algorithm is developed for a constrained combinatorial optimization problem called the Traveling Salesman Problem. The algorithm has shown some promise in that the idea of group chases and escapes could be generally utilized for optimization problems.

Finally, we provide a sketch of a broader perspective for the benefit of a pack and living together.

5.2 Issues of the Basic Model

5.2.1 Boundary Conditions

One of the relevant criticisms of the basic model is the boundary conditions. Their role is non-trivial in the chasing context. Strictly speaking, the periodic boundary condition we introduced in the basic model corresponds to the case of chases and escapes on a torus, a surface of revolution generated by revolving a circle in three-dimensional space about an axis coplanar with the circle. The geometry is ideal and convenient for simulating the system; however, applications to specific real situations would not be straightforward. For example, in the case of chasing, there may be an event such that an already escaped particle suddenly reappears at the back of the chasing group and it is the slowest chaser who may catch it. This kind of edge effect can also occur when motions of chasers and targets are restricted on a spherical surface.

On the other hand, what kind of boundary condition is appropriate is highly non-trivial and probably depends on aspects of the system one wants to investigate. If

one introduces fixed walls at the boundaries, events of the sudden appearance of agents, mentioned above, could be avoided. However, the effects of walls definitely affect the results because they introduce an additional way of pursuing; for example, the chasers can drive the target into a corner of the walls to catch it. This may reduce or enhance the effect of increasing the number of chasers studied in the basic model, and the shapes of the walls may also change the results.

The ambiguity of the boundary conditions suggests the difficulty of elucidating the general behavior of group chase and escape. One of the expectations in our attempt of the group chase and escape is that, even though the pursuit curves in one-to-one cases are highly sensitive to specific setups as outlined in Chapter 2, the introduction of a large degree of freedom (particles) results in a kind of regularity, analogous to that in statistical mechanics, in a sense that the behavior of the system does not depend on the details of the setup. One pessimistic view is, however, in the case of chasing and escaping, such a universal behavior does not exist. On the other hand, the general tendency of having the optimum number of chasers, given the number of targets, seems to exist in the different geometry of systems.

In any cases, quantitative methods to evaluate the relevance of the boundary conditions to specific problems remain to be developed for possible applications of the basic models to real problems.

5.2.2 Characterization of the Chasing and Escaping Processes

In order to understand the nature of the model, we introduce the time for catching all the targets from the initial conditions, and clarify the two distinct regions with different numbers of chasers (see Fig. 4.5). The quantity is intuitively reasonable as a measure of efficient chasing and escaping because objectives of the group of chasers and targets are, respectively, to decrease and increase the time, naturally reflecting the conflicting behavior of the system. However, the quantity is measurable only in cases that all the targets are captured in finite simulation times, and there may be other appropriate candidates to characterize typical chasing and escaping processes. In fact, how much the quantity is sensitive to the initial condition is still not sufficiently clarified. In the basic model, the distribution of the time has a single peak (Fig. 4.2) so that there seems no clear evidence that the initial condition drastically changes the time.

On the other hand, we found that there are two typical chasing patterns observed in our simulation. In pattern A in Fig. 4.9, a number of chasers follow a target in a linear formation. In pattern B in Fig. 4.9, a number of chasers surround a target, and a catch-up event typically follows. The two distinctive regions of the time correspond to how frequent the chasing pattern A appears, and more frequent appearance of pattern A prolongs the time because it takes more time to shift to surrounding the target to catch it.

One non-trivial perspective of the chasing and escaping processes is that if there may be a case that, in several independent and identical samples, some samples de-

velop chasing pattern A, i.e., it takes a longer time to catch the targets, while the other samples do not and all the targets are caught, maybe by pattern B, within a relatively short time. Then one may say that the chasing patterns within the former/latter samples share a kind of similarity, more than the samples between the former and the latter samples. In this case, the distribution of the chasing pattern takes a non-trivial form in the system, reflecting the existence of multiple stable configurations of chasing. Even though we do not find any clues to characterize such behavior in the basic model, the viewpoints may provide another promising direction of studying chasing and escaping.

5.2.3 Possibility of Developing Continuum Theory

The method of modeling we adopted in the basic model is based on simplified units (chasers and targets) to simulate the collective behavior of large ensembles. The approach has now a history, especially in statistical mechanics, in which particles originally represented atoms or molecules. Such "individual-based" modelings are becoming useful with the rapid increase in computing power and a growing appreciation of "simulations" to understand the system.

In parallel with the "microscopic" models, developments of macroscopic models are also of particular interest to explain the dynamics of the system. While the macroscopic models are restricted to describing the collective behavior in terms of the spatial density $\rho(x,t)$ and the average velocity $\mathbf{v}(x,t)$ as a function of the position x and time t, they are often preferred for their numerical efficiency, and their suitability for analytical investigations and comparison with empirical data.

Substantial efforts have been devoted to developing hydrodynamic equations in the field of collective motion. Here, we briefly introduce two representative examples for flocking and traffic flow.

The first theory for the Vicsek model was introduced by Toner and Tu [97]. Analogous to the Navier–Stokes equation, they derived the continuous, long-wavelength description by writing down the general equations of motion for the velocity field $\mathbf{v}$ and density ρ consistent with the symmetries and conservation laws of the problem.

The only symmetry of the system is rotation invariance: all the directions of space are equivalent to other directions. It suggests that the continuous equations of motion cannot have a special direction a priori. In addition, it is noteworthy that the model does not have Galilean invariance, that is, changing the velocities of all the particles by a constant velocity does not leave the model invariant.

By keeping only the lowest-order terms in spatial gradients and time derivatives of $\mathbf{v}$ and ρ, the resulting equations are

$$\begin{aligned}&\partial_t \mathbf{v} + \lambda_1 (\mathbf{v}\cdot\nabla)\mathbf{v} + \lambda_2 (\nabla\cdot\mathbf{v})\mathbf{v} + \lambda_3 \nabla\left(|\mathbf{v}|^2\right)\\ &= \alpha\mathbf{v} - \beta|\mathbf{v}|^2\mathbf{v} - \nabla P + D_L \nabla(\nabla\mathbf{v}) + D_1\nabla^2\mathbf{v} + D_2(\mathbf{v}\nabla)^2\mathbf{v} + \xi,\end{aligned} \tag{5.1}$$

$$P = P(\rho) = \sum_{n=1}^{\infty} \sigma_n (\rho - \rho_0)^n \tag{5.2}$$

and

$$\partial_t \rho + \nabla (\rho \mathbf{v}) = 0. \tag{5.3}$$

In Eq. (5.1), D_L, D_1, D_2 are diffusion constants and ξ is an uncorrelated Gaussian random noise. The λ terms on the left-hand side of the equation are the analogs of the convective derivative of the coarse-grained velocity field $\mathbf{v}$ in the conventional Navier–Stokes equation. Here, the absence of Galilean invariance allows the terms with λ_2 and λ_3, in addition to the term with λ_1. If the Galilean invariance holds, it requires $\lambda_2 = \lambda_3 = 0$ and $\lambda_1 = 1$. The terms with $\alpha, \beta > 0$ enable the equation to have a solution of $\mathbf{v}$ with non-zero magnitude, corresponding to the ordered phase. The pressure P depends on the local density only as Eq. (5.2), where ρ_0 is the mean of the local number density, and σ_n denotes a coefficient in the pressure expansion. Eq. (5.3) represents the conservation of mass (the number of particles).

The first macroscopic traffic model was developed by Lighthill and Whitham [58], and Richards [85]. Their fluid-dynamic model is based on the fact that the number of vehicles is constant in a one-dimensional lane. This conservation of vehicles leads to the continuum equation

$$\frac{\partial \rho(x,t)}{\partial t} + \frac{\partial Q(x,t)}{\partial x} = 0, \tag{5.4}$$

where $Q(x,t) = \rho(x,t)V(x,t)$ is the product of the density $\rho(x,t)$ and the average velocity $V(x,t)$, indicating the traffic flow per lane.

If one introduces the total derivative

$$\frac{d}{dt} = \frac{\partial}{\partial t} + V \frac{\partial}{\partial x}, \tag{5.5}$$

describing temporal changes in a coordinate system moving with velocity $V(x,t)$, then Eq. (5.4) is rewritten as $d\rho(x,t)/dt = -\rho(x,t)\partial V(x,t)/\partial x$. From this, one can conclude that the vehicle density increases in time ($d\rho/dt > 0$), when the velocity decreases in the course of the lane ($\partial V/\partial x < 0$), and vice versa.

The first steady-state speed density relation was introduced by Greenshields, who proposed a linear relationship,

$$V(\rho) = V_{max} \left(1 - \frac{\rho}{\rho_{max}} \right), \tag{5.6}$$

where V_{max} is the maximum velocity and ρ_{max} is the maximum density of the road.

By inserting $Q(x,t) = \rho(x,t)V(x,t)$ into Eq. (5.4), we obtain

$$\frac{\partial \rho}{\partial t} + U(\rho) \frac{\partial \rho}{\partial x} = 0, \tag{5.7}$$

where

$$U(\rho) = \frac{dQ}{d\rho} = V(\rho) + \rho \frac{dV}{d\rho}.$$

This is a nonlinear wave equation to describe the propagation of kinematic waves with velocity $U(\rho)$. Because $dV(\rho)/d\rho < 0$, $U(\rho) < V(\rho)$. Thus, the kinematic waves always propagate backward with respect to the average velocity $V(x,t)$ of the traffic, with the speed $u(\rho) = U(\rho) - V(\rho) = \rho dV(\rho)/d\rho \leq 0$. The $U(\rho)$ is the speed of the characteristic lines and depends on density. Because the speed in congested areas is lower, the characteristic lines intersect. This gives rise to changes of wave profile and to the formation of shock waves.

The macroscopic models are often very instructive and sometimes useful for analytical investigations and numerical efficiency. Development of macroscopic models to explain aspects of chasing and escaping in terms of the spatial density and the average velocity remains one of challenging and potentially important future problems for applications of our results.

5.3 Potential Applications

5.3.1 Hunting in Nature

Here, we briefly review the works in classical and ethological studies on hunting in nature, and appreciate the importance of group size.

5.3.1.1 Wolf-Pack

In nature, situations relating to chases and escapes arise in predator–prey interactions and hunting. Though it is not common, group or cooperative hunting has been observed in certain species. Examples include lions [93], wild dogs [21], wolves [66], bottlenose dolphins [29], and Stegodyphid spiders [79]. Observations of hunting behaviors by these species have been performed to understand what kinds of communications and interactions exist to make such cooperations possible.

As a representative example, we briefly describe a computational model of wolf-pack hunting [66]. Northern gray wolves are known to perform group hunting on moose and bison. It has been argued that cooperation and social hierarchies in packs increase the efficiency of hunting prey. The basis of these arguments is two types of hunting behaviors: ambush and relay chasing. Ambush is the strategy that one or more wolves hide and wait for prey being chased by other pack members. Relay chasing is a cooperative and continuous chase where multiple members in the pack take alternate turns to play different roles.

In a recent work [69], however, a hypothesis is proposed that the wolf-pack hunting is rather a collective emergent motion arising from simple rules. In other words,

the hypothesis argues that no sophisticated mechanisms are necessary such as intentional behavior, high skills of communication, and the social hierarchy for wolf-pack hunting. This view is similar in spirit to the mathematical models of Boids and the Vicsek model.

To justify the hypothesis, the authors proposed two rules for each member in a wolf pack [69]. Here, each wolf in the pack is assumed to follow these rules autonomously.

Rule 1: A wolf moves towards the prey until a pre-determined minimum safe distance to the prey is reached.

Rule 2: Once the wolf reaches the safe distance, it moves away from the other wolves at the safe distance.

They performed computer simulations to analyze a case of wolf-pack behavior in which there are a single prey and several wolves. Here, they assume that the speed of wolves is faster than that of the prey.

The formation of the pack depends on initial positions of the wolves and the motion of the prey. When the pack is located far away from the safe distance, the wolves move directly toward the prey. If the prey does not move, then as the pack reaches the safe distance, they start to spread over a circle centered at the prey. This is analogous to the encircling formation observed in real wolf-pack hunting.

On the other hand, relay chasing hunting and ambushing formations arise depending on the way the prey moves.

Thus, some of the wolf-pack behavior can be explained without assuming intelligent communication and social hierarchy in a pack. It will be interesting if their work is extended to consider cases of multiple prey. Then, it would be an example of group chases and escapes which can be compared with observations in the real world.

5.3.1.2 Lotka–Volterra Equations

Natural predator–prey systems have been attracting much interest and the most commonly known classical model is the Lotka–Volterra equations. The equations are a pair of first-order nonlinear differential equations to describe the population dynamics of prey and predators:

$$\frac{dx}{dt} = ax - bxy,$$
$$\frac{dy}{dt} = cxy - dy,$$

where x and y are the number of prey and predators, respectively, and a, b, c, and d are positive parameters.

The first equation describes the dynamics of prey. The model assumes an unlimited food supply, and the prey reproduce exponentially unless subject to predation:

the first term ax represents the assumption. The rate of predation is assumed to be proportional to the rate at which the predators and the prey meet, represented by the term bxy. The second equation describes the dynamics of the predator. In the equation, the first term cxy represents the growth of the predator population. Here, the different constant c is used because the rate at which the predator population grows is not necessarily equal to the rate at which it consumes the prey. The second term dy represents the loss/death of the predators. The equations have periodic solutions and both prey and predators coexist.

Because of the advances of computer technology, the commonly used model schemes shifted from population dynamics based on differential equations to discrete individual-based models. Still, the differential equations play essential roles to explain some aspect of the individual-based model. For example, the log-normal distribution of time for the entire catch T (for $N_C = 100$ and 500 in Fig. 4.2 of Chapter 4) can be explained as follows. One can write the differential equations corresponding to the setup of the basic model in which the number of targets decreases by encounters with the chasers. If we denote the number of chasers and targets, respectively, by n_C and n_T, the decreases in n_T are written as

$$\frac{dn_T}{dt} = -kn_C n_T,$$

where k is a rate constant. The number of chasers remains a constant so that the solution for n_T gives $n_T = n_T(0)\exp(-kn_C t)$. By rewriting the equation as $d\log(n_T)/dt = -kn_C$, one can see that the quantity $\log(n_T)$ decreases by the constant rate kn_C. If one assumes that the constant rate fluctuates with a normal distribution by stochastic elements of the system, the number of targets n_T exhibits a log-normal distribution.

5.3.1.3 Cooperative Hunting - Relevance of Group Size

The Lotka–Volterra equations assume that the rate of hunting events is proportional to the number of predators. It might be intuitively reasonable to assume that the rate is proportional to the number of predators if solitary hunting is dominant. However, the effect of interactions among predators, i.e., cooperative hunting, could give rise to non-trivial nonlinear effects.

Actually, previous field studies have reported that increases in group size above a certain threshold reduce their success per capita. Data from a range of social predators suggest that success initially increases, then levels off, or even declines with group size despite apparent cooperation among predators. Several studies show that carnivore hunting success peaks at 2–5 hunters and remains constant or declines over larger group sizes [79, 60].

Two relevant factors are commonly accepted for the nonlinear dependence: interference and free-rider. The interference factor explains the nonlinear dependence because individual predators impede each other's actions. Even if the predators are proficient, simple overcrowding of predators can inhibit the ability of each predator

and consequently, the hunting success can reach a limit or be reduced. The free-rider can also contribute to the dependence because in large groups individual predators withhold effort to participate in successful hunting while remaining nearby to get access to the prey.

5.3.2 Optimization Problems

Along with increasing interest in collective motions, emergence of intelligence from a large number of autonomous agents is actively explored in the field of artificial intelligence. Such a direction of research is called Collective Intelligence [61] and Swarm Intelligence [35]. Researchers from various fields of robotics, information sciences, control engineering, biology, and physics are joining to expand the developing research area. We briefly present here one application of group chases and escapes in this direction.

One of the main problems in the field is called a constrained combinatorial optimization problem, in which the objective is to find the minimum (or maximum) of a target function. Often, local updating algorithms are employed to incrementally search for the minimum state. The main difficulty associated with such algorithms is, however, the existence of multiple local minima in the target function. Through the course of incremental optimization, it is commonly difficult for the system to escape from the local minima because one cannot find incrementally better states or combinations by local updating rules at these local minima, even though there exists the global optimum state. Thus, providing a solution to overcome this problem to reach the global optimum is one of the main issues, and various algorithms such as simulated annealing [53, 14] have been developed.

Let us consider here one such representative example of the constrained optimization problems, namely, the Traveling Salesman Problem [18]. A task for the salesman is to travel multiple N cities once and only once, but the salesman wants to minimize the total traveling path length, thus, the length represents the target function. The problem is easily solved when N is small because one can compare all the possible paths, but it becomes considerably difficult with increasing N as the number of possible paths increases explosively.

We number all the N cities by integers $(1,2,...,N)$, and each possible path to visit all the N cities is represented by a permutation of the N numbers. For each possible path, we refer to a state and a "cost" is defined as the total traveling path length. The task is to find a permutation (a path) with the minimum cost, out of $(N-1)!$ permutations. Here, each closed path is represented by N permutations (the salesman would return to the starting city, and the N permutations represent the same closed path with different starting city). Thus, the number of possible different paths is $N!$ divided by N, i.e., $(N-1)!$.

Methods of local updating of states have been developed to find the optimum path [59]. One example of local updating is to pick two cities randomly and exchange their position as a permutation. If the permutation leads to a shorter total

path length, we accept the new state, otherwise discard it. We repeat this process aiming to minimize the total path length. However, the state is commonly trapped at a local minimum state (permutation) from which one cannot improve the target function by the same updating rule.

To overcome the problem, an idea is employed from group chase and escape [78] (see Fig. 5.1). First, we prepare several states (permutations) and calculate their path length. Then, we designate the best state with the shortest length as an escapee and all the other states as chasers. For each round of updating, the escapee performs the local updating for a better state with a shorter length, while the chasers update their state so that they approach the escapee by a prescribed distance measured between permutations. After the updating, we evaluate all the states and choose the best one with the shortest length to be the escapee for the next round. This process is repeated until a steady state is achieved. We expect that the states assigned as the chasers may find a better state during their approaches to the escapee, and can help avoid the trapping problem with local minima.

We apply the above algorithm to the Traveling Salesman Problem with 52 cities, for which the shortest path is known.[1] Fig. 5.2(A) shows the known shortest path which length is approximately 7544. On the other hand, Fig. 5.2(B) shows one example of the path obtained by the proposed algorithm with chase and escape. To highlight the overlap between the two lines, the two paths are shown together in Fig. 5.2(C).

Also, we evaluate the proposed algorithm by comparing with simple parallel multiple searches, given the same number of initial states, in Fig. 5.3. The algorithm with chase and escape performs better because it finds a shorter path faster than the simple algorithm.

The algorithm with chase and escape can be extended in various directions. For example, we can assign multiple escapees in addition to the best one with the shortest length. Also, a combination with other optimization algorithms such as the simulated annealing [53, 14] can be envisioned. Further applications of group chases and escapes are expected not only in optimization but also to other problems in engineering.

[1] The following website has a collection of Traveling Salesman Problems. We have used one with 52 cities, named in the list as berlin52.tsp and berlin52.opt.tour. http://elib.zib.de/pub/Packages/mptestdata/tsp/tsplib/tsp/index.html

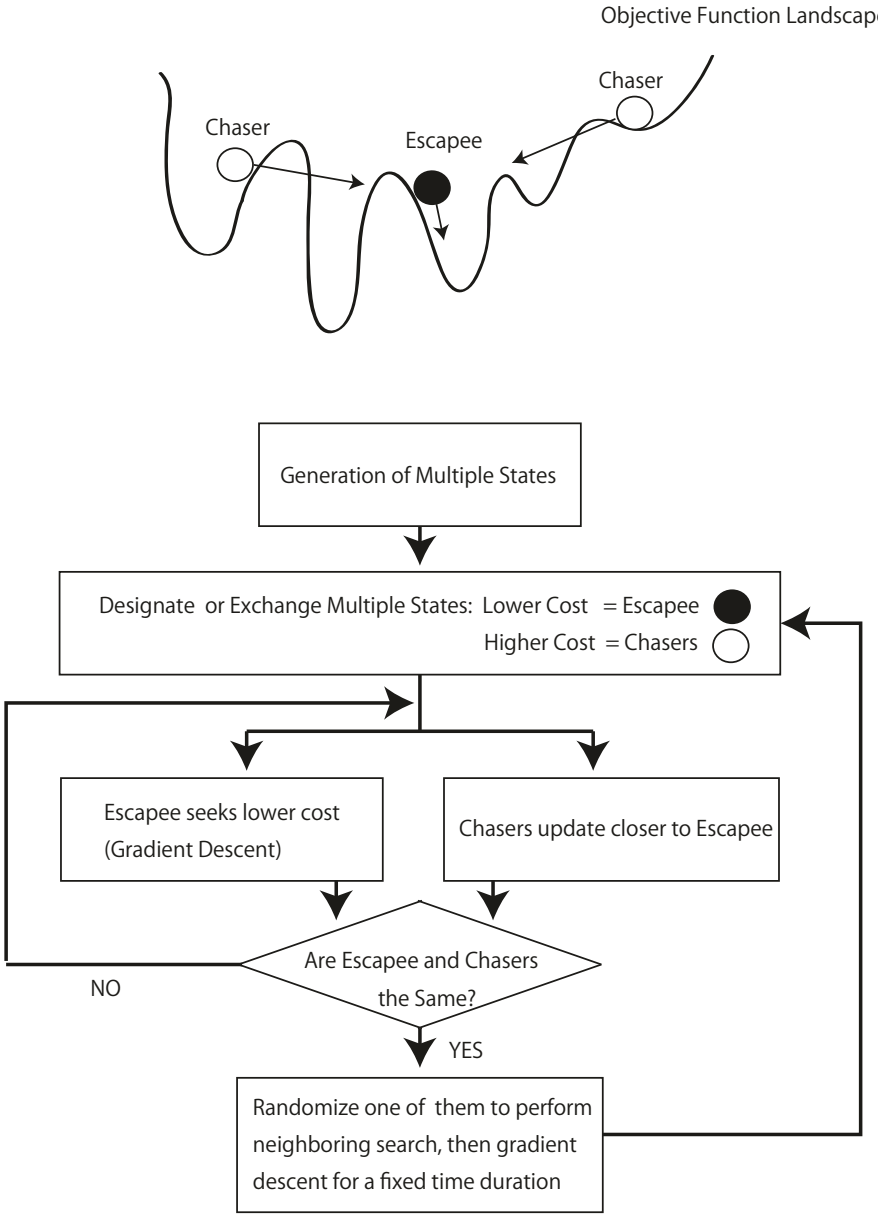

Fig. 5.1 Implementation of chase and escape to the optimization problem of finding the global minimum of the target function. Modified from [78] with permissions (© 2015 International Society of Artificial Life and Robotics).

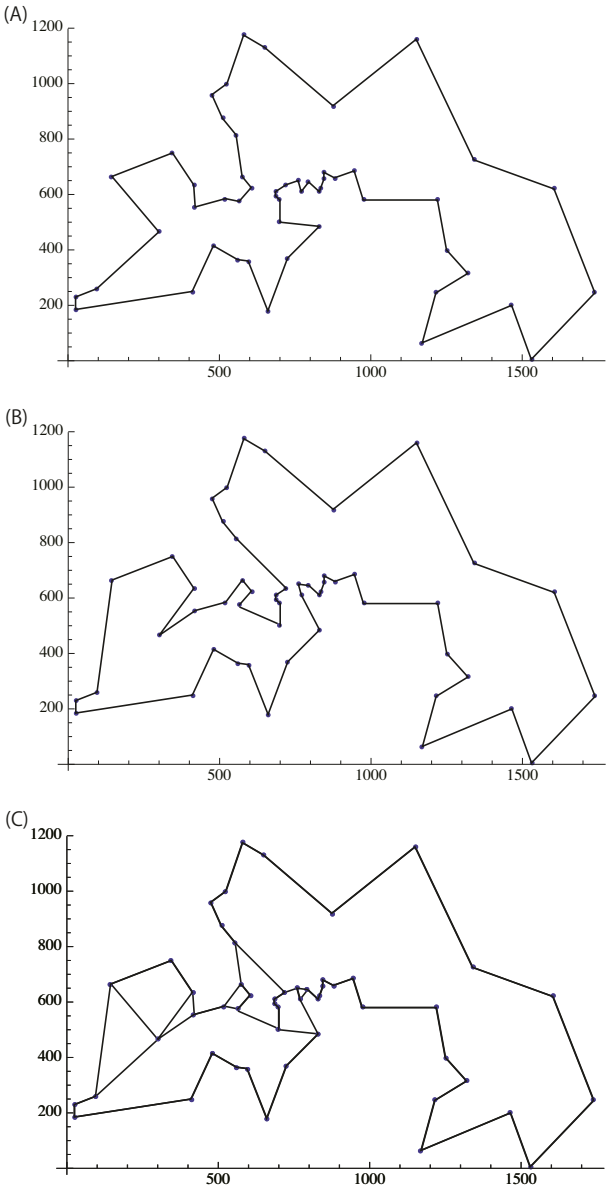

Fig. 5.2 Traveling Salesman Problem with 52 cities. (A) The line shows the known shortest path. This optimal path length is approximately 7544. (B) One example of the path for the problem obtained with our algorithm using chase and escape. This path length is approximately 7940. (C) The two paths in (A) and (B) are shown together to highlight the overlap. Modified from [78] with permissions (© 2015 International Society of Artificial Life and Robotics).

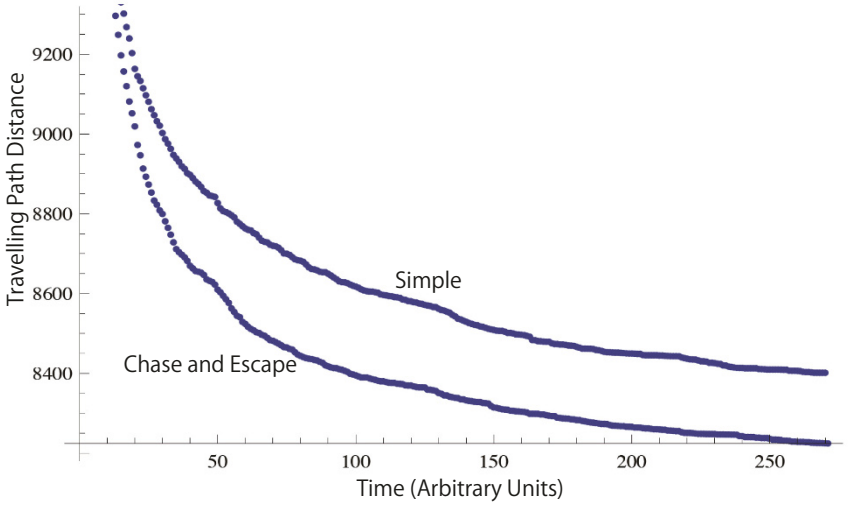

Fig. 5.3 The path distance length generated in time by the "Simple" and "Chase and Escape" algorithms. The algorithm with chases and escapes performs better because it finds a shorter path faster than the simple algorithm. Modified from [78] with permissions (© 2015 International Society of Artificial Life and Robotics).

5.3.3 A Sketch

To provide a general perspective on the power of living together, we quote here from *Crowds and Power* by Elias Canetti [13]. The work was based on empirical observations and studies from psychological and anthropological viewpoints.

> From earliest times the pack has had *four* different forms, or functions. They all have something fleeting about them, and each changes easily into another, but it is important to determine first of all the respects in which they differ. The truest and most natural pack is that from which our word derives, the hunting pack; and this forms wherever the object of the pack is an animal too strong and too dangerous to be captured by one man alone. It also forms whenever there is a prospect of a mass of game, so that as little as possible of it shall be lost. If the slaughtered animal is very large, a whale or an elephant for example, its size means that it can only be brought in and divided up by numbers of men working together, even if it was originally struck down by one or two individuals. Thus the hunting pack enters the stage of *distribution*. Distribution need not always be preceded by hunting, but the two stages, or states, are closely connected and should be examined together. The object of both is the *prey*; and the prey alone, its behaviour and nature, whether alive or dead, determines the behaviour of the pack which forms with it as object.
>
> The second type of pack is the war pack, and this has much in common with the hunting pack and is, indeed, connected with it by many transitional states. It postulates a second pack of men, and is always directed against what it feels to be one, even where this has not yet had time to form. In earlier times its object was often a single life, one man on whom it had to take revenge. In the certainty with which it knows its victim it comes particularly close to the hunting pack.

> The third type is the *lamenting pack*. This forms when a member of a group is torn from it by death. The group is small and feels every loss as irreplaceable, and unites for the occasion into a pack. It may be primarily concerned with keeping back the dying man, or with snatching from him, before he disappears completely, as much of his life as it can incorporate into itself; or it may want to propitiate his soul so that it does not become an enemy to the living. In any case, action of some kind is felt to be necessary, and there are no human beings anywhere who forgo it entirely.
>
> Fourthly, I shall summarise a variety of phenomena which, in spite of all their diversity, have one thing in common: the intent to increase. Increase packs are formed so that the group itself, or the living beings, whether plants or animals, with which it is associated, should become more. They manifest themselves in dances to which a definite mythical significance is attributed. Like the other packs they are found everywhere where there are men living together; and what they express is always the group's dissatisfaction with its numbers. One of the essential attributes of the modern crowd, namely its urge to grow, thus appears very early, in packs which are not themselves capable of growth. There are rites and ceremonies which are intended to compel growth and, whatever one may think of their effectiveness, the fact remains that, in the course of time, they have resulted in the formation of large crowds.

The group chase and escape we proposed in this book would be mainly categorized into an attempt to model the first type of pack, the hunting pack. Besides, the vampire problem presented in section 4.3.2.1 may also include the form of the increase pack because the chasers pursue the targets in order to increase their group.

Recent works by one of the authors [45, 48, 50] highlight the benefit of being together in the form of the increase pack. The works specifically consider how a few biomolecules got together to increase at the primitive stage of life. To increase the molecules, each of the molecules should be properly replicated so that the sequences of the polymer molecules are copied to transfer the information. The simplest reaction scheme for such a replication is $X \rightarrow 2X$, in which the replication of the molecule X occurs with the template molecule X to produce another copy of X (Fig. 5.4A). This results in exponential growth of the population. How such complex molecules capable of self-replication could have first arisen attracts much interest because this kind of reaction is the basis for one of the main hypotheses on the origin of life, namely, the RNA world [30] which premises that self-replicating molecules precede the beginning of life.

There are still, however, a number of conceptual problems even if one assumes, in any way, such a self-replicating molecule appeared. First, the self-replication process is much harder than one might guess because numerous copying errors, or mutations, arise. At the primitive stage of life, inevitable copying errors occur. Because typical functional molecules are substantially long enough and most of the errors hinder the molecule's ability, the bad mutations accumulate over time and it fails to continue replicating the sequences to maintain the functions. This problem is called error catastrophe [23].

Theoretical studies have shown that such a problem can be avoided if different kinds of molecules catalyze the replication of each other [24, 25]. For example, instead of one type of molecule, there could have been two types (X and Y), each of them able to duplicate itself only if the other one was present as

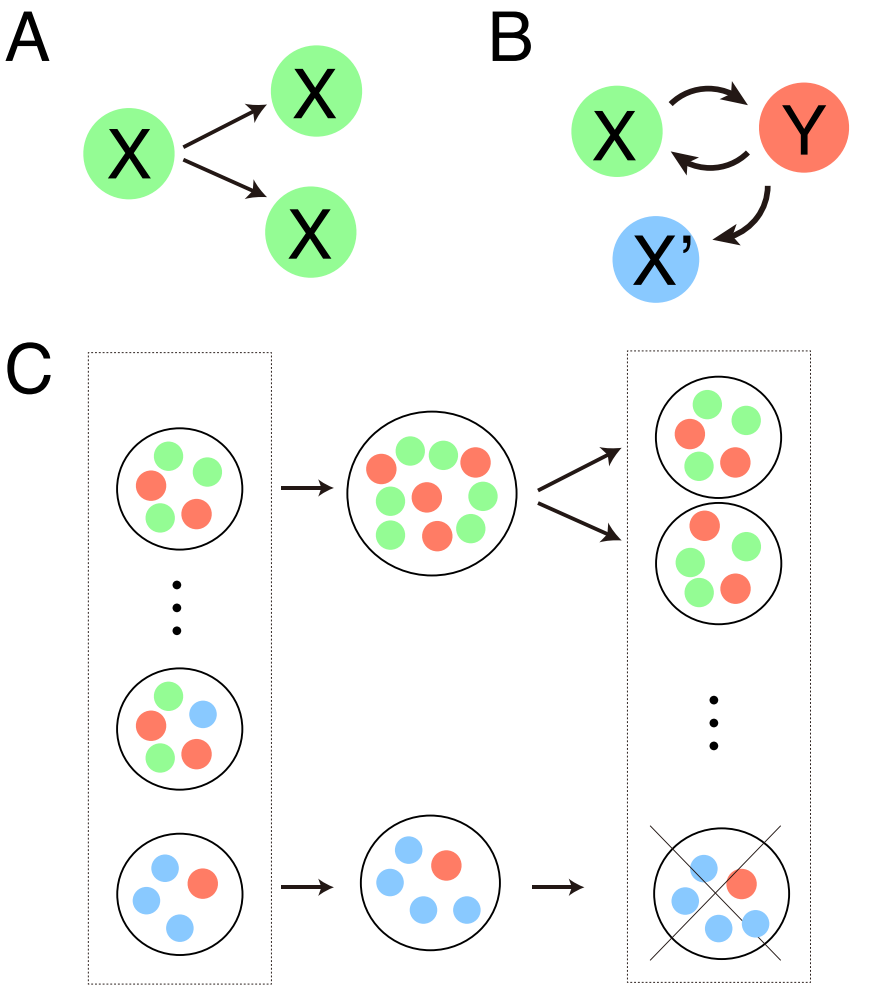

Fig. 5.4 (A) The simplest scheme for a replication is $X \rightarrow 2X$, in which the replication of the molecule X occurs with the template molecule X to produce another copy of X. (B) Two types of molecules (X and Y) are able to duplicate themselves with the aid of the other type. The parasites (X') also duplicate with the aid of the other type (Y), but they do not help the other's replication. (C) If the system is compartmentalized into a number of "protocells", the cells with good copies can continue growth, while those dominated by parasites cannot grow and are selected out.

$$X + Y \rightarrow 2X + Y, \quad Y + X \rightarrow 2Y + X. \tag{5.8}$$

Here, the pair of molecules can increase in proportional to the square of the concentrations. By this way, errors would not accumulate because when one molecule produced a defective copy of itself, that copy would not help the second molecule to

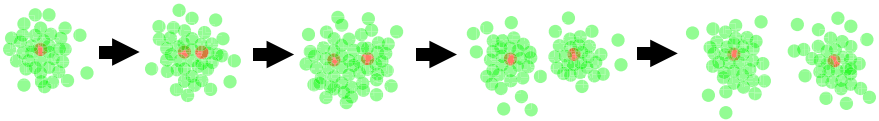

Fig. 5.5 Schematics of the behavior after the replication of Y. The green semitransparent particles represent the X molecules. The red particles represent the Y molecules, located deep within the clusters. Time evolves from the left to the right.

replicate. Then, the concentration of the second molecule would fall, and as a result, the ability of the defective first molecule to replicate decreases.

But this model also has a problem because many parasitic copies could still be replicated with the help of others, while the parasites do not help the other's replication (X' in Fig. 5.4B). Such parasites increase and dominate the space, therefore, finally resulting in keeping the good copies from reaching each other.

The introduction of compartment-level selection, in addition to the molecules' level, can find a way to overcome the problem of parasites [64, 95]. If the system is compartmentalized into a number of "protocells" [83], the cells with good copies can continue growth, while those dominated by parasites cannot grow and are selected out [Fig. 5.4C].

But how do the molecules get together and organize growth and divisions of such protocells, even in the absence of sophisticated mechanisms? To answer this, we consider the two types of molecules X and Y, catalyzing the replications of each other as in Eq. (5.8). Here, we give three essential assumptions: i) the replication rate of one type, say Y, is much slower and that of the other, X, is much faster; ii) the fast-replicating type X degrades faster while the slow type Y lasts longer, and iii) the molecules are giant so that the excluded volume effect is relevant.

Fig. 5.5 shows the behavior of the system under the assumptions. Here, replications of X (green) occur fast only where the Y molecules (red) are present. In contrast, the degradations of X are also fast so that X molecules diffused away from the Ys die out. This results in a formation of clusters of X molecules around each of the Y molecules. In the clusters, the molecules are crowded so that each interacts only with nearby molecules. In this sense, the clusters have the effect of compartments, and in fact, the clusters play the role of the units of selection: those with the good ones can grow, while those dominated by parasites cannot grow (see [45] for detail).

In addition, the cluster shows a division process synchronous with each replication of the slow molecule Y. When the replication of Y occurs, the two molecules of Y are in the crowd of X, and each helps the replications of X. Therefore, as the two Ys diffuse away to the size of the cluster, the number of X molecules distribute around each of the Y molecules. This completes the division process. Because the division occurs after the replication of Y, it appears as if the growth of the clusters is controlled by the minority species Y.

The relevance of “minority” is generally attributed to controllability and evolvability of the system. For example, a simple model suggests that in guiding animal groups, only a very small proportion of informed individuals is required to achieve great accuracy [20]. In the context of primitive cells, it is suggested that if the number of gene copies in the system is infinitely large, a “good” mutation in a gene is hindered by the majority of other genes so that there is no coupling of phenotype (growth) with genotype [56, 74]. Thus, Darwinian evolution is essentially stopped. The advantage of having multiple copies is also discussed because multiple copies can avoid a loss of the genes at division events when an accurate segregation mechanism of genes is absent. The above study suggests that the accurate segregation mechanism may be possible even at a primitive stage of life, i.e., earlier than when modern prokaryotes arose.

Appendix A
Discrete Search Game on Graphs

We introduce here a variation of chases and escapes called Discrete Search Games. In the problem, a target chooses one post from many finite distinct posts, and stays there to hide from a chaser. The chaser repeatedly hops from one post to another until he/she finds the target. In this context, the target and the chaser are often called the hider and the searcher, respectively.

The problem is formulated by a graph with vertices and edges. The vertices represent the posts, one of which is chosen by the hider to stay at. The searcher moves from one vertex to another only when they are connected by an edge. In other words, the game is a problem of chases and escapes on a graph, except that the hider does not move and the searcher does not recognize the location of the hider.

The purpose of the game for the hider is to hide as long as possible in general. On the other hand, that for the searcher is to find the hider in as small a number of hops as possible. Then, the main interest is the minimum number of hops, V, from the start of the game until the finding of the hider, given the network structure of the graph.

From the setup of the game, the following conditions are satisfied:

- The upper limit of V is given by the shortest path length with which all the vertices are visited by the searcher.
- V is finite.
- V depends on the structure of the graph, i.e., the number of vertices and how they are connected by the edges.

Here, we introduce the following three types of graphs; complete graph, cyclic graph, and linear graph (Fig. A.1). A complete graph is a graph in which every pair of vertices is connected by an edge. Thus, the searcher can hop from one to any other vertex. A cyclic graph consists of N vertices $\{x_1, x_2, x_3, \ldots, x_N\}$ such that a vertex x_i is only connected to x_{i+1} and x_{i-1} for $1 < i < N$. The vertex x_N is connected to x_{N-1} and x_1, and the vertex x_1 is connected to x_2 and x_N. Here, the searcher can hop only two neighboring vertices. A linear graph is obtained by deleting the edge between x_N and x_1 from the cyclic graph.

© Springer Nature Singapore Pte Ltd. 2019

A. Kamimura and T. Ohira, *Group Chase and Escape,*
Theoretical Biology, https://doi.org/10.1007/978-981-15-1731-0

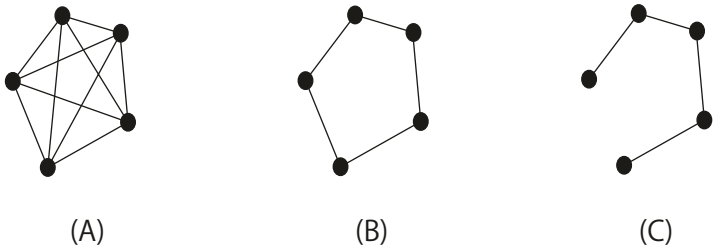

Fig. A.1 Three types of graphs for $N = 5$ vertices: (A) a complete graph, (B) a circular graph, (C) a linear graph.

Interestingly, it turns out that for all the above types of graphs, the value of V can be calculated explicitly as

$$V = \frac{1}{2}(N+1). \tag{A.1}$$

We sketch the outline of the proof in the case of the linear graph. Here, we assume that the hider chooses one vertex out of N vertices with equal probability of $1/N$. Let us denote the vertex as x_k $(1 \leq i \leq N)$. As the searcher does not recognize the position of the hider, the best strategy for the searcher is to minimize the path to cover all vertices. It is realized only for the two cases of starting from either end x_1 or x_N, and moving in one direction. If the searcher starts from x_1, then he/she can find the hider after k steps. On the other hand, if starting from the other end x_N, the hider is found after $N-k+1$ steps. Because the searcher should assume that the hider is at x_j in the ranges of $1 \leq j \leq N/2$ and $N/2 \leq j \leq N$ with the equal probability of $1/2$, the best strategy is to choose the two options accordingly. Then, the value of V can be calculated as

$$V = \frac{1}{2}k + \frac{1}{2}(N-k+1) = \frac{1}{2}(N+1). \tag{A.2}$$

For the case of the other two types of graphs, the searcher can have more options for his/her paths to visit the entire vertices. It can be shown, however, that the value of V is the same as in the case of the linear graph (see [86]).

Discrete search games on the graphs can be extended into different directions. One such example is to include a "missing" factor that the searcher fails to find the hider with some probabilities even though the hiding vertex is visited. One can consider such situations when the searcher is careless, or when the hider can occasionally escape from the searcher in some other way. Another extension is that the hider can also move among the vertices. One classic example is called the Monster–Princess problem, where the princess (the hider) moves in the hope that she can evade the monster (the searcher) for as long as possible. These extensions naturally complicate the problem and the solutions are more intricate (see [41] and [71]).

Appendix B
Chase and Escape with Delays

In this section, we introduce another extension of chases and escapes where delays in pursuits are present [77]. The factor of delays is inevitably present in reality because it takes a finite time to transmit a signal from an object. For example, if we point to the location of the sun in the sky, the position is actually where it was about eight and a half minutes in the past. Another example is a delay caused by maneuvering a ship or a plane to point to the position of the target.

Delays often bring rather complex behavior in dynamical systems, and various examples have been investigated. As a first step to consider delays in chases and escapes problems, we extend the circular pursuit problem discussed in section 2.3.1.

We introduce a state-dependent time delay into the original circular pursuit problem. It is assumed that the signal from the target takes some time (delay) to reach the chaser. Then, the chaser points not to the target's present position as in the original model, but to its past position by a time delay τ.

If τ is constant, then the problem can be mapped to the original problem with a different target's initial position. Thus the pursuit task is qualitatively unchanged: a constant delay is equivalent to the introduction of a fixed phase shift.

However, more complex behavior appears when τ is an increasing function of the distance ρ between the chaser and the target. To show this, we consider the simplest case: τ is a linear function of ρ as $\tau = \tau_0 \rho$, where τ_0 is a constant scale factor. Here, the chaser's precision in pointing to the target's position decreases in proportion to the distance between them.

We rely on computational simulations to investigate the extended model with state-dependent delays. Fig. B.1 shows the behavior of the chaser and the target as a function of τ. Increases of τ_0 lead to a variety of trajectories for the chaser with the target moving in the unit circular path.

We observe that, when the speed of the target is faster than that of the chaser, the chaser cannot catch the target, irrespective of the presence of delay (Fig. B.1b without delay and Fig. B.1e with delay). In contrast, when the speed of the target is slower than that of the chaser and without delay, the chaser can catch the target (Fig. B.1a). However, with the delay increases beyond a critical value, the chaser cannot

© Springer Nature Singapore Pte Ltd. 2019

A. Kamimura and T. Ohira, *Group Chase and Escape,*
Theoretical Biology, https://doi.org/10.1007/978-981-15-1731-0

catch the target (Figs B.1c, d, and f–h). As the delay increases, trajectories of the chaser can be quite complex (Figs B.1c–h).

As mentioned above, the complex trajectories of the chaser in Fig. B.1 arise because τ is a function of the distance ρ. To give an insight why the simple linear-dependency results in the complex trajectories, we consider a change in ρ by a movement of the chaser in a short time interval dt. If ρ increases, then τ increases in the next step. This decreases the chaser's precision for the target's position in the next time interval. On the other hand, if ρ decreases, then the chaser points to the present target's position more accurately. The change of ρ is determined only by the relative position of the chaser and the target. One expects that if the spatial distribution of the change is rough and saw-toothed, the trajectory of the chaser is inevitably complex because the chaser should change its velocity very frequently.

To visualize the spatial distribution, we take $(x_T, y_T) = (1,0)$ as the present position of the target. Here, we fix the radius of the circle $a = 1$. The chaser is located at $(x_C, y_C) = (r\cos\lambda, r\sin\lambda)$ (see Fig. B.2). The distance ρ between the chaser and the target is written as

$$\rho = \sqrt{(r\cos\lambda - 1)^2 + (r\sin\lambda)^2} = \sqrt{1 + r^2 - 2r\cos\lambda}.$$

The delay is defined as $\tau = \tau_0\rho$. By taking the angular velocity of the target as ω, the target's position in the past by time τ is given by $(x_T^\tau, y_T^\tau) = (\cos 2\pi\omega\tau, -\sin 2\pi\omega\tau)$, to which the chaser at (x_C, y_C) points its velocity. The direction of velocity of the chaser is written as

$$(v_x, v_y) \equiv (\cos 2\pi\omega\tau - r\cos\lambda, -\sin 2\pi\omega\tau - r\sin\lambda).$$

This, in turn, enables us to compute the position of the chaser with this velocity in the future by dt as

$$(x_C', y_C') = (r\cos\lambda + dtv_x/V, r\sin\lambda + dtv_y/V),$$

where $V = \sqrt{v_x^2 + v_y^2}/V_C$ and V_C is the speed of the chaser.

After time dt, the position of the chaser is at (x_C', y_C') as shown above, and that of the target is approximated to the first order in dt as $(1, 2\pi\omega dt)$. Then, we derive the distance ρ' between them at time dt as

$$\begin{aligned}\rho' &= \sqrt{(r\cos\lambda + dtv_x/V - 1)^2 + (r\sin\lambda + dtv_y/V - 2\pi\omega dt)^2} \\ &= \sqrt{\rho^2 + \Delta\rho},\end{aligned}$$

where

$$\Delta\rho = \left\{v_x^2/V^2 + (v_y/V - 2\pi\omega)^2\right\}dt^2 + 2\left\{v_x(r\cos\lambda - 1)/V + (v_y/V - 2\pi\omega)r\sin\lambda\right\}dt.$$

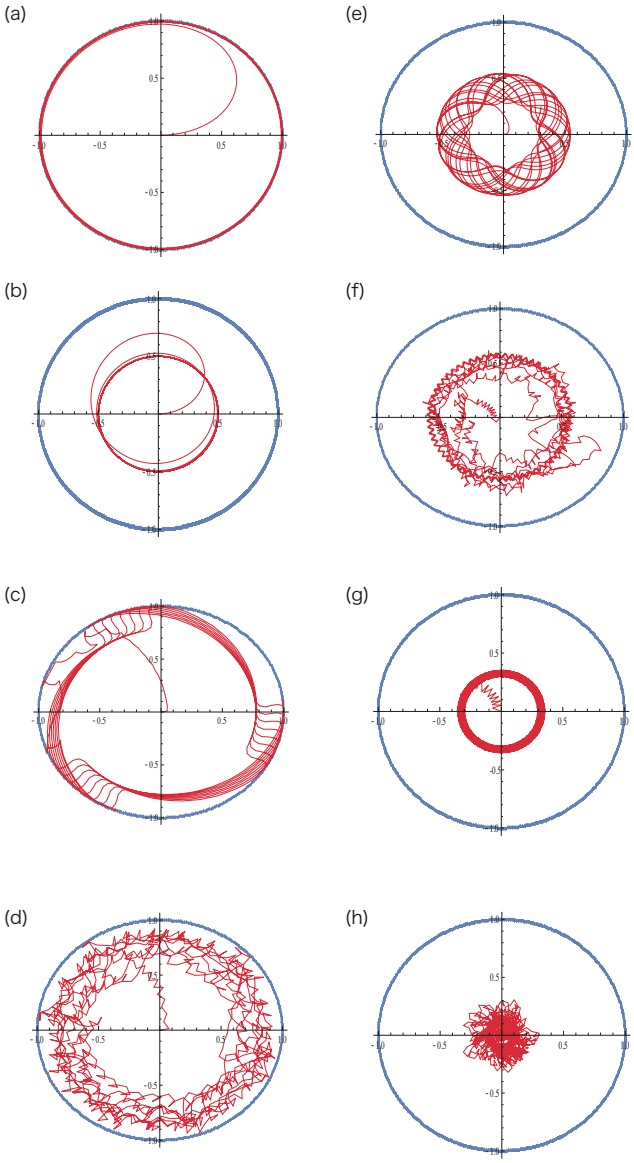

Fig. B.1 Examples of pursuit trajectories of the chaser (red) with the distance-dependent delays. The blue curves indicate the circular path on which the target moves. The scale factor and speed ratio $[\tau_0, n]$ are given as $(a)[0, 1.01]$, $(b)[0, 0.5]$, $(c)[500, 1.01]$, $(d)[500, 1.5]$, $(e)[500, 0.5]$, $(f)[1050, 1.01]$, $(g)[700, 1.5]$, $(h)[1500, 1.01]$. Here, the target's velocity is given as $v = 0.05$ (the period the target takes to go around the unit circle is $T \approx 126$). Reproduced from [77].

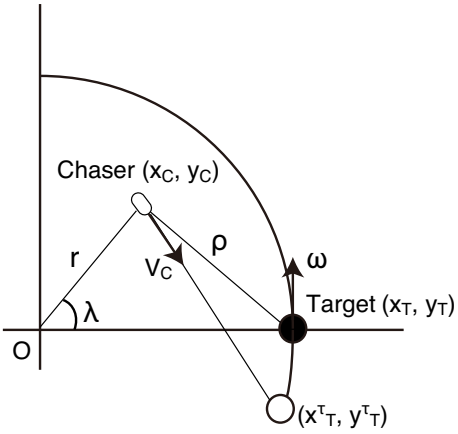

Fig. B.2 Position of the chaser and the target.

The sign of $\Delta\rho$, thus, tells us whether the distance between them increases (when $\Delta\rho > 0$) or decreases (when $\Delta\rho < 0$) by the movement.

Figs B.3 to B.6 show the spatial distribution of the sign of $\Delta\rho$ as a function of the chaser's position (x_C, y_C), with relevant parameters set as $\omega = 1$, $V_C = 1$, $dt = 0.001$, and $\tau_0 = 0, 10, 100, 1000$. In the plots, the target is located at $(x_T, y_T) = (1, 0)$. The color at each point represents the absolute value of $\Delta\rho$, and they are shown separately for the cases $\Delta\rho$ is positive and negative. For all the cases, there is a tendency that the change is negative, $\Delta\rho < 0$, if the chaser is in the upper half of the plane, i.e., the chaser gets closer to the target. This is because, from the position of the target at $(x_T, y_T) = (1, 0)$, the target moves into the upper (positive y) part of the plane.

Without delay (Fig. B.3), the structure of $\Delta\rho$ is quite smooth. As we increase the delay, however, with larger τ_0 (Figs B.4–B.6), they have complex structures, suggesting that a small difference of the chaser's position relative to the target can sensitively affect the increase or decrease of the distance ρ.

We also consider the case as a reference, where we assume the target does not move in dt. In Fig. B.7, we plot the change of the distance between the chaser (x_C, y_C) and the point $(1, 0)$ for the case of $\tau_0 = 10000$. In this case, the intricate pattern is symmetric with respect to the x axes as expected.

In summary, we show that even a simple model with a state-dependent delay can bring complex trajectories to the chase and escape problems. Even though the detailed studies remain in the future, it will be of interest to see how delay can change the qualitative behavior of "group chase and escape".

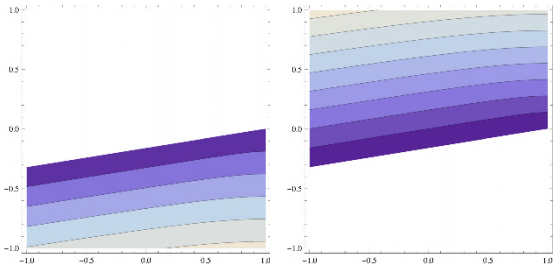

(a) $\Delta\rho > 0$ (b) $\Delta\rho < 0$

Fig. B.3 $|\Delta\rho|$ for the case of $\tau_0 = 0$ plotted as a function of initial position of the chaser. Darker color reflects the smaller value of $|\Delta\rho|$ (no data for white region). Reproduced from [77].

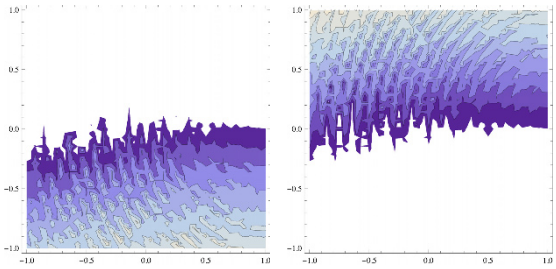

(a) $\Delta\rho > 0$ (b) $\Delta\rho < 0$

Fig. B.4 $|\Delta\rho|$ for the case of $\tau_0 = 10$ plotted as a function of initial position of the chaser. Darker color reflects the smaller value of $|\Delta\rho|$ (no data for white region). Reproduced from [77].

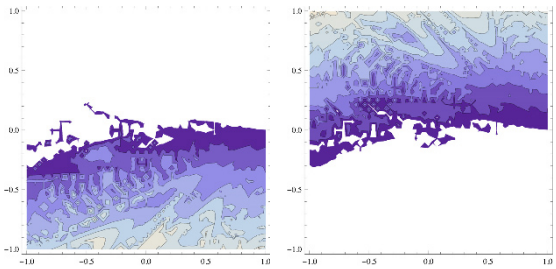

(a) $\Delta\rho > 0$ (b) $\Delta\rho < 0$

Fig. B.5 $|\Delta\rho|$ for the case of $\tau_0 = 100$ plotted as a function of initial position of the chaser. Darker color reflects the smaller value of $|\Delta\rho|$ (no data for white region). Reproduced from [77].

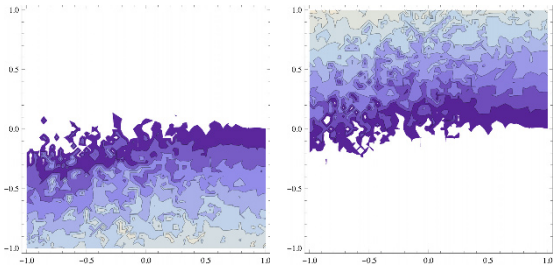

(a) $\Delta\rho > 0$ (b) $\Delta\rho < 0$

Fig. B.6 $|\Delta\rho|$ for the case of $\tau_0 = 1000$ plotted as a function of initial position of the chaser. Darker color reflects the smaller value of $|\Delta\rho|$ (no data for white region). Reproduced from [77].

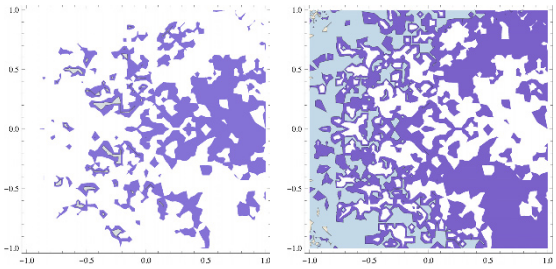

(a) $\Delta\rho > 0$ (b) $\Delta\rho < 0$

Fig. B.7 $|\Delta\rho|$ for the case of $\tau_0 = 10000$ with the fixed target at $(1,0)$, plotted as a function of the position of the chaser (x_C, y_C). Darker color reflects the smaller value of $|\Delta\rho|$ (no data for white region). Reproduced from [77].

Appendix C
Virtual Stick Balancing

We have discussed predator–prey interactions as an example of chases and escapes in section 5.3.1.2. Besides that, a tracking task is observed in a number of biological and social systems where the task can be modeled as chases and escapes. For example, our eyes track motions of an object in sight continuously. As a result, we can perform rather well the task of tracking targets which move along a complex and rapidly changing trajectory. Such a tracking task is modeled in general as chases and escapes with delays. Here, delays occur as a result of various factors such as time taken to identify the target, to formulate a strategy and then to act upon it.

As a typical example of the tracking task, we present here a study of virtual stick balancing (VSB) [67]. VSB is an experimental paradigm which has been well suited for investigating complex visuomotor tracking tasks. It requires a subject (human) to track a target dot that moves on the computer screen by a pointer controlled through a computer mouse. The name, "virtual stick balancing", reflects that the task is considered as a model of balancing a stick vertically on a fingertip. In the real stick balancing, a subject tries to control the motion of his/her fingers so that the stick does not fall. The task is often performed well by tracking a point of the stick visually and controlling our movements. The advantage of VSB is that relevant parameters such as task difficulty can be easily adjusted.

Two different approaches are mainly adopted to model VSB. The first approach considers VSB as a problem of stabilizing an unstable fixed-point with time-delayed feedback and noisy fluctuations. The second approach considers VSB as a chase and escape problem with delays and fluctuations. We will adopt here the second approach.

We describe the setup of VSB. The subject is asked to move a computer mouse in order to keep both the mouse position (pointer or cursor) and a moving target dot on the computer screen as long as possible (the screen is a 20-inch CRT monitor with a 75 Hz refresh rate).

The dynamics of the target are given by the following equation:

$$\frac{d^2}{dt^2}\mathbf{T} = R(\mathbf{T} - \mathbf{C}), \tag{C.1}$$

© Springer Nature Singapore Pte Ltd. 2019

A. Kamimura and T. Ohira, *Group Chase and Escape,*
Theoretical Biology, https://doi.org/10.1007/978-981-15-1731-0

where $\mathbf{C} = (C_x, C_y)$ and $\mathbf{T} = (T_x, T_y)$ are the positions of the mouse cursor and the target on the two-dimensional screen, respectively. The dynamics describe that an acceleration of the target decreases with decreasing distance between the target and the cursor. If the subject can locate his/her cursor close to the position of the target, the target does not accelerate much and pointing is successful. The dynamics are qualitatively analogous to the balance control of sticks on a fingertip in which the subject can control the stick well and the stick is close to its vertical position. On the other hand, once the cursor is far from the target, the target accelerates and moves away from the mouse cursor. This corresponds to the case of failure of controlling stick so that it falls faster as it tilts away from its vertical position. Thus, it is reasonable to assume that the difficulty of the pointing (balancing) task is controlled by the parameter R: the pointing task gets more difficult as R increases.

We now show results of the experiments. Fig. C.1 shows the average balancing time (time duration a subject can keep the target dot on the computer screen) of the VSB experiment for up to 14 subjects. The value of R is set at approximately $5.25[s^{-2}]$. Each subject was asked to practice for up to seven days over a two-week period. Each day, about 25 trials were taken to calculate the average balancing time. Each circle corresponds to each subject. Six subjects participated for all seven days, and the solid curve represents the average balancing time over these six subjects. We observe that the balancing time distributes among subjects and the time increases as the skill improves by practice. The improvement is about threefold for the six subjects.

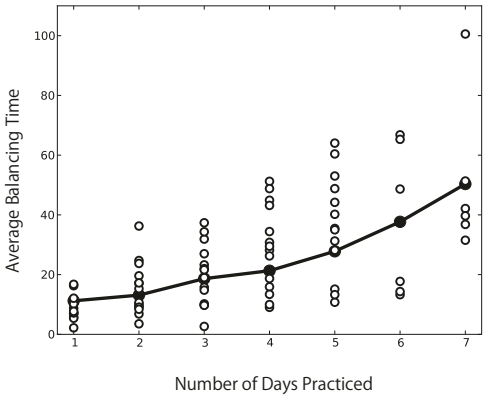

Fig. C.1 Average virtual stick balancing time (in seconds) measured for 14 subjects who practiced up to seven days over a two-week period for $R \approx 5.25$. At least 25 trials were used to estimate the average time. Six subjects participated on all seven days, and the solid curve shows the average time (the average of the averages) of the six subjects. Modified from [67] with permissions (© 2013 The Institute of Electronics, Information and Communication Engineers).

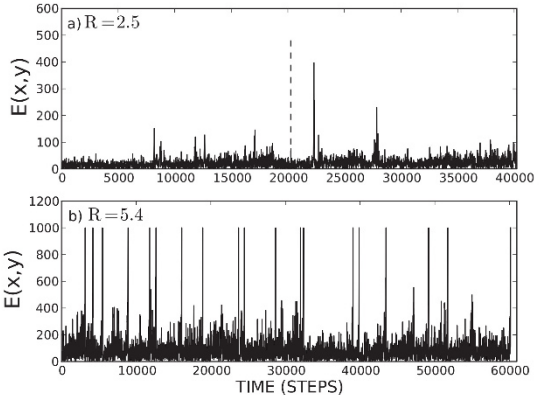

Fig. C.2 Tracking error, $E[C(t),T(t)]$, as a function of time measured at two different levels of task difficulty. (a) Data for $R \approx 2.5$ is for two consecutive trials (separated by vertical dashed line) and (b) for $R \approx 5.4$ for 19 consecutive trials (separated by vertical solid lines). For $R \approx 2.5$ the subject stopped at a given trial voluntarily and for $R \approx 5.4$ each trial ended when the target escaped off the computer screen. Data was taken at a 75 Hz sampling rate. Modified from [67] with permissions (© 2013 The Institute of Electronics, Information and Communication Engineers).

In order to quantify the balancing skill, the tracking error $E[C(t),T(t)]$ is defined as the distance between the cursor and the target on the computer screen:

$$E[C(t),T(t)] = |\mathbf{C}-\mathbf{T}| = \sqrt{(C_x-T_x)^2+(C_y-T_y)^2}, \tag{C.2}$$

where T_x, T_y and C_x, C_y are the (x,y) coordinates of the target and the cursor respectively.

The tracking error is recorded for $R \approx 2.5$ and $R \approx 5.4$ for one subject (Fig. C.2). The time series show burst-like characteristics, in which the distance between the cursor and the target intermittently becomes large. Here, for $R \approx 2.5$, the subject reported little difficulty with the task (the subject voluntarily stopped the task at ≈ 5 minutes to avoid fatigue). On the other hand, for $R \approx 5.4$, the task was difficult for the subject and the target always ran off the computer screen. This was observed even when the subject improved his/her skill by repeated trials. Trial-to-trial variability was also considerable as shown in the figure.

In order to characterize difficulties of the task from another viewpoint, we compute the complementary cumulative distribution function (CCDF) from the empirical data. The CCDF function $F_{ccdf}(s)$ is defined as a probability that the tracking error $E[P(t),T(t)]$ is larger than s,

$$F_{ccdf}(s) = Prob(s < E[C(t),T(t)]). \tag{C.3}$$

For the six subjects, this function is plotted on the log–log scale (Fig. C.3). It is clearly observed that, for all subjects, the occurrences of smaller errors are more

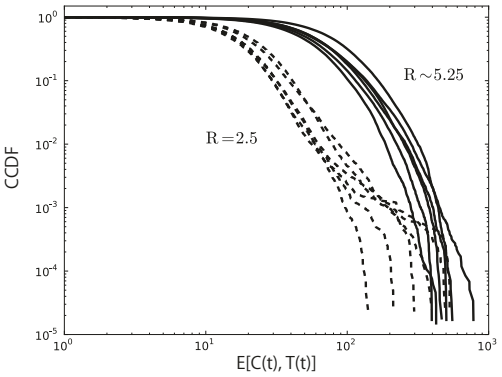

Fig. C.3 Log–log plots for the complementary cumulative distribution function (CCDF), $F_{ccdf}(s)$, as a function of the tracking error, $E[C(t),T(t)]$, for the six subjects with two different levels of task difficulty: $R \approx 2.5$ (dashed lines) and $R \approx 5.25$ (solid lines). Modified from [67] with permissions (© 2013 The Institute of Electronics, Information and Communication Engineers).

notable for $R \approx 2.5$ indicating the balancing task in VSB is less difficult compared to the cases for $R \approx 5.25$.

In order to explain the observation, we propose a simple model based on random walks. As a first step, we consider two interacting random walks in one–dimensional space with discrete time and space: one is the target and the other is the cursor. The target is assumed to move randomly as modeled by a simple symmetric random walk. Then, the probability $P_T(y,t)$ that the target is at spatial position y at time t is given by

$$P_T(y,t+1) = \frac{1}{2}P_T(y-1,t) + \frac{1}{2}P_T(y+1,t), \quad P_T(y,0) = \delta_{y,0}. \tag{C.4}$$

On the other hand, the subject moves the cursor based on a visual feedback with delays. We model this effect by a delayed random walker whose movement is biased toward the position of the target. Then the probability, $P_C(x,t)$, of the position of the cursor x at time t is influenced by the position y of the target at time $t-\tau$ steps in the past, following

$$\begin{aligned} P_C(x,t+1) = &\sum_y \frac{1}{2}\{1-\beta(x-1-y)\}P(x-1,t:y,t-\tau) \\ &+\sum_y \frac{1}{2}\{1+\beta(x+1-y)\}P(x+1,t:y,t-\tau), \end{aligned} \tag{C.5}$$

where β is a positive parameter controlling the bias between the two random walkers. $P(x,t:y,t-\tau)$ is the mixed joint probability with the target at the position y at $t-\tau$ and the cursor at the position x at t. This model accounts for the two elements

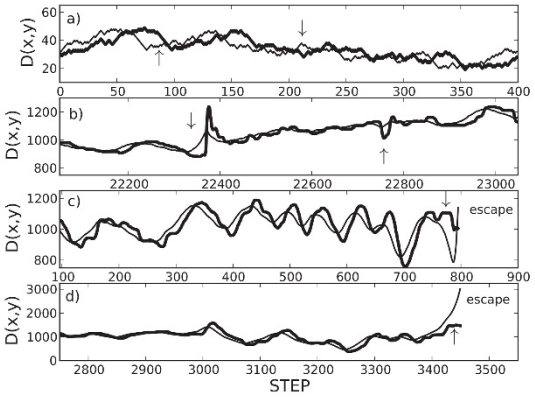

Fig. C.4 Movements of the mouse cursor (thicker lines) and the target dot (thinner lines) in the VSB. $D(x,y)$ represents the distance from a common reference point as the origin to the positions of the cursor and the target. (a) The coupled delayed random walk model with $\beta = 0.5$. The delay is introduced as $\tau = 20$. (b) The experimental observation of VSB for $R \approx 2.5$. (c,d) Two different trials showing escapes for $R \approx 5.4$. Modified from [67] with permissions (© 2013 The Institute of Electronics, Information and Communication Engineers).

in the VSB experiment: fluctuation of the perception of the movements and delays in the control of the mouse cursor.

When $\tau = 0$, the cursor has a bias to move closer to the target by the terms with β. By setting $\tau > 0$, the bias can be controlled to depend on the position of the target in the past. As a result, the dynamics become more complicated because the delay τ can result in the movement of the cursor either toward or away from the target.

We compared the behavior of this coupled delayed random walk model to the experimental results. Fig. C.4 shows representative examples of the movements of the mouse cursor and the target: Fig. C.4(a) shows a result of the model, Fig. C.4(b) shows the observations with $R \approx 2.5$, and Fig. C.4(c,d) show observations with $R \approx 5.4$ in the experiment.

For both our model and experimental observations, an oscillatory behavior is observed in the trajectories of the cursor and the target. This suggests that the time delay causes "over-shoot" of the cursor by the subject in the tracking task. As the skill improves by practice, the oscillatory behavior is less noticeable.

Also, we observe occasional events in which the cursor moves in an unexpected way so that the tracking error $E[P(t),T(t)]$ increases. They are indicated by up and down arrows. In the coupled delayed random walk model, such events have little effect because they do not affect the movement of the target (it follows just the symmetric random walk). Also, the model neglects inertia of the random walks, which may result in strong over-shoots as seen in the experimental data. In the experiments, such occasional increases of the error can be enhanced by the dynamics of the target. For $R \approx 2.5$, however, the subject can typically move the mouse cursor fast enough so that he/she can manage to control the target. On the other hand, for

$R \approx 5.4$, the increases lead to enhancements in $E[P(t), T(t)]$ with which the subject cannot manage the mouse cursor fast enough to overcome. As a result, the target typically escapes off the computer screen resulting in a failure of the task.

The statistical results in the VSB experiments can be also explained by the coupled delayed random walk model. Fig. C.5 plots on the log–log scales the CCDF function $F_{ccdf}(s) = Prob(s < E[C(t), T(t)])$ against a "normalized" error $\hat{E} = E[C(t), T(t)]/E[0.5]$. Here $E[0.5]$ is the error which gives the median of the CCDF function, i.e, $F_{ccdf}(E[0.5]) = Prob(E[0.5] < E[C(t), T(t)]) = 0.5$. The model is in a relatively good agreement with the experiment in the range $\hat{E} < 10^1$, particularly for $R \approx 5.25$. On the other hand, discrepancies are noticeable in the range $\hat{E} > 10^1$, particularly for $R \approx 2.5$. The discrepancy in the large error $\hat{E}$ can arise because the subject can manage and regain the control of the target for $R \approx 2.5$, even once the mouse cursor is located far from the target. For $R \approx 5.25$, such corrections typically fail and the task is stopped so that the large errors are rarely recorded in the experiment.

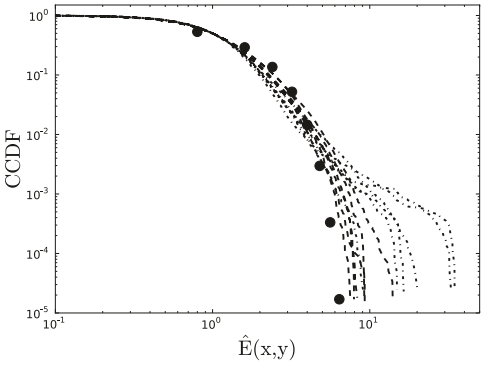

Fig. C.5 Comparison of the model (dots) with the experimental results with the log–log plot of the CCDF function against the normalized error: VSB for $R \approx 2.5$ (dashed–dotted lines) and VSB for $R \approx 5.25$ (dashed lines). Parameters are the same as in Fig. C.3. Modified from [67] with permissions (© 2013 The Institute of Electronics, Information and Communication Engineers).

Further issues remain to be investigated. One is the effects of inattention and blinking of the subject's eyes. Intuitively, inattention and eye blinking increase the failure of the task in which the target escapes from the screen. In the experiment, however, we were not able to identify a causal relationship between the length of inattention time and the failure of the task. At this point, one could say that origins of large tracking errors, which lead to the failure, are mainly from the intrinsic dynamics of the tracking, and the effects of inattention and blinking would be secondary. This view is supported by the fact that the occasional unexpected movements are also observed in the coupled delayed random walk model.

Appendix D
Minority Games

The concept of group chase and escape shares a similarity with a class of problems in game theory. First, conflict of interests exists between the players: chasers and targets. Each chaser tries to capture a target as soon as possible. On the other hand, each target tries to survive as long as possible. Second, each player takes actions independently from the others' actions. For both chasers and targets, the action (movement) is determined only from the distance to the nearest opponent. Yet, from our simulations, the players collectively behave as if they cooperate within each group.

The Minority Game [16] is one of such problem to share the two characteristics: conflict of interests and independent pursuit of its own interest. As described below, the game also exhibits collective behavior of players as if they are cooperative.

The Minority Game was initiated by a problem named after a small bar, El Farol Bar, in Santa Fe, United States [3, 40]. A fixed number of people independently decide to go to this small bar or to stay at home every Thursday. If all the people go there, it is no fun because the bar is crowded. The problem is to avoid the crowd at the bar. One can have a better time if he/she chooses to go there when the number of people is small at the bar. In contrast, it is better to stay home when too many people go there. Each player has to decide without communications with others or knowledge of the status of the bar.

This "El Farol Bar" problem is generally extended and formulated as binary betting by a fixed number of players. A player wins if the number of players is smaller for the same bet, i.e., if one belongs to the minority group. The critical question is "What is the best strategy for each player to win the game?" If every player follows the same deterministic strategy, all the players make the same choice and no one can belong to the minority group. More interesting is if one introduces multiple strategies and each player chooses one of them in a probabilistic manner. These "mixed strategies" can produce an equilibrium state where every player has a chance to win on average.

As an example of the Minority Game, we introduce here a simple game called the Standard Minority Game, proposed by [15]. We consider N (odd integer) players, and they play a repeated game of binary betting. The game assumes that each

© Springer Nature Singapore Pte Ltd. 2019

A. Kamimura and T. Ohira, *Group Chase and Escape,*
Theoretical Biology, https://doi.org/10.1007/978-981-15-1731-0

player decides on one of the two choices, in each time step, based on a strategy card that the player independently prepares in advance. The strategy card determines the next choice, given the winning history of the previous m (memory) time steps. An example of the strategy table card for $m = 3$ is shown in Fig. D.1; we label the two choices of betting as "0" and "1". Here, the information of the winning history is available to all the players. The history is then updated according to the current outcome of every time step.

For each time step, the winning outcome is either of the two choices. Then, the winning history of the m steps has 2^m combinations. For each of the combinations, the next choice is defined in the strategy card, as shown in Fig. D.1. And, for each combination of the m-step history, the next choice is either of 0 or 1. Thus, 2^{2^m} different strategy cards can be produced. With $m = 3$, one can produce $2^8 = 256$ strategy cards. For example, if $m = 3$, there are $2^3 = 8$ combinations of the winning history. When the winning history of the immediate $m = 3$ steps is "010", the strategy card in Fig. D.1 determines the next choice is "0".

The game assumes that each player is allowed to hold s strategy cards, out of the 2^{2^m} cards. Each player randomly chooses the cards in advance, and they cannot be altered or exchanged during the game.

0	0	0	1
0	0	1	0
0	1	0	0
0	1	1	1
1	0	0	0
1	0	1	1
1	1	0	0
1	1	1	1

Fig. D.1 One example of the strategy table card for $m = 3$. For each of the $2^3 = 8$ combinations of the winning history (the left three columns), the next choice is determined as the rightmost column.

At the beginning of the game, the history used for the next choice is randomly generated, and it is updated according to the winning outcome. For example, if the randomly-generated history is "110" ($m = 3$), then, the history is updated to "101" if the group of the choice "1" wins, and to "100" if the group of the choice "0" wins.

Each player uses the s strategy cards as follows. The player assigns points for each card with the initial value of 0. In each step, the player bets according to the strategy card with the highest points among his/her s strategy cards (if multiple cards have the highest points, one is chosen randomly). If the player wins, then the points of the strategy card increase by one, otherwise, the points decrease by one.

The game was investigated by computer simulations. Here, the number of players is fixed at $N = 201$. The number of strategy cards each player can hold is varied as $s \in \{2,5,10,16,32,64\}$ with the memory $m = 3,4$. For each set of $\{s,m\}$, the betting is repeated up to 10^4 times in the game.

Fig. D.2 shows typical time series of the number of winning players (the number of players in the minority group) with two holding strategies ($s = 2$). The time series are shown for the memory $m = 3$ [(a); red], $m = 4$ [(b); blue], and the case when the players select the choices randomly with equal probability of $1/2$ [(c); gray].

The numbers of the winning players with strategy cards [(a), (b)] are closer to the maximum of 100, compared to the random case (c). In addition, the fluctuation in the number is less with strategy cards.

In order to characterize their statistics, we show in Fig. D.3 the average (a) and the standard deviation (b) for the number of winning players as a function of s. As a reference, we also show the case in which all the players randomly choose either of the options without any strategies. In this case, the average is approximately 94.9 and its standard deviation is approximately 5.2.

For both $m = 3,4$, the average number of the winning players decreases with the number of holding strategies s. In addition, the standard deviations increase with s. Surprisingly, when s is smaller than ≈ 16 ($m = 3$), the average number of the winning players is larger than that of the random case. This means that more players can win the game than in the random case, by following their own interests with a smaller number of strategies.

We also show in Fig. D.4 the number of wins, i.e., how many times each player won for all the $N = 201$ players in 10^4 bets in the game. For the memory $m = 3$ [(a); red] and 4 [(b); blue], the number of wins falls mostly within a range of 4800 to 5000. On the other hand, the number is mostly below 4800 for the random case [(c); gray]. Thus, most of the players have higher winning numbers than in the case of random choices.

Hence, given the appropriate sets of parameters of $\{s,m\}$, all the players can enjoy a fair number of wins, almost all of which have higher winning numbers than in the case of random choices. These results look as if the players cooperate to maximize the benefit of all the players, even though each player independently makes decisions to seek his/her own interest. This counter-intuitive behavior results from various factors. Relevant factors have been discussed and investigated, including the assumption of the model that all the players refer to the same winning history, and how the result of betting is affected by a small change of individual players' decisions.

It is one of the promising perspectives to study if the framework of the Minority Game is applied to extend the chasing and escaping strategies in group chases and escapes. For example, when too many chasers try to move toward a single target, chasers tend to block each other's way. This intimately suggests that the number of chasers should not be biased to a specific target to efficiently catch all the targets. On the other hand, it might be better also for the targets to distribute themselves across the spatial field to avoid being rounded up. It would be interesting to develop effi-

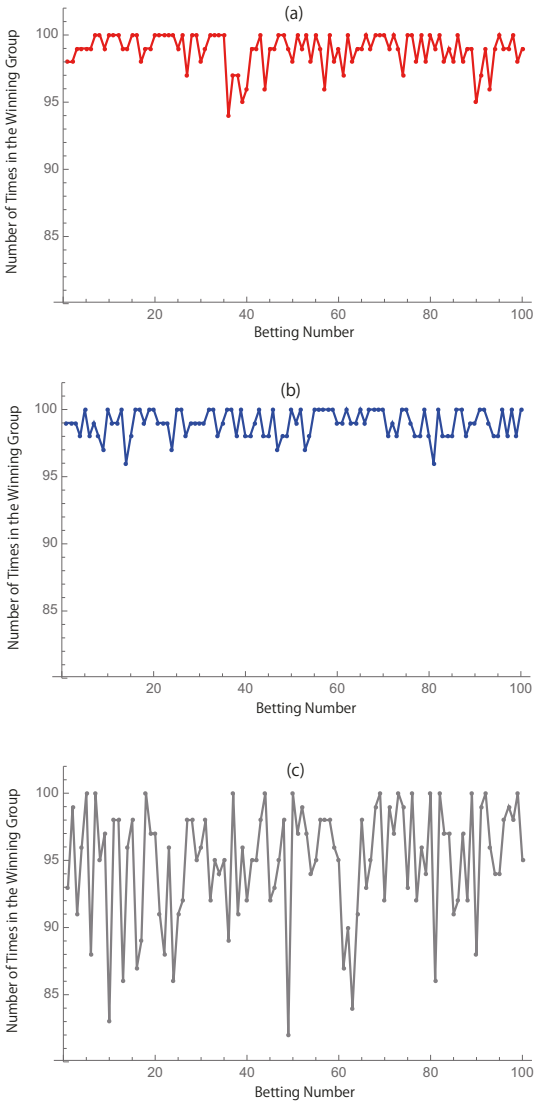

Fig. D.2 Typical time series of the number of the winning players with two holding strategies. (a) $m = 3$ (red) (b) $m = 4$ (blue), and (c) the case where the players select the choices randomly with equal probability of $1/2$ (gray). Data is taken for 100 bets between the time $[9900, 10000]$.

cient strategies for both chasers and targets, even though each player independently moves to seek its own interest.

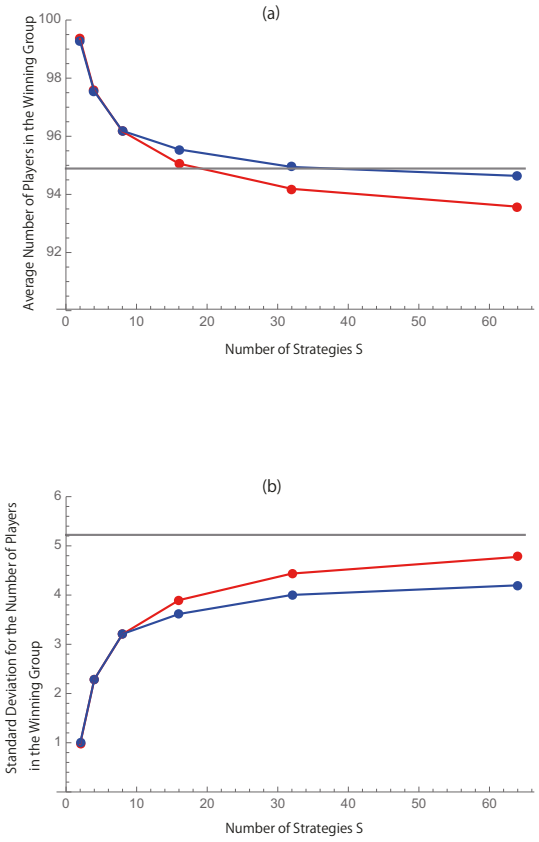

Fig. D.3 (a) The average and (b) the standard deviation for the number of winning players with $m = 3$ (red) and $m = 4$ (blue). The horizontal gray line is the case when all the players choose one of the options with equal probability of $1/2$.

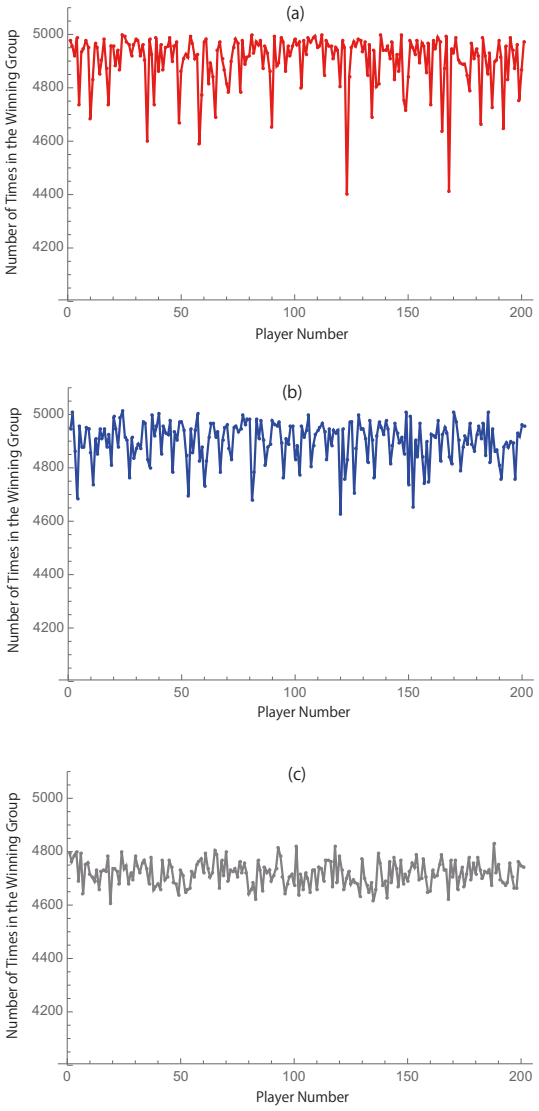

Fig. D.4 For each of the $N = 201$ players, we show the number of wins, i.e., how many times the player won, out of 10^4 bets. (a) $m = 3$ (red) (b) $m = 4$ (blue), and (c) the random choice. The number of holding strategies is set to $s = 2$.

References

1. Angelani, L., Collective predation and escape strategies, Physical Review Letters, **109**, 118104 (2012)
2. Archibald, R. C. and Manning, H. P., Historical remarks on the pursuit problem, American Mathematical Monthly, **28**, 91–93 (1921)
3. Arthur, W. B., Inductive reasoning and bounded rationality, American Economic Review, **84**, 406-411 (1994)
4. Bando, M., Hasebe, K., Nakayama, A., Shibata A., and Sugiyama, Y., Dynamical model of traffic congestion and numerical simulation, Physical Review E, **51**, 1035 (1995)
5. Barton, J. C. and Eliezer, C. J., On pursuit curves, Journal of the Australian Mathematical Society Series B, **41**, 358-371 (2000)
6. Bishop, J. M., Stochastic searching networks, in 1st IEE Conf. on Artifical Neural Networks, 329-331, London, UK (1989)
7. Bonabeau, E., Theraulaz, G. and Deneubourg, J. L., Fixed response thresholds and the regulation of division of labor in insect societies. Bulletin of Mathematical Biology, **60**, 753-807 (1998)
8. Bonabeau, E., Dorigo, M. and Theraulaz, G., Swarm Intelligence: From Natural to Artificial Systems. Oxford University Press, New York (1999)
9. Boole, G., A Treatise on Differential Equations. Macmillan and Company, Cambridge (1859)
10. Bouguer, P., Lines of pursuit, Memories de l'Aacademie Royale des Sciences, 1-14 (1732)
11. Bulsara, A. R. and Gammaitoni, L., Tuning in to noise, Physics Today, **49**, 39 (1996)
12. Cabana, A., Cimarelli, A., Giardina, I., Parisi, G., Santagati, R., Stefanini, F. and Viale, M., Scale-free correlations in starling flocks, Proceedings of the National Academy of Sciences of the United States of America, **107**, 11865-11870, (2010)
13. Canetti, E., Crowds and Power, Victor Gollancz Ltd, (1962). [Translation by Carol Stewart of *Masse und Macht*, originally published by Claassen Verlag, 1960]
14. Cerny, V., Thermodynamical approach to the traveling salesman problem: An efficient simulation algorithm, Journal of Optimization Theory and Applications, **45**, 41-51 (1985)
15. Chalet, D. and Zhang, Y.-C., Emergence of cooperation and organization in an evolutionary game, Physics A, **246**, 407 (1997)
16. Chalet, D., Marsili, M. and Zhang, Y.-C., Minority Games: Interacting Agents in Financial Markets. Oxford University Press, Oxford (2005)
17. Coleman W. J. A., A curve of pursuit. Bulletin Institute of Mathematics and its Application, **27**, 45-47 (1991)
18. Cook, J. W.: In Pursuit of the Traveling Salesman: Mathematics at the Limits of Computation. Princeton University Press (2012)

© Springer Nature Singapore Pte Ltd. 2019

A. Kamimura and T. Ohira, *Group Chase and Escape,*
Theoretical Biology, https://doi.org/10.1007/978-981-15-1731-0

19. Couzin, I. D. and Franks, N. R., Self-organized lane formation and optimized traffic flow in army ants, Proceedings of the Royal Society B, **270**, 139–146 (2003)
20. Couzin, I. D., Krause, J., Franks, N. R. and Levin, S. A., Effective leadership and decision-making in animal groups on the move, Nature, **433**, 513–516 (2005)
21. Creel, S. and Creel, N.M., Communal hunting and pack size in African wild dogs, Lycaon pictus, Animal Behaviour, **50**, 1325–1339 (1995)
22. Dorigo, M. and Stutzle, T., Ant Colony Optimization. MIT Press, Cambridge, MA (2004)
23. Eigen, M., Selforganization of matter and the evolution of biological macromolecules, Naturwissenschaften, **58**, 465–523 (1971)
24. Eigen, M. and Schuster, P., The Hypercycle. Springer, New York (1979)
25. Eigen, M., Steps Towards Life. Oxford University Press, Oxford (1992)
26. Eliezer, C. J. and Barton, J. C., Pursuit curves. Bulletin Institute of Mathematics and its Application, **28**, 182–184 (1992)
27. Eliezer, C. J. and Barton, J. C., Pursuit curves II. Bulletin Institute of Mathematics and its Application, **31**, 139–141 (1995)
28. Gammaitoni, L, Hanngi, P., Jung, P. and Marchesoni, F., Stochastic resonance, Reviews of Modern Physics, **70**, 223 (1998)
29. Gazda S. K., Connor R. C., Edgar R. K. and Cox F., A division of labour with role specialization in group-hunting bottlenose dolphins (Turnips truncates) off Cedar Key, Florida, Proceedings of the Royal Society B, **272**, 135–140, (2005)
30. Gilbert, W., Origin of life: The RNA world, Nature, **319**, 618 (1986)
31. Ginelli, F., Peruani, F., Pillot, M-H., Chate, H., Theraulaz, G. and Bon, R., Intermittent collective dynamics emerge from conflicting imperatives in sheep herds, Proceedings of the National Academy of Sciences of the United States of America, **112**, 12729–12734 (2015)
32. Guha A. and S. Biswas, S., On Leonardo da Vinci's cat and mouse problem, Bulletin Institute of Mathematics and its Application, **30**, 12–15 (1994)
33. Hara, I., Moving direction of japanese sardine school on the basis of aerial surveys, Bulletin of the Japanese Society of Scientific Fisheries, **55**(12), 1939–1945 (1985)
34. Hara, I., Swimming speed of sardine school on the basis of aerial survey, Nippon Suisan Gakkaishi, **53**(2), 223–227 (1987)
35. Hassanien, A. E. and Emary, E., Swarm Intelligence: Principles Advances, and Applications, CRC Press (2015)
36. Hayakawa, Y., Spatiotemporal dynamics of skeins of wild geese, Europhysics Letters, **89**, 48004 (2010)
37. Helbing, D. and Molnar, P., Social force model for pedestrian dynamics, Physical Review E, **51**, 4282 (1995)
38. Helbing, D., Schweitzer, F., Keltsch, J. and Molnar, P., Active walker model for the formation of human and animal trail systems, Physical Review E, **56**, 2527-2539 (1997)
39. Helbing, D., Traffic and related self-driven many-particle systems, Reviews of Modern Physics, **73**, 1067 (2001).
40. Huberman, B. A., The Ecology of Computation, Studies in Computer Science and Artificial Intelligence vol. 2, North Holland (1988)
41. Isaacs, R., Differential Games. Wiley, New York (1965)
42. Iwama, T. and Sato, M., Group chase and escape with some fast chasers, Physical Review E, **86**, 067102 (2012)
43. Janosov, M., Viragh, C., Vasarhelyi, G. and Vicsek, T., Group chasing tactics: how to catch a faster prey, New Journal of Physics, **19**, 053003 (2017)
44. Kamimura, A. and Ohira, T., Group chase and escape, New Journal of Physics, **12**, 053013 (2010)
45. Kamimura, A. and Kaneko, K., Reproduction of a protocell by replication of a minority molecule in a catalytic reaction network, Physical Review Letters, **105**, 268103 (2010)
46. Kamimura, A., Matsumoto, S., Nogawa, T., Ito, N. and Ohira, T., Stochastic resonance with group chase and escape, 21st International Conference on Noise and Fluctuations (ICNF), 200 (2011)

47. Kamimura, A. and Kobayashi T. J., Information processing and integration with intracellular dynamics near critical point, Frontiers in Physiology, **3**, 203 (2012)
48. Kamimura, A. and Kaneko, K., Compartmentalization and cell division through molecular discreteness and crowding in a catalytic reaction network, Life, **4**, 586–597 (2014)
49. Kamimura, A. Matsumoto, S. and Ohira, T., Chases and escapes: From singles to groups, in Ohira, T. and Uzawa, T. (Eds) Mathematical Approaches to Biological Systems, Springer, 139–166 (2015)
50. Kamimura, A. and Kaneko, K., Exponential growth for self-reproduction in a catalytic reaction network: relevance of a minority molecular species and crowdedness, New Journal of Physics, **20**, 035001 (2018)
51. Kandel, E., Schwartz, J., Jessell, T., Siegelbaum, S. and Hudspeth, A. J., Principles of Neural Science. McGraw-Hill Education, New York (2012)
52. Kennedy, J., Eberhart, R. C. and Shi, Y., Swarm Intelligence. Morgan Kaufmann, San Francisco (2001)
53. Kirkpatrick, S., Gelatt Jr, C. D. and Vecchi, M. P., Optimization by simulated annealing, Science, **220** (4598), 671-680 (1983)
54. Kobayashi, T. J., Implementation of dynamic bayesian decision making by intracellular kinetics, Physical Review Letters, **104**, 228104 (2010)
55. Kobayashi, T. J. and Kamimura, A., Dynamics of intracellular information decoding, Physical Biology, **8**(5), 055007 (2011)
56. Koch, A. L., Evolution vs the number of gene copies per primitive cell, Journal of Molecular Evolution, **20**, 71–76 (1984)
57. LeCun, Y., Bengio, Y. and Hinton, G., Deep learning, Nature, **521**, 436–444 (2015)
58. Lighthill, M. J. and Whitham, G. B., On kinematic waves II. A theory of traffic flow on long crowded roads, Proceedings of the Royal Society London, Series A, **229**, 317 (1955)
59. Lin, S. and Kernighan, B. W., An effective heuristic algorithm for the traveling-salesman problem, Operations Research, **21**, 498–516, (1973)
60. MacNulty, D. R., Smith, D. W., David Mech, L., Vucetich, J. A. and Packer, C., Nonlinear effects of group size on the success of wolves hunting elk, Behavioral Ecology, **23**, 75–82 (2012)
61. Malone, T. W. and Bernstein, M. S. (Eds.), Handbook of Collective Intelligence, The MIT press (2015)
62. Masuko, M., Hiraoka, T., Ito, N. and Shimada, T., The Effect of laziness in group chase and escape, Journal of the Physical Society of Japan, **86**, 085002 (2017)
63. Matsumoto, S. Nogawa, T. Kamimura, A. Ito, N. and Ohira, T., Fluctuation effect for group chase and escape, Proceedings of the Symposium on Simulation of Traffic Flow, **16**, 1–4 [in Japanese] (2010)
64. Maynard-Smith, J., Hypercycles and the origin of life, Nature, **280**, 445 (1979)
65. McCulloch, W. and Pitts, W., A logical calculus of the ideas immanent in nervous activity, Bulletin of Mathematical Biophysics, **5**, 115–133 (1943)
66. Mech, L. D. and Boitani, L. (Eds.), Wolves: Behavior, Ecology and Conservation, University of Chicago Press, Chicago (2003)
67. Milton, J. G., Fuerte, A., Christophe B., Lippai, J., Kamimura, A. and Ohira, T., Delayed pursuit-escape as a model for virtual stick balancing, Nonlinear Theory and Its Applications, IEICE, **4**, no. 2, 129–137 (2013)
68. Moyle, P. B. and Cech, J. J., Fishes: An Introduction to Ichthyology, Benjamin Cummings (2003)
69. Muro, C. Escobedo, R. Spector, L. and Coppinger, R. P., Wolf-pack (canis lupus) hunting strategies emerge from simple rules in computational simulations, Behavioural Processes **88**, 192-197 (2011)
70. Nagy, M., Akos, Z., Biro, D. and Vicsek, T., Hierarchical group dynamics in pigeon flocks, Nature, **464**, 890–893 (2010)
71. Nahin, P. J., Chases and Escapes: The Mathematics of Pursuit and Evasion. Princeton University Press, Princeton (2007)

72. Nakayama, A., Hasebe, K. and Sugiyama, Y., Instability of pedestrian flow and phase structure in a two-dimensional optimal velocity model, Physical Review E, **71**, 036121 (2005)
73. Nakayama, A., Hasebe, K. and Sugiyama, Y., Effect of attractive interaction on instability of pedestrian flow in a two-dimensional optimal velocity model, Physical Review E, **77**, 016105 (2008)
74. Niesert, U., Harnasch, D. and Bresch, C., Origin of life between scylla and charybdis, Journal of Molecular Evolution, **17**, 348–353 (1981)
75. Nishi, R., Kamimura, A., Nishinari, K. and Ohira, T., Group chase and escape with conversion from targets to chasers, Physica A, **391**, Issues 1-2, 337 (2012)
76. Ohira, T. and Sawatari, R., Phase transition in a computer network traffic model, Physical Review E, **58**, 193 (1998)
77. Ohira, T., Kamimura, A. and Milton, J. G., Pusuit–escape with distance-dependent delay, 7th European Nonlinear Dynamics Conference (ENOC2011), Rome, Italy, MS-11 (2011)
78. Ohira, T. Hosaka, T. and Nogawa, T., Chases and escapes, and optimization problems, Artificial Life and Robotics, **20**, 257–261, (2015)
79. Packer, C. and Ruttan, L., The evolution of cooperative hunting, The American Naturalist, **132**, 159-198, (1988)
80. Parrish, J. K. and Hammer, W. H. (Eds.), Animal Groups in Three Dimensions. Cambridge University Press, Cambridge (1997)
81. Pavlov, D. S. and Kasumyan, A. O., Patterns and mechanisms of schooling behavior in fish: A review, Journal of Ichthyology, **40**, Suppl. 2, S163–S231 (2000)
82. Portugal, S. J., Hubel, T. Y. Fritz, J. Heese, S., Trobe, D., Voelkl, B., Hailes, S., Wilson, A. M. and Usherwood, J. R., Upwash exploitation and downwash avoidance by flap phasing in ibis formation flight, Nature, **505**, 399–402 (2014)
83. Rasmussen, S. (Ed.), Protocells Bridging Nonliving and Living Matter. MIT Press, Cambridge, MA (2008)
84. Reynolds, C. W., Flocks, herds and schools: A distributed behavioral model, Computer Graphics, **21**(4) (SIGGRAPH '87 Conference Proceedings), 25–34 (1987)
85. Richards, P. I., Shock waves on the highway, Operations Research, **4**, 42 (1956)
86. Ruckle, W. H., in Stochastic Games and Related Topics (T. E. S. Raghavan et al., Eds.), Kluwer Academic, 29–43 (1991)
87. Saito, T., Nakamura, T. and Ohira, T., Group chase and escape model with chasers' interaction, Physica A, **447**, 172–179 (2016)
88. Sato, M., Chasing and escaping by three groups of species, Physical Review E, **85**, 066102 (2012)
89. Schaller, V., Weber, C., Semmrich, C., Frey, E. and Bausch, A. R., Polar patterns of driven filaments, Nature, **467**, 73–77 (2010)
90. Sengupta, A., Kruppa, T. and Lowen, H., Chemotactic predator-prey dynamics, Physical Review E, **83**, 031914 (2011)
91. Shiraishi, M., Takeuchi, R., Nakaghawa, H., Nishimura, S-I., Awazu, A. and Nishimori, H., Diverse stochasticity leads a colony of ants to optimal foraging, Journal of Theoretical Biology, Vol. 465, 7–16, (2019)
92. Shunyakov, V. M. and Lavrik, L. V., Analytical solution of curvilinear motion on an inclined plane, American Journal of Physics, **78**, 1406 (2010).
93. Stander, P.E., Cooperative hunting in lions: the role of the individual, Behavioral Ecology and Sociobiology, **29**, 445–454 (1992)
94. Sugiyama, Y., Fukui, M., Kikuchi, M., Hasebe, K., Nakayama, A. and Nishinari, K., Traffic jams without bottlenecks – experimental evidence for the physical mechanism of the formation of a jam, New Journal of Physics, **10**(3), 033001 (2008)
95. Szathmary, E. and Demeter, L., Group selection of early replicators and the origin of life, Journal of Theoretical Biology, **128**, 463 (1987)
96. Tadaki, S., Kikuchi, M., Fukui, M., Nakayama, A., Nishinari, K., Shibata, A., Sugiyama, Y., Yosida, T. and Yukawa, S., Phase transition in traffic jam experiment on a circuit, New Journal of Physics, **15**, 103034 (2013)

97. Toner, J. and Tu, Y., Long-range order in a two-dimensional dynamical XY model: How birds fly together, Physical Review Letters, **75**, 4326 (1995)
98. Vasarhelyi, G., Viragh, C., Somorjai, G., Nepusz, T., Eiben, A. E. and Vicsek, T., Optimized flocking of autonomous drones in confined environments, Science Robotics, **3**(20), eaat3536 (2018)
99. Vicsek, T., Czirok, A., Ben-Jacob, E., Cohen, I. and Shochet, O., Novel type of phase transition in a system of self-driven particles, Physical Review Letters, **75**, 1226 (1995)
100. Vicsek, T., Fluctuations and Scaling in Biology. Oxford University Press, New York (2001)
101. Vicsek, T., Statistical physics: Closing in on evaders, Nature, **466**, 43 (2010)
102. Vicsek, T. and Zafeiris, A., Collective motion, Physics Reports, **517**, Issues 3-4, 71 (2012)
103. Wiesenfeld, K. and Moss, F., Stochastic resonance and the benefits of noise: from ice ages to crayfish and SQUIDs, Nature, **373**, 33 (1995)
104. Wilson, D. J., Issacs' princess and monster game on a circle, Journal of Optimization Theory and Applications, **9**, 265-288 (1972)
105. Yamamoto, K. and Yamamoto, S., Analysis of group chase and escape by honeycomb grid cellular automata, SICE Annual Conference (SICE), 2013 Proceedings of. IEEE, 1004–1009 (2013)